

Mechanistic and Computational
Studies of Ferroin, Simple Organic Acids,
and Bromine Oxides

Elucidating the Complex Electrochemical Dance in an Oscillating Reaction

A thesis presented to
Faculty of the Graduate School of Chemistry
At the University of Missouri-Columbia

In partial fulfillment
of the requirements for the
degree of Master of Science

By:
Cory Camasta
Dr. Rainer Glaser, Ph.D., Thesis Supervisor
December 2016

The undersigned, appointed by the Dean of the Graduate School, have examined the thesis entitled:

MECHANISTIC AND COMPUTATIONAL STUDIES OF
FERROIN, SIMPLE ORGANIC ACIDS, AND BROMINE OXIDES

presented by Cory Camasta, a candidate for the Master of Science degree,
and hereby certify that, in their opinion, it is worthy of acceptance.

Dr. Rainer E. Glaser

Dr. Thomas D. Sewell

Dr. Aigen Li

Acknowledgement

The scientist's journey is a long and challenging one. Though I do not know where mine will end, I have high hopes for it. In this short preface to the work that has directly consumed a large amount of my last nine months at the University of Missouri (and indirectly quite a bit longer), I would like to take a moment to give due thanks:

Thank you to all of the dedicated researchers that allowed me to write this thesis without ever putting on a pair of protective eyewear – including the one that gave me a job.

Thank you to those who loved every second of the research you did. Your sincere efforts to extend our collective knowledgebase certainly show in the fruits of your labor.

Thank you to those who hated every second of the research you did. Even though you may have thought so at the time, your struggles were not all in vain. I hope they taught you something useful and that you find your way onto the path that you deserve to follow.

Thank you to those who have shown me love and acceptance, both in academia and in the real world. It is for you that I am motivated to better myself and, by doing so, better the world. I am grateful to have received some of your light and hope to find more people like you in the next leg of my journey.

Thank you to those who have shown me the ugly side of academia. I know a lot more now than I once knew (despite also feeling that smaller-fraction-of-everything-that-exists thing), and will use what you have taught me to become a wiser and all-around better human being. Even so, I hope to avoid people like you in the next leg of my journey.

For better or for worse, our lives are constantly impacted by different people and new things. Instead of letting the evil in the world consume us, as it is so easy to do sometimes, please join me now if you have not already in this quest to turn copper to orichalcum, coal to carbene, and eventually turn lead to gold. It is time to science!

Table of Contents

ii. Acknowledgement	
iv. List of Figures, Schemes, Tables and Equations	
v. List of Abbreviations	
1. Introduction	iv
1.1 Abridged History of Belousov and Zhabotinsky's Reaction	3
1.2 Components and General Mechanisms of a BZ Reaction	5
1.2.1 Metal	5
1.2.2 Reducing Agent	7
1.2.3 Halogen Oxides and Strong Acid	8
1.3 Ferrum and Ferrioin	10
2. Materials & Methods	12
2.1 Theory	18
2.2 Calibrating the System	21
2.3 The Importance of Phase	27
3. Results	29
3.1 The Arrow of Time	29
3.2 Proposed Mechanisms	32
3.2.1 The Induction Period and Rise of Oscillations	32
3.2.2 Propagation via One-Electron Oxidations	38
3.2.3 Termination via Two-Electron Oxidations	41
3.2.4 Products of a BZ Reaction	44
3.2.5 Elusive Intermediate: Bromotartronic Acid	49
3.3 Metal Catalysis	51
3.3.1 Evidence for the Outer-Sphere Electron Transfer	51
3.3.2 Tautomerizations	56
3.4 Modeling the Metal Catalysis	60
3.4.1 First Attempts	60
3.4.2 Ligand Field Analysis	61
3.4.3 Ligand Fields in Another Practical Model	65
3.5 Bromine Oxide/Oxoacid Equilibria	67
3.5.1 What is Known	67
3.5.2 What is Less Known	68
3.5.3 What We Can Speculate – Brozone and Bonding	76
3.6 Fruits of Labor	80
4. Discussion	86
4.1 Potential Flaws, Fixes, and Side Notes	86
4.2 Conclusions and Future Direction	89

List of Figures, Schemes, Tables and Equations

Figure 1. Morse potential plot for $^{79}\text{Br}-^{81}\text{Br}$	15
Figure 2. Aqueous optimized structures of bromine-free derivatives of malonic acid	35
Figure 3. Aqueous optimized structures of brominated derivatives of malonic acid	37
Figure 4. Radical recombination products and subsequent decompositions.	45
Figure 5. Aqueous optimized structure of hypothetical ferriin-bromomalonic acid adduct	48
Figure 6. Additional theorized intermediates and byproducts of a BZ reaction	50
Figure 7. Spin density isosurfaces of malonic and bromomalonic acids and neutral radicals	58
Figure 8. Molecular orbital bonding schemes of iron in the context of ligand field theory.....	63
Figure 9. Aqueous optimized structures of assorted singlet (S=0) bromine oxides.....	72
Figure 10. Electrostatic potential of BrOOOOOBr.....	75
Figure 11. Oxidation of BrOBr by acidic bromate.....	77
Figure 12. Acid-mediated condensation of bromate and bromous acids.....	80
Figure 13. Decomposition of bromine dioxide dimer, oxygen evolution.....	81
Figure 14. Decomposition of $\text{O}_2\text{BrOBrO}_2$ by bromide and acid.....	82
Figure 15. Decomposition of OBrOBrO_2 by bromide	83
Figure 16. Decomposition of BrOBrO_2 by hydrobromic acid.....	84
Figure 17. The acidic bromide-mediated decomposition of BrOBrO_2	85
Scheme 1. Mechanisms describing the formation of bromo- and dibromo-malonic acids	33
Scheme 2. Mechanisms describing the oxidation of malonic acid enol and tartronic acid	42
Scheme 3. Mechanisms describing the degradation of mesoxalic acid into oxalic acid and CO_2	42
Scheme 4. Mechanisms describing a route to the formation of bromoethenetetracarboxylic acid	46
Scheme 5. Mechanism describing the electron transfer from ferriin to oxidized bromomalonic acid	55
Table 1. Calibration data for iron and bromine using density functional theory.....	25
Table 2. Calibration data for iron and bromine using traditional higher level theories.....	26
Table 3. Table of selected solvation energies	28
Table 4. Reaction matrix containing acid-consuming single-electron oxidations	40
Table 5. Table of two-electron oxidation reactions	43
Table 6. Table of ketone to enol tautomerization energies.....	57
Table 7. Thermodynamic data for $\text{Fe}(\text{NH}_3)_6^{3+}$ in different conformations	61
Table 8. Gas-phase thermodynamics of ligation and spin crossover for iron complexes.	64
Table 9. Thermodynamics of the bromine oxide reactions described by the MBM model.....	68
Table 10. Thermodynamics of ozone formation	78
Equation Set 1. Thermodynamics calculations in Gaussian	13
Equation Set 2. Basic definitions in <i>ab initio</i> molecular modeling.....	18
Equation Set 3. Summary of density functional theory	19
Equation Set 4. Summary of many-body perturbation theory	19
Equation Set 5. Summary of coupled cluster theory	20
Equation Set 6. The Eyring equation.....	79

List of Recurrent Abbreviations

BZ – Belousov-Zhabotinsky

MA – Malonic Acid ($C_3H_4O_4$), MAyl – Malonyl radical

BMA – Bromomalonic Acid ($C_3H_3O_4Br$), BMAyl – Bromomalonyl Radical ($C_3H_2O_4Br$)

DBMA – Dibromomalonic Acid ($C_3H_2O_4Br_2$)

TA – Tartronic Acid ($C_3H_4O_5$), TAyl – Tartronyl Radical ($C_3H_3O_5$)

MOA – Mesoxalic Acid ($C_3H_2O_5$)

GOA – Glyoxalic Acid ($C_2H_2O_3$)

OA – Oxalic Acid ($C_2H_2O_4$)

FA – Formic Acid (H_2CO_2), Cbxyl – Carboxyl Radical (HCO_2)

CA – Carbonic Acid (H_2CO_3)

BTA – Bromotartronic Acid ($C_3H_3O_5Br$)

BrAA – Bromoacetic Acid ($C_2H_3O_2Br$), BrAyl – Bromoacetyl Radical ($C_2H_2O_2Br$)

Br₂AA – Dibromoacetic Acid ($C_2H_2O_2Br_2$), Br₂Ayl – Dibromoacetyl Radical ($C_2HO_2Br_2$)

Br₃AA – Tribromoacetic Acid ($C_2HO_2Br_3$)

DFT – Density Functional Theory

MP2 – Møller-Plesset Second-Order Perturbation Theory

CIS(T) – Configuration Interaction, Single-excitation, (Triple-excitation)

PCM – Polarizable Continuum Model

SMD – Solvent Model Density

MBM – Marburg-Budapest-Missoula

GTF – Györgyi-Turányi-Field

FKN – Field Körös Noyes

kcal/mol – Kilocalories per mole \sim 4.184 Kilojoules per mole

MO – Molecular orbital

Note: In sections 3.5 and 3.6 expanded molecular formulas reflect atomic connectivity.

1. Introduction

Before the year 1950, many chemists in their 'right mind' held the archaic belief that all chemical reactions proceed strictly from reactants to products, though some could be coaxed into reverse. What we now know colloquially as a potential energy surface was only visualized in more than two dimensions by the greatest thinkers at the time. The Belousov-Zhabotinsky (BZ) reaction is perhaps the most well-known of the 'chemical oscillators' and a prime example of a phenomenon that simply cannot be demystified given a two-dimensional data set. Though simulations of the BZ reaction produce reasonable results, to this day, not one published model has been capable of completely describing the chemistry that occurs. Some sort of halide-halogen-oxide cycle drives almost, if not, all known inorganic chemical oscillators, including those that proceed naturally in Earth's atmosphere. Catalytic indicators like cerium and ferroin, when added to the reaction mixtures, provide intuitive views of the chemical environment that we cannot normally see while moderately altering the reaction dynamics. Researchers worldwide have invested countless man-hours into producing different sets of data, from which the ultimate goal of describing this type of oscillating chemical reaction in detail will eventually be realized. In this study, we examine both basic and obscure chemical processes that proceed in a BZ mixture with a focus on those prepared in a continuously stirred tank reactor (CSTR), ideally in order to pave a new path for researchers that choose to fixate on this phenomenon in the future and help complete the already daunting collections of reactions that have been devised to describe the peculiar chemistry that occurs. Most everyone that has studied the BZ reaction in the past knows that it is perhaps the single most influential process in the modern era of knowledge regarding non-linear chemical dynamics. Since we opt for an entire laboratory *in silico*, this study will primarily examine physical and electronic mechanisms at the single-

molecule scale. Detailed mathematics are not presented in this study, however we do present a niche of non-equilibrium chemical mechanics and some applications of university-level quantitative chemistry to computational problems. Consequently, interested chemists are encouraged to treat many of the largely extrapolated ensemble-scale conclusions herein with scrutiny and perhaps try to prove what they may find intriguing themselves. That being said, most potential inadequacies have already been identified and discussed. The initial goal of this study was to model the oxidation of bromomalonic acid (BMA) by $\text{Fe}(1,10\text{-phenanthroline})_3^{3+}$ (a.k.a. ferriin) and determine the mechanism by which electrons are transferred. Following many months of unpublished work, the initial models were determined to be inadequate and the project underwent a transformation, eschewing the model in an effort to focus on the ‘real deal’ and favoring a new theoretical approach, determined to be capable of examining many different systems as efficiently and accurately as possible given all other constraints. This is the culmination of those efforts. By the end of this thesis, the reader should at the very least gain: 1) An appreciation for both empirical and theoretical methods in the hard sciences and the roles of mathematics therein; 2) Knowledge of many hypothetical and documented processes that occur during the oxidation of organic acids by acidic bromate, specifically derivatives of malonic acid, and why the term ‘oscillating chemical reaction’ might be more accurately replaced with ‘chaotic chemical pendulum’ (but will not be hereafter); 3) Some insight into the nature of electrons – how they behave and why, for instance, a thermodynamically favorable chemical reaction might not proceed appreciably in practice or why an unfavorable reaction may still proceed in practice; and 4) New leads to follow down the path of elucidating bizarre and oft-neglected chemistry of the halogen oxides, specifically of bromine. These are some things that I learned more about, too. In the meantime, the reader may also expect to learn a bit of biochemistry as a tribute to our good friends, Борис Белоусов and Анатолий Жаботинский.

1.1 Abridged History of Belousov and Zhabotinsky's Reaction ¹

As is the case in most monumental scientific discoveries, the BZ reaction was originally discovered in the context of something else and met with plenty of undue criticism. Circa 1950, biophysics professor and department head at the USSR Ministry of Health, Boris Pavlovich Belousov, then in his late fifties, was attempting to simulate the tricarboxylic acid (TCA) cycle, our primary means of liberating electrons for use in the mitochondrial respiratory chain where their motion provides energy to pump protons against a voltage/concentration gradient as the electrons are shuttled through the mitochondrial membrane, eventually reducing elemental oxygen to water. Belousov decided to oxidize citric acid in an acidic solution of cerous (III) ions and bromate, which when mixed together resulted in a color-changing solution, cycling from yellow to clear and back again while evolving CO₂ for over an hour. Since no one had ever described such a phenomenon at the time, Belousov began studying the reaction in detail and eventually tried to publish his findings. He accredited A. P. Safronov, one of his colleagues, with perfecting the recipe and suggesting the use of ferroin as an indicator/catalyst, which eventually lead to Belousov's observation of redox waves in a test tube variant of the reaction.

Unfortunately, despite popularizing the chemical oscillator and spurring further studies worldwide, attempts to publish his own research were met with criticism from the editors of journals to which he had sent the manuscripts. His first submission was shot down because the referee could not see his findings as anything but "impossible". Belousov was told that in order for his work to have scientific merit, he would have to disprove the accepted chemical theory at the time because it had never predicted any sort of chemical reaction that could be thought of as 'oscillating'. To be fair, the original manuscript reportedly had zero outside references.

Around the same time, Alan Mathison Turing was in Manchester, England modeling reaction-

diffusion systems of biological 'morphogens' with differential equations and independently predicted the existence of chemical oscillations.² All the while, William C. Bray had published his recipe for an iodine-iodate- H_2O_2 oscillator in the US about thirty years prior, which cites even older literature.²² It is unfortunate for Belousov that they did not have the internet at that time. Either way, in response to his first rejection, Belousov spent six years studying his reaction and put together a new, more detailed manuscript with rudimentary descriptions of the chemical mechanism, however when submitted it was dismissed again, this time with a suggestion to cut out all of his hard work and resubmit the findings as a letter to the editor. At this point Belousov was done with the manuscript and it remained unpublished for more than twenty years.

Biochemistry graduate student Anatol Zhabotinsky at Moscow State University comes into the picture in late 1961 when he is told to study the reaction by his graduate advisor, another one of Belousov's colleagues named Simon El'evich Schnoll. Zhabotinsky grew attached to this work and made several attempts to talk face-to-face with Belousov while he studied the phenomenon, however they only ever communicated in writing. During this time, a lot of literature was published describing oscillating reactions deriving from Belousov's original recipe, including Zhabotinsky's review of the unpublished manuscript in 1964. Unfortunately, Boris Belousov did not live long enough to accept the Lenin Prize in 1980 that was awarded to himself, Zhabotinsky, V. I. Krinsky and G. R. Ivanitsky for the discovery of the oscillating chemical reaction that now bears his name, but at least he got to see it published.

Today, many different models devised to describe the BZ reaction exist in literature, notably including the Brusselator,³ Oregonator,⁴ Field Körös Noyes (FKN)⁵, Györgyi-Turányi-Field (GTF)⁶ and Marburg-Budapest-Missoula (MBM)⁷ models. They consist of chemical and arithmetic equations that, *in silico*, reasonably reproduce the behavior of cerium-catalyzed BZ reactions when given reasonable initial concentrations of reactants.

1.2 Components and General Mechanisms of a BZ Reaction

1.2.1 Metal

Ferriin, a complex formed from one part iron and three parts 1,10-phenanthroline, ($\text{Fe}(\text{o-phen})_3^{2/3+}$), is commonly used as the metal catalyst in a BZ reaction because it also functions as a high-contrast reduction-oxidation (redox) indicator, cycling from reduced red ferriin(II) to oxidized blue ferriin(III) and back, however it is among the more expensive options if one cannot synthesize their own phenanthroline. Chemical waves seen in two-dimensional, non-stirred variants of the reaction are redox fronts made visible by this metastable iron complex, but in a stirred vessel the entire solution changes color in response to its dominant oxidation state. Iron in its free ionic form can also reportedly catalyze bromate oscillators, cycling between ferrous(II) and ferric(III) states. Despite the draws of using an abundant, non-toxic metal, it is not commonly employed due to its lackluster ability to sustain chemical oscillations in comparison to the other hydrated metal cations.⁸

The first noteworthy free metal cation used in batch-reactor BZ reactions is cerium because it has been studied the longest and frequently referenced mathematical models are parameterized for it. Cerium cations cycle between yellow cerous(III) and colorless ceric(IV) forms. Studies of a bromate-resorcinol-[catalyst] chemical oscillator found that starting with a ceric catalyst results in more pronounced oscillations as long as they persist, as one with previous knowledge of the chemical mechanisms at play would probably expect.⁹

Manganese is also commonly used as a free metal catalyst, cycling between reduced manganous(II) and oxidized manganic(III) states. It is the most reactive of all the free metal catalysts in resorcinol-based chemical oscillators.^{9,10} Manganese-containing BZ solution appears very pale pink to colorless (depending on the concentration) when the metal is reduced and

reddish when oxidized to its +3 state. The manganic(III) form of manganese is not commonly found elsewhere, thus this reaction presents a novelty occurrence.

A ruthenium complex that cycles between reduced Ru(II)tris-bipyridine and oxidized Ru(III)tris-bipyridine, very similar to ferroin, is also a viable catalyst for BZ reactions, though no studies report the successful use of ruthenium alone. Orange solution indicates that the complex is in its reduced state and green indicates that it is oxidized. A number of studies note the strong sensitivity of the ferro-group complexes to light, including one that effectively determined a way to manipulate the chemical waves inside of Ru-BZ-containing droplets with high-intensity illumination and direct the motion of the droplets on an oil-coated surface.¹¹ Ruthenium is directly below iron on the periodic table, thus one wonders whether an Osmium complex might also facilitate redox oscillations. Since the red-to-blue color change is the most pronounced of those discovered, ferroin is often chosen for use in chemistry demonstrations.

Known reactions that oscillate in the absence of a metal catalyst include chlorine dioxide-iodine-malonic acid (MA) and chlorite-iodide-MA reactions, though these still require starch as an indicator if one wants to observe the oscillations without electrochemical equipment.¹² Since bromine does not form a polybromide complex inside starch helices, the metal appears to be required in a bromate oscillator if one relies on visual oscillatory cues, however at least one metal-free oscillator has been identified with a bromine-sensitive electrode that utilizes catechol as the reducing substrate.¹³ The uncatalyzed bromate oscillator is very sensitive to increasing temperature between 303 and 323 K, which significantly decreases the induction time and lengths of oscillatory periods.

1.2.2 Reducing Agent

The organic reducing component can vary even more so than the metal complex, at least according to a query of what has been done already. Though many researchers choose to use malonic acid as Zhabotinsky did years ago, some natural antioxidants including catechol,¹⁴ resorcinol¹⁴ and gallic acid¹⁵ have also been used successfully, in addition to synthetic benzene-derived compounds like *p*-benzoquinone¹⁶ and *p*-aminophenol.⁸ Belousov was using citric acid when he discovered the reaction and other Russian researchers at the time apparently had success with different TCA-cycle intermediates as well. A 1978 study reports that malic and oxaloacetic acids are also effective in a Mn-BrO₃⁻ oscillator, however they report that fumaric acid is not effective, which, given the inner-sphere mechanism of the Mn-catalyzed reaction (similar to Ce as discussed later), makes sense due to the difficulty fumarate has complexing multivalent metal cations.¹⁷ By this logic, we might reason that succinate would have been a better choice due to its enhanced flexibility. More recently, another group successfully utilized 1,4-cyclohexanedione in a bromate oscillator with three different metal catalysts (Mn^{2/3+}, Ce^{3/4+} and Ru(trisbipyridine)^{2/3+}) and isolated a hydroquinone intermediate, providing rationale for multiple probable mechanisms.¹⁸

We notice that all of the reducing agents mentioned contain at least one oxygen atom and learn from past experiments that they are often brominated during the reaction. Given this, all signs indicate that a good organic component must be physically capable of participating in redox chemistry with the metal catalyst, and results also suggest that it should also be prone to bromination. Different metal catalysts govern different physical mechanisms, but all of the aforementioned reagents contain either conjugated π -systems or a means of direct complexation to the metal, whether inherently or following a chemical modification (like acid-

catalyzed tautomerization or decarboxylation). Some researchers have even managed to create Manganese-catalyzed minimal bromate oscillators without *any* organic components, though the concentration regimes in which they oscillate are extremely narrow.¹⁹

Oscillating reactions can typically continue until enough of the organic reducing agent has been “redox bleached”, or is no longer collectively intact enough to mediate its intermediate chemistry. When using an open-chain reagent like citric or malonic acid (MA), the redox-bleaching event is the complete oxidation of the organic acid to carbon dioxide and water, though this would take an extremely long time (or additional heat) to actually occur in practice. Since the oxidations rarely proceed to completion, Glyoxalic acid (GA) and/or oxalic acid (OA) tend to accumulate during this process, which likely also occurs when using phenolic reducing agents, though perhaps more slowly. Formic (FA) and carbonic acids (CA) may eventually become significant in longer reactions as well, though are not commonly discussed.

1.2.3 Halogen Oxides and Strong Acid

Given all of the research presented, it appears the only common components found in all chemical oscillators are strong acids and halogen oxides, the latter of which is not at all surprising due to the natural presence of a halide-halogen-oxide cycle in Earth’s atmosphere. In the cycle, radical halogen species are produced by photolysis which then have the capacity to mediate ozone decomposition and oxidation of metallic mercury, perhaps also playing roles in other atmospheric processes.^{20,21}

The recipe for the first oscillating reaction known to academia was published by William Bray in 1921. It contained KIO_3^- , H_2O_2 and H_2SO_4 , and is often called the “Iodine Clock” or Bray-Liebafsky reaction today.²² Other chemical oscillators discovered after the BZ reaction include

the Briggs-Raucher reaction, which is essentially a BZ reaction substituted with iodate and H_2O_2 instead of bromate,²³ and some more recently discovered novel oscillators based on chlorine dioxide-iodine¹² and chlorite-iodate²⁴ redox couples. Neither of the aforementioned oscillators require a catalytic metal, and the chlorite-iodate reaction reportedly oscillates measurably in the presence of a variety of both organic and inorganic reducing substrates; namely Ascorbic acid, MA(+KI), $\text{K}_4\text{Fe}(\text{CN})_6$, $\text{Na}_2\text{S}_2\text{O}_3$, Na_2SO_3 , $\text{NaHSO}_2\cdot\text{OCH}_2$, and $\text{As}(\text{OH})_3$.

The strong acid provides protons for organic tautomerizations and contributes additional ionic strength to the solution, allowing effective transfer of electrons among species without transmuting them. Given that the acid must be relatively inert, HCl is not a good choice (Cl^- is reactive). Almost all literature reports success with H_2SO_4 and occasionally HClO_4 , but H_3PO_4 and HNO_3 are viable alternatives.¹⁰

As the solution in a BZ reaction vessel approaches equilibrium, bromine is reduced from Br(V) (BrO_3^-) to Br(-I) (Br^-) and eventually regresses to elemental Br(0) (Br_2 , $\text{Br}\bullet$) when there are no more organics left to react with. If no bromide is added to the vessel initially, it must be allowed to accumulate during what is known as the induction period, which may take many minutes to over an hour, depending on the specific initial conditions. When it has an appreciable presence in solution, bromide facilitates reductive disproportionation reactions among bromine oxides, getting oxidized itself as a result. When the reductive wave is spent ($[\text{Br}^-]$ is low), an oxidizing environment dominates and the cycle continues until either the bromine oxides are used up or there are no longer enough oxidizable substrates to use them up. Brominated organics release HBr as they slowly decompose to CO_2 , CO, and H_2O . A steady supply of bromide feeds the autocatalytic bromine oxide stint of the cycle and protects the reducing agent from redox-bleaching, thus allowing the reaction to oscillate perpetually.

1.3 Ferrum and Ferroin

Iron is the most thermodynamically stable and abundant transition metal in the universe, existing predominantly as iron-56. It can be found on Earth as an integral component of the planet itself, and in much of the biochemical machinery of its inhabitants. The metal has been taken advantage of for the following reasons, among others: Iron is able to catalyze a wide variety of chemical reactions depending on its chemical environment, it is ferromagnetic, well-studied, abundant, and available at fairly low price from chemical suppliers. In addition to its many uses in synthetic chemistry, this particular metal was chosen by evolution billions of years ago (on Earth) to catalyze a huge array of biological functions ranging from the high-temperature Archean hydrogenase in deep-sea trenches, Mammalian oxygen-shuttling myoglobin that gives red meat its characteristic color (as well as its smell when irreversibly oxidized) and its ubiquitous incorporation in electron-shuttling metal-sulfur clusters, among multitudes of other uses. We narrow our focus in this study to one specific organic complex of iron, named ferroin when the iron center is in its second oxidation state and ferriin when in its third. The main reason that this particular compound is so useful is due to the brilliant color that it confers to aqueous solutions even at very low concentrations; aqueous ferroin solution is observed a deep red color and ferriin a cool blue. This oxidative color change has been exploited in attempts to quickly query concentrations of compounds such as antioxidants, neurotransmitters, pharmaceuticals and biological metabolites in the aqueous phase, among other things.^{25,26,27} It has also recently been promoted as a much-preferred alternative to blue dot solution (a mixture of potassium ferricyanide and phenolphthalein) in the assessment of passive film growth on stainless-steel rods used in nuclear power plants. The rods are coated with oxide films in order to protect them from chemical damage, but over time the films

degrade, leaving the rods vulnerable to corrosion and oxidation. While blue dot solution is fairly corrosive and toxic, ferroin solution is less toxic and non-corrosive, in addition to being a more useful indicator, with a color change from red to blue indicating a fickle film that should be renewed.²⁸ In non-aqueous liquids, ferriin and ferroin have been used successfully to query the reducing powers of edible oils,²⁹ redox-coupled to their cobalt (II and I) analogs for use in a rechargeable redox-flow battery that has the potential to be optimized for efficient, large-scale energy storage,³⁰ and attached to activated carbon frameworks that show great promise as pseudo-supercapacitors, outperforming many commonly used materials in experimental trials in terms of both energy density and cyclability.³¹ Another particularly novel recent use of ferroin (ferriin, in this case) is as a DNA hybridization sensor, when covalently attached to a strand of DNA. In this application, it is redox-coupled to ferrocene, which is covalently attached to another strand of differing sequence. A long, synthetic strand that contains sequences complimentary to both of the aforementioned strands, separated by five deoxythymidine phosphorothiolate residues, is covalently attached to a gold-sputtered quartz-crystal-microbalance by means of the extremely strong Au—S bond, which functions as the reference electrode. When both query strands hybridize to the synthetic strand, ferriin is near enough to ferrocene to oxidize it, which is then detected as an electromotive force.³² The procedure could use some optimization before it is practically usable, but it still represents a novel use of the compound. In addition to these uses, ferroin is widely applicable for other nonspecific uses as a general redox titrant.

2. Materials & Methods

All calculations herein were carried out by the Gaussian09 program, revision D.01,³³ and structures queried in Gaussview 5.0.9.³⁴ Schemes were drawn in ACD/ChemSketch (Freeware) 2015.^{Error! Bookmark not defined.} The most computationally intensive were sent via SSH client to Lewis3, the main computing hub of the University of Missouri Bioinformatics Consortium (UMBC), otherwise they were completed with a Dell Latitude E6440 laptop boasting an Intel® Core™ i7-4610M 3 GHz CPU. Geometrically optimized stationary structures were classified as either minima or first-order saddles (i.e. transition states) following harmonic frequency calculations, also required for calculating thermochemical parameters, which were not modified following extraction from the Gaussian output. When geometric isomer(s) of relevant molecules exist, data provided herein refer to the most Gibbs-stable isomer that was found at the given level of theory unless otherwise noted, with prominent exceptions to this in when discussing bromine oxides. All instances of bromine in calculations herein refer to ⁷⁹Br, the lighter and minutely more prevalent isotope (50.69% versus 49.31%) according to slightly outdated (1997) IUPAC data.³⁵ Important quantities reported in this study include the change in total electronic energy (ΔE_{tot} , henceforth referred to simply as ΔE), enthalpy (ΔH) and/or Gibbs free energy (ΔG) at room temperature for as many of the discussed chemical processes as possible. Considering the calculated enthalpy or free energy rather than total electronic energy does not make a significant difference in comparisons made for calibration purposes, however when more atoms are optimized and the geometry become more complex, entropy and thermal energy become much more significant driving forces in chemical equilibrium, thus we must consider free energy and enthalpy when approaching more complex chemical problems in detail. The exact thermodynamic sums employed by Gaussian are provided in **Equation Set 1**.³⁶

1. $U(T) = E_{trans} + E_{rot} + E_{vib} + E_{elec}$
2. $E_{elec} = 0$

3. $pV = (N)k_B T$
4. $H_u(T) = U(T) + k_B T$
5. $H = E_{tot} + H_u$

6. $S_u = S_{trans} + S_{rot} + S_{vib} + S_{elec}$

7. $G_u(T) = H_u + T S_u$
8. $G = E_{tot} + G_u$

Equation Set 1. Relevant thermodynamic equations in Gaussian:

Temperature, $T = 298.15$ Kelvin for all calculations herein.

Pressure, p , volume, V , number of particles, N . In molar quantities; $N = N_a \approx 6.022 \times 10^{23} \frac{\text{particles}}{\text{mole}}$.

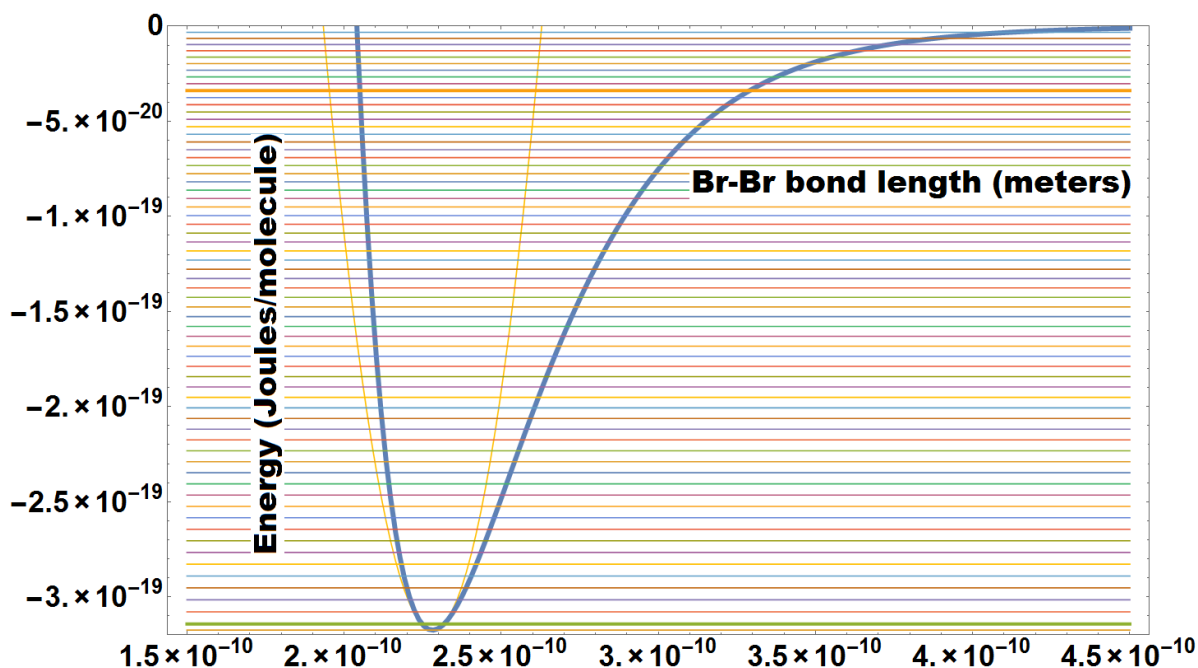
Boltzmann's constant, $k_B \approx 1.381 \times 10^{-23} \frac{\text{Joules}}{\text{Kelvin}}$.

Internal energy, $U(T)$, setting $E_{elec} = 0$ subject to the assumption that contributions from excited electronic states are negligible, which could actually be a source of error in this particular study. S_{elec} reduces to $\ln(2s + 1)$, where $s = \text{total spin}$. Both quantities are zero for closed-shell singlets.

Wave energy, E_{tot} , calculated in **Section 2.1**.

We notice, specifically from equations **4** and **7**, that the accuracy of the absolute free energy, G , and enthalpy, H , very much depend on the accuracy of the wave energy, E_{tot} , as well as the validity of approximations made while calculating components of internal energy, U , and entropy, S . Approximations include the ideal gas assumption, fixed electronic ground states, equally partitioned low-frequency harmonic modes, and the assumption that it is reasonable to use the bottom of harmonic potential wells as energy zeroes. In a more rigorous study, the ground vibrational state might be set to $n = 1$. Though currently unreasonable in terms of required computing power, true anharmonic vibrations would also give more accurate results because we know that the distance-dependent energy of a chemical bond is better described with a Morse potential well rather than a simplified harmonic potential well. In fixed ground-

state, low temperature models, this approximation is fine, however for molecules at high temperatures and/or subject to intense electromagnetic radiation, a harmonic potential well overestimates the energy of increasing nuclear separation. While these assumptions do introduce small errors into the thermodynamics at all levels of theory, a poor basis set or inadequate treatment of the electron density could individually cause errors magnitudes larger. Besides, the errors are only relevant in calculations when molecules are allowed to deviate from their equilibrium geometry, as can be seen in **Figure 1**, where the Morse potential and harmonic approximation for 64 theoretical vibrational levels of gaseous $^{79}\text{Br}-^{81}\text{Br}$ are compared directly using data obtained in reference 37. We find D_e , the total bond energy, at the very bottom of the well, however since all matter has intrinsic zero-point vibrational energy, the value that one actually measures for a given molecule in its vibrational ground state is described by D_0 , which is found directly above the line tangent to the bottom of the well and is smaller in magnitude. The allowed intranuclear distance at the D_0 level, r_0 , is actually defined as a range of distances around ten picometers wide. Near the center of that range lies the equilibrium bond length, r_e .



$$\alpha = \sqrt{\frac{k_e}{2 D_e}}$$

$$V_{Morse}(r) = D_e \left[(1 - e^{-\alpha(r-r_e)})^2 - 1 \right]$$

$$E_{vib}(n) = hc \left[\omega_e \left(n + \frac{1}{2} \right) - \omega_e \chi_e \left(n + \frac{1}{2} \right)^2 + \omega_e y_e \left(n + \frac{1}{2} \right)^3 \right]$$

$$D_n = D_e - E_{vib}(n)$$

Figure 1. Morse potential plot compared to the harmonic approximation. The Morse potential plots well depth, D_e , as a function of bond length, r , as a negative displacement from zero. Horizontal lines represent the anharmonic vibrational levels, corrected to the third order. The zero-point vibrational energy level, D_0 , and energies for 64 theoretical excited vibrational levels of gaseous elemental bromine ($^{79}\text{Br}-^{81}\text{Br}$) in its electronic ground state ($^1\Sigma_g^+$) are included on the plot. In this case, the parabolic equation only reasonably approximates bond energies displaced by less than 20 picometers from their equilibrium distance, r_e . The equilibrium bond length was obtained from reference 56 and D_e , the well depth, from Gaussian, found as $\Delta E_{tot}(\text{Br}_2 \rightarrow 2 \text{ Br})$. Geometry optimizations indicate that the bond length and well depth should not change significantly from $^{79}\text{Br}_2$ to $^{79}\text{Br}-^{81}\text{Br}$, however the vibrational frequency, ω_e , decreases by about 2.08 cm^{-1} and harmonic force constant, k_e , increases by 0.06 J/m^2 (neither of which changes are terribly significant). The force constant for the $^{79}\text{Br}-^{81}\text{Br}$ bond was extracted from Gaussian output at the U ω B97X-D/6-311G* level. Spectroscopic constants: ω_e , $\omega_e \chi_e$, and $\omega_e y_e$, were derived in reference 37 from spectroscopic data and provided from a more precise source. The coefficients used in this figure are weighted combinations, treating the cited values therein as more correct. Vibrational energies calculated using these parameters match Rydberg-Klein-Rees (RKR) second differences ($\Delta G_{v'}$) obtained spectroscopically in 37. Directly relevant equations are included below the plot. Lines representing the zero-point energy and 55th excited vibronic energy are bolded because reference 37 reports that a Br_2 molecule excited past the 55th vibronic level has reached its dissociation limit. We note that the Morse potential does not reflect this. Also note that the spacing between energy levels decreases slightly as the dissociation limit is approached. Gaussian predicts the well depth to be 45.70 kcal/mol, which is consistent with the value of D_0 (1.9707 eV) reported in reference 56. The graph was produced in Mathematica. Error! Bookmark not defined.

Using the ideal gas equation to calculate standard-state pressure-volume work, pV , is only truly valid in a closed, adiabatic system. Since BZ reactions are traditionally run in a petri dish or a beaker, free pressure and heat exchange with the surroundings are both allowed. This could potentially cause errors in absolute Enthalpy on the order of RT , or about 0.5925 kcal/mol at room temperature, which is well within the margin of computational error anyway. Fortunately, even if the error is significant, it should theoretically be about the same for every calculation in the same model system, thus ΔH and ΔG are still valid approximations. Additionally the “absolute” values of H and G that Gaussian calculates for a given geometric conformer of a given query molecule are assigned reference zeroes relative to infinitely separated component particles, thus can philosophically already be thought of as ΔH and ΔG , with the initial state being non-interacting component nuclei plus non-interacting free electrons, and the final state being the specific geometric conformer of the query molecule. Using this convention, ΔE , ΔH , and ΔG , as notated herein, become $\Delta(\Delta E)$, $\Delta(\Delta H)$, and $\Delta(\Delta G)$, respectively.

It is important to calibrate the system of interest before jumping to conclusions gathered from a few calculations, especially since theoretical single-molecule systems tend to not accurately model specific experimental conditions. Combinations of Density Functional Theory (DFT),^{38,39,40,41} Møller-Plesset Second Order Perturbation Theory (MP2)⁴² and Coupled-Cluster methods including single, double, triple and quadruple excitations (CCSD(T) and CCSD(TQ))^{43,44}, primarily with Pople double- ζ ,^{45,46} triple- ζ ,^{47,48} and Huzinaga-Dunning^{49,50} bases, were used to calibrate the system. Comparing calculated results to experimental values of relevant properties ensured selection of a standard theory that would reasonably model real experiments. The calibration is discussed in **Section 2.2**.

Molecules were reoptimized from gas-phase to aqueous-phase geometric minima subject to the Integral-Equation-Formalism Polarizable Continuum Model (IEF-PCM), specifically the Solvent Model Density (SMD) algorithm, in order to correct free reaction energies for solvation.⁵¹ Errors in the semi-empirical procedure are reportedly up to 4 kcal/mol for charged molecules and 1 kcal/mol for neutrals, which is not too bad. Like before, at least in this particular study, the additional potential term could benefit from including excited state contributions.

The Configuration Interaction (CI)⁵² method, including electronic contributions from single and triple excitations (CIS(T)), was used to query excitation energies of some bromine oxides. Results are not reported in the interest of space, time, and accuracy, but interesting observations are noted in the text. Note that geometry optimizations produce somewhat misleading results in these types of calculations due to the Born-Oppenheimer effect, so structures optimized at U ω B97X-D/6-311G* were used as the reference species (as is common, correct practice). Excited-state geometry optimizations can be used to predict irradiative decomposition products.

2.1 Theory

Details regarding the calibration procedure and knowledge resolved are given following a brief look at some of the computational methods, which underlie all of the quantum chemistry that was used to model the system of interest herein. Details of the Configuration Interaction (CI) method are not included in this section because it was not used extensively herein and the theory is fairly straightforward, even to novice computational chemists. Equations were mostly adapted from Introduction to Computational Chemistry by Frank Jensen.⁵³ In the equations sets below (which may also include definitions, expressions, and inequalities), bolded variables indicate a matrix, operator, or determinant.

$$\mathbf{Eq\ 1:} \quad \Psi = \frac{1}{\sqrt{N!}} |\psi_1(q_1), \psi_2(q_2), \dots, \psi_N(q_N)|$$

$$\mathbf{Eq\ 2:} \quad E_{\text{tot}} \Psi = \mathbf{H} \Psi$$

$$\mathbf{Eq\ 3:} \quad E_{\text{tot}} = \int \dots \int \Psi^* \mathbf{H} \Psi \, dq \equiv \langle \Psi | \mathbf{H} | \Psi \rangle$$

$$\mathbf{Def\ 1:} \quad \mathbf{H} \equiv \left(\frac{-\hbar^2}{2m} \nabla^2 + U(q) \right)$$

Equation Set 2. These mathematical statements underlie all *ab initio* molecular chemistry. Psi (Ψ) is the all-electron wavefunction, proportional to the determinant of the Hermitian matrix formed from all single-particle vectors (each vector also has a spin component). In practice, Ψ is optimized numerically by minimizing the energy, E , in the time-independent Schrödinger equation (**Eq 2**). This equation makes use of an operator called the Hamiltonian, which generally takes the form shown above in **Def 1**, but is modified when applied to DFT and some other higher-level methods. $U(q)$ is the potential energy function of all electron coordinates, which are often abbreviated with the letter q . **Eq 3** illustrates the shorthand bra-ket notation that is often used in place of integrals. Ψ^* is the complex conjugate of Ψ .

Eq 1: $\rho(\mathbf{q}) = \sum_{j=1}^N |\psi_j(\mathbf{q}_j)|^2$

Eq 2: $\int_{-\infty}^{\infty} \dots \int_{-\infty}^{\infty} \rho \, dq = \text{Number of electrons}$

Eq 3: $E_{DFT}[\rho] = T[\rho] + V_{n,e}[\rho] + V_{e,e}[\rho]$

Eq 4: $E_{DFT}[\rho] = T_s[\rho] + V_{n,e}[\rho] + C_{e,e}[\rho] + E_{xc}[\rho]$

Eq 5: $E_{xc}[\rho] = (T[\rho] - T_s[\rho]) + (V_{e,e}[\rho] - C_{e,e}[\rho])$

Eq 6:⁵⁴ $E_{DFT-D}[\rho] = E_{DFT}[\rho] + E_{dispersion}[\rho]$

Equation Set 3. A set of functionals that capture the idea of DFT. The variable $\rho(\mathbf{q})$ represents the electron density as a function of position and is defined simply as a sum of the probability densities of all electrons as per Hohenberg-Kohn theory. The additional terms in **Eqs 4** and **5**, notably the exchange-correlation energy (E_{xc}), arise to account for the portions of exact kinetic energy (T) and electron-electron interaction ($V_{e,e}$) that the partial kinetic energy, T_s , and Coulomb interaction, $C_{e,e}$, do not model. The dispersion correction term in **Eq 6** introduces damped, semi-empirical atom-atom dispersion interactions that improve calculated results. An improvement makes sense because there is no nuclear repulsion term in **Eq 3**.

Exp 1: $(\mathbf{H}_0 + \lambda \mathbf{H}')(\lambda^0 \Psi_0 + \lambda^1 \Psi_1 + \lambda^2 \Psi_2 + \dots + \lambda^n \Psi_n)$

Ineq 1: $0 \leq \lambda \leq 1$

Eq 1: $\lambda^n (\mathbf{H}_0 \Psi^n + \mathbf{H}' \Psi^{n-1}) = \lambda^n \sum_{i=0}^n W_i \Psi_{n-i}$

Eq 2: $W_i = \int \dots \int \Phi_0^* \mathbf{H}' \Psi_{i-1} \, dq$

Eq 3: $E_{PT} = \sum_{i=1}^{order} W_i$

Equation Set 4. One expression (Exp), one inequality (Ineq), and three equations (Eq) that summarize n^{th} order perturbation theory. **Eq 1** is derived by collecting λ^n terms from **Exp 1**, with W_i and Ψ_i representing the i^{th} -order energy and perturbed wavefunction, respectively. **Ineq 1** represents the “mixer dial” inequality, manifesting a theory of completely non-interacting electrons when $\lambda = 0$ and a complete treatment when $\lambda = 1$. Φ_0^* is the complex conjugate of the reference (i.e. unperturbed) Slater determinant, \mathbf{H}_0 is the reference Hamiltonian, and \mathbf{H}' is the perturbation operator. Note that W_1 is equivalent to the Hartree-Fock energy.

Eq 1: $E_{CC} = \int \dots \int \Phi^* \mathbf{H}(\mathbf{P}\mathbf{e}^T\Phi) d\phi dq$

Def 1: $\mathbf{P}\mathbf{e}^T \equiv 1 + \mathbf{T}_1 + \left(\mathbf{T}_2 + \frac{1}{2}\mathbf{T}_1^2\right) + \left(\mathbf{T}_3 + \mathbf{T}_2\mathbf{T}_1 + \frac{1}{6}\mathbf{T}_1^3\right) +$
 $\left(\mathbf{T}_4 + \mathbf{T}_3\mathbf{T}_1 + \frac{1}{2}\mathbf{T}_2^2 + \frac{1}{2}\mathbf{T}_2\mathbf{T}_1^2 + \frac{1}{24}\mathbf{T}_1^4\right) +$
 $\left(\mathbf{T}_5 + \mathbf{T}_4\mathbf{T}_1 + \frac{1}{2}\mathbf{T}_3\mathbf{T}_2 + \frac{1}{2}\mathbf{T}_3\mathbf{T}_1^2 + \frac{1}{6}\mathbf{T}_2^2\mathbf{T}_1 + \frac{1}{120}\mathbf{T}_1^5\right) +$
 $\left(\mathbf{T}_n + \dots + \frac{1}{n!}\mathbf{T}_1^n\right) + \dots$

Equation Set 5. Summary of Coupled Cluster theory to any excitation level. The permuted excitation operator described by **Def 1** is shown all the way to quintuple contributions here, but in practice does not really benefit beyond the triple excitation permutation for reasonably small systems. Note that the operator \mathbf{T}_n^m generates m n -electron excited determinants when applied to a wavefunction, meaning the total number of electrons excited per operator can be expressed as n times m . The general higher-order formula includes all permutations of excitation terms such that the number of electrons excited for each combination/product of operators adds up to the order of excitation (i.e. 3-electron excitations in triples, 2-electron excitations in doubles and only one in singles), weighted by $1/p!$ for increasing p from zero after each decrement of the first excitation term. The final term appears to be weighted by $1/n!$ regardless of its place in the logical sequence.

2.2 Calibrating the System

As any computational chemistry textbook will tell you, all mathematical methods and basis sets have their own unique strengths and weaknesses, and even some of the best computational chemists have some trouble predicting which theory would be best suited for a specific problem. Given this, it is always important to calibrate the system of interest against experimental results before meaningfully interpreting the outputs of the many required computations. In order to do this effectively and efficiently, three fairly well-known DFT methods and three reliable basis sets (plus variants therein) were chosen and compared both to high-level calculations (MP2(full) and CCSD(T)) with large basis sets and experimental data. The calibration data is provided and referenced in **Table 1**. Interestingly enough, at least for the system of interest, the ω B97X-D functional provided with a double- or triple-zeta basis set is found to outperform even the “state-of-the-art” coupled-cluster method (CCSD(T)) provided with a quadruple-zeta basis set when considering certain properties, which is also a testament to the method’s unique combination of *ab initio* terms and empirical corrections for disperse interactions. This method was selected because it has proven among the most reliable density functionals available; for the current author in unpublished work involving transition metals and organic molecules, its creators in work involving small halogenated hydrocarbons,⁵⁴ and at least one other group in work involving noble gases.⁵⁵ The creators note that ω B97X-D excels in describing non-bonding interactions, and this is verified. The current author notes anecdotally that the functional sometimes fails when attempting to describe larger systems with shallow potential energy wells, hence why data for the ferriox and Fe(ligand)₆ systems are perhaps not as fleshed-out as they could be herein. That being said, many of the convergence issues can be worked out with enough probing, though the process is tedious. Following calibration analyses,

the current author's choice to use ω B97X-D was verified as good, however a mixed-method, *i.e.* treating iron atoms with a different theory, would surely give even better results.

Structures queried with coupled-cluster methods were not optimized to geometric stationary minima, which is likely why the methods appear to fail in this case. As expected, adding diffuse functions to Pople series basis sets improve electron affinity calculations that include the bromide anion, but tend to diminish the empirical agreement of ionization energy calculations that include iron cations when the core electrons are not considered. In contrast, adding diffuse functions to the Dunning series basis sets appears to improve all calculations of energy. Some of the optimized geometries are improved upon the addition of diffuse functions to the basis, but others are negatively affected. The empirical Br—Br bond length reported was reproduced most accurately by ω B97X-D/aug-cc-pVQZ theory ($\Delta \sim -0.124$ pm), the empirical bond energy of elemental bromine by ω B97X-D/6-311G* theory ($\Delta \sim -1.06$ kJ/mol), and the electron affinity of bromine by MP2/aug-cc-pVDZ theory ($\Delta \sim 3.565$ kJ/mol). Empirical values for the electron affinity of atomic bromine and the Br—Br bond length were obtained to three-decimal precision while the third ionization energy of iron is the least precise, however the lack of precision in this case is okay because only a handful of the most computationally intensive theories predict the third ionization energy of iron within less than 25 kJ/mol of the empirical quantity. The level of theory that most accurately reproduces the third ionization energy of iron of all queried, by far, is MP2(full)/aug-cc-pVTZ ($\Delta \sim 4$ kJ/mol); an augmented quadruple- ζ basis passed to the same method is the second most accurate ($\Delta \sim -20$ kJ/mol), followed closely by the non-augmented double- ζ variant ($\Delta \sim -22$ kJ/mol).

In this dataset, considering all (valence and core) electrons always improves the third ionization energy of iron when treating the system with MP2, which performs better than both CCSD(T) and CCSD(TQ) given the same bases. One speculates based on this finding that double excitations are the dominant terms in accurate descriptions of valence activity around the iron nucleus. In contrast, when calculating properties of bromine, notably the Br—Br bond energy and optimized Br—Br bond length, including core electrons in the Huzinaga-Dunning (HD) calculations tends to *decrease* the empirical agreement. We rationalize the bromine trends fairly easily since, as far as we know, core electrons do not participate in covalent bonding. One notes that electrons in contracted core shells are subject to greater repulsive forces from both themselves and the valence electrons, causing them to move at higher velocities than those on the outside. Particles moving at velocities closer to the speed of light experience an effective length contraction that is not accounted for in the standard HD bases.

Addition of ‘tight functions’ to the bases might remedy relativistic errors, however that would require either a lot more optimization or choosing physically unsound numbers, neither of which the author cared to do.

The benefit that iron experiences from the inclusion of all electrons appears to be due to the fact that its true valence shell includes filled 3s and 3p subshells, in addition to the 4s and 3d orbitals, which appear to be neglected in Gaussian’s frozen-core approximation unless requested with the keyword ‘full’. This error could be fixed in the next release of the program, however it would likely come at the cost of additional computing time. Consistent with that logic, bromine does not benefit from an all-electron treatment because the 3d orbitals are filled, thus compacting the entire third fundamental energy level into the core. In this case, the frozen-core approximation holds, and treating only 4s and 4p subshells as the entire set of valence

electrons is valid; in fact, relativistic error met by inclusion of the $n \leq 3$ electrons apparently outweighs the potential benefit of treating the system more completely. **Table 1** and **Table 2**, the best theory for treating a system containing both iron and bromine, all things considered, was determined to be the combination ω B97X-D/6-311G**. Using this theory, the paired d_z^2 ground state of iron was determined to be ~ 0.52 kcal/mol less stable than the paired d_{xy} ground state – just shy of RT at room temperature. Both Hartree-Fock (HF) and Parameterized Model (PM) treatments were ineffective, but HF predicted a reasonable Br_2 bond length. It should also be noted that as more light, organic elements are included in the calculations, results obtained using UB3LYP/6-31G** theory better agree with results obtained using the chosen DFT, $U\omega$ B97X-D/6-311G**. As most any accomplished computational chemist will tell you, the increased efficiency and adequate accuracy is a huge draw to the hybrid methods. Then again, as in the case of iron, sometimes the extra computing time is necessary to get accurate results, as we learn in this calibration.

Theoretical Level	⁷⁹ Br— ⁷⁹ Br Length (pm)	⁷⁹ Br— ⁷⁹ Br Bond Energy (kJ/mol)	⁷⁹ Br· → ⁷⁹ Br ⁻ e ⁻ Affinity (kJ/mol)	Fe ²⁺ → Fe ³⁺ Ionization Energy (kJ/mol)
Empirical	228.105 ⁵⁶	-190.14 ⁵⁶	-324.537 ⁵⁷	2957 ⁵⁸
PM3	244.323	-203.18	-347.192	--
PM6	232.849	-203.20	-337.510	2678.15
HF/aug-cc-pVDZ	229.702	-50.74	-240.785	2767.97
ωB97X-D/6-31G* (5d)	229.817	-201.44	-282.596	2998.71
ωB97X-D/6-31G* (6d)	228.797	-221.23	-279.734	2997.30
ωB97X-D/6-31+G*(5d)	229.847	-197.10	-343.034	3023.29
ωB97X-D/6-31+G*(6d)	228.874	-218.45	-340.278	3022.02
ωB97X-D/6-311G*	229.655	-191.20	-318.727	2993.33
ωB97X-D/6-311+G*	229.551	-192.08	-339.498	3006.79
ωB97X-D/ADZP ⁵⁹	231.175	-191.44	-345.300	3002.15
ωB97X-D/cc-pVDZ	229.836	-191.87	-283.080	3011.72
ωB97XD/aug-cc-pVDZ	229.992	-191.78	-343.108	3013.37
ωB97XD/aug-cc-pVTZ	228.249	-206.51	-335.297	3004.90
ωB97XD/aug-cc-pVQZ	227.981	-208.40	-334.741	3008.83
B3LYP/6-31G* (5d)	233.600	-204.33	-276.102	3020.34
B3LYP/6-31+G* (5d)	233.453	-198.43	-347.198	3052.03
B3LYP/6-31+G* (6d)	232.359	-219.38	-345.272	3050.68
B3LYP/ADZP	234.509	-192.55	-349.577	3050.68
B3LYP/cc-pVDZ	233.499	-194.61	-277.105	3052.37
B3LYP/aug-cc-pVDZ	233.499	-209.15	-277.105	3051.92
PBEPBE/6-31G* (5d)	232.775	-240.46	-270.695	3025.81
PBEPBE/aug-cc-pVDZ	233.022	-229.32	-342.425	3060.89

Table 1. Calibration data for bromine and iron according to some semi-empirical, HF and DFT methods. Bolded quantities represent deviations in Br—Br bond length (r_0) less than 2 picometers, Br—Br bond energy less than 5 kilojoules per mole, atomic bromine electron affinity less than 6 kilojoules per mole, and atomic iron third ionization energy less than 40 kilojoules per mole in each column, respectively. All wavefunctions were unrestricted (U) and geometries optimized to stationary minima if applicable.

Theoretical Level	⁷⁹ Br— ⁷⁹ Br Length (pm)	⁷⁹ Br— ⁷⁹ Br Bond Energy (kJ/mol)	⁷⁹ Br· → ⁷⁹ Br ⁻ e ⁻ Affinity (kJ/mol)	Fe ²⁺ → Fe ³⁺ Ionization Energy (kJ/mol)
Empirical	228.105	-190.14	-324.537	2957
MP2/6-311G*	230.792	-171.52	-280.664	2865.00
MP2(full)/6-311G*	230.369	-175.73	-283.224	2920.93
MP2/6-311+G*	230.699	-173.50	-302.518	2877.44
MP2(full)/6-311+G*	230.279	-177.64	-305.116	2935.32
MP2/cc-pVDZ	231.482	-170.97	-250.382	2900.73
MP2(full)/cc-pVDZ	231.392	-173.01	-250.529	2935.84
MP2/aug-cc-pVDZ	232.381	-180.54	-328.103	2900.97
MP2(full)/aug-cc-pVDZ	232.386	-183.38	-328.187	2935.82
MP2/aug-cc-pVTZ	227.868	-223.44	-336.447	2907.53
MP2(full)/aug-cc-pVTZ	226.875	-237.66	-336.264	2960.98
MP2/aug-cc-pVQZ	226.073	-237.98	-345.734	2920.27
MP2(full)/aug-cc-pVQZ	225.590	-246.11	-345.380	2976.50
CCSD(T)/aug-cc-pVTZ	--	-191.61	-319.991	2903.10
CCSD(T,full)/aug-cc-pVTZ	--	-203.78	-319.414	2874.59
CCSD(T)/aug-cc-pVQZ	--	-202.78	-329.644	2913.92
CCSD(T,full)/aug-cc-pVQZ	--	-209.07	-319.414	2933.58

Table 2. Calibration data for iron and bromine at some levels of theory traditionally regarded as more accurate. Bolded values represent deviations in Br—Br bond length (r_0) less than 2 picometers, Br—Br bond energy less than 5 kilojoules per mole, atomic bromine electron affinity less than 6 kilojoules per mole, and atomic iron third ionization energy less than 40 kilojoules per mole in each column, respectively. Required geometry optimizations for CCSD calculations were carried out at the MP2/aug-cc-pVTZ level. All wavefunctions were unrestricted (U) and geometries optimized to stationary minima if applicable.

2.3 The Importance of Phase

Taking solvation into account, in general, highly favors charged species over neutral ones. For example, the dissociation of HBr by proton transfer to water is thermodynamically unfavorable in both the aqueous phase and the gas phase queried at U ω B97X-D/6-311G** (potentially exposing another source of error), however the magnitude is very different. As one expects, modeling the system in the aqueous phase greatly improves the probability of the proton abstraction, decreasing the reaction free energy change from 166.00 (gaseous) all the way to 12.51 (aqueous) kcal/mol; a difference of -153.49 kcal/mol. The magnitude of the change is almost equal to those of BrOH (-157.95), BrO₂H (-154.87) and BrO₃H (-152.54), all in kcal/mol, with BrOH dissociation benefiting the most from solvation. The good news is that not all of the gas-phase data collected in this study is useless, but the bad news is that a lot of it is, at least in the context of a BZ reaction. In order to provide aqueous corrections, all of the compounds were reoptimized using the SMD algorithm and some hydration energies were calculated, shown in **Table 3**. The only chemical species that appears to prefer the gas phase out of all examined is HBr, though Br, BrO, and BrOBr are stabilized by less than 2 kcal/mol in the aqueous phase, likely allowing for their dissolution into the gas phase and thereby driving a lot of atmospheric chemistry in the marine-boundary layer. The ionization energy of ferroin to ferriin also decreases by more than half when attempting to model it in the aqueous phase. Though the aqueous geometry never converged completely, the energy appears to converge to unit precision. In this case, the calculated (low-spin) ionization energy decreases from about 272 kcal/mol to 114 kcal/mol, both of which are at least a half magnitude greater than values calculated from empirical potentiometric data (24.4 kcal/mol in 1 M H₂SO₄, discussed later).⁶⁰

Chemical Species	$\Delta E(\text{Solv})$ (kcal/mol)	$\Delta H(\text{Solv})$ (kcal/mol)	$\Delta G(\text{Solv})$ (kcal/mol)
H ₂ O	-8.29	-8.45	-8.46
H ₃ O ⁺	-105.67	-105.50	-105.44
BrO	-1.75	-1.74	-1.74
BrO ⁻	-65.17	-65.14	-65.12
HBrO	-4.09	-4.16	-4.16
BrO ₂	-4.29	-4.30	-4.31
BrO ₂ ⁻	-66.08	-66.11	-66.15
HBrO ₂	-8.36	-8.33	-8.26
BrO ₃	-2.55	-2.58	-2.60
BrO ₃ ⁻	-62.62	-62.74	-62.79
HBrO ₃	-7.11	-7.23	-7.23
Br	-0.77	-0.77	-0.77
Br ⁻	-54.00	-54.00	-54.00
HBr	2.61	2.52	2.51
Br ₂ O	-1.64	-1.64	-1.64
MA	-12.95	-13.53	-13.69
MA enol	-8.86	-9.76	-10.03
MA ⁺	-70.55	-70.40	-70.17
MA ⁺ enol	-8.86	-9.76	-10.03
BMA	-10.36	-10.81	-10.49
BMA enol	-9.55	-10.33	-10.49
BMA ⁺	-62.85	-63.72	-64.05
BMA ⁺ enol	-62.09	-62.26	-62.35

Table 3. Electronic energy, enthalpy and Gibbs energy of solvation for selected compounds. Computed by subtracting the absolute gas-phase values from the reoptimized PCM/SMD values. Notice that enthalpy and Gibbs energy rarely deviate from the total electronic energy by more than 1 kcal/mol in these types of calculations and the gain when considering geometry (which includes terms for both internal energy and entropy when calculating enthalpy and Gibbs energy, respectively) is generally favorable, if only slightly. This is largely because we are dealing with small molecules. Recall, though, that an additional 1 kcal/mol is more than half (0.59) RT at room temperature.

3. Results

3.1 The Arrow of Time

Thermochemical data from this study suggest that when a Belousov-Zhabotinsky reaction is allowed to proceed indefinitely, all bromine eventually reaches its elemental or first oxidation state (0 or +1) and readily observable chemical oscillations cease. When bromate and bromous acid are depleted, two-electron oxidations slow and the chemistry is likely dominated by radical reactions, with relevant oxidized species liberating electrons from reduced catalysts and recombining with one another. When using ferroin as an indicator/catalyst, the resultant solution at or sufficiently near equilibrium appears blue, which means that iron is primarily in its +3 oxidation state and the electrons it started with were transferred. Similarly, cerium and manganese solutions appear clear, meaning that they, too, are stripped of readily oxidizable electrons. Specific manganese chemistry is not particularly well-described. In pure water, the (mostly) *ab initio* results of this study predict only one near-equilibrium process of all queried that is capable of reducing ferriin to ferroin in the aqueous phase: Reduction by bromide. Since the oscillating reaction does not visibly proceed without bromide, this is consistent with what is observed, however it is probably not safe to assume that bromide is the dominant reducing agent. In the gas phase, only the acid-consuming symproportionation of HBrO_2 and radical bromine to two BrOH (of all reactions queried) has the potential to *oxidize* ferroin to ferriin, according to the numbers generated, though in the aqueous phase this is no longer true. If we then substitute the appropriate empirical redox energy of ferroin (computed shortly), many plausible reactions liberate enough energy to oxidize it. The reductions of all radical organic species by ferroin are thermodynamically favorable in the aqueous phase by a significant margin (>70 kcal/mol), however the physical ability of ferroin to reduce them varies. Even if we consider

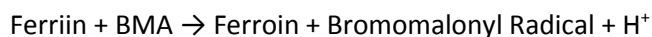
the computed organic reduction potentials as overestimated, they are still greater than both the electrode potential and the DFT potential of ferriin by enough to regard the general flow of electrons as: Ferriin \rightarrow Organic acids \rightarrow Bromine oxides (though not necessarily in chronological succession). Ferriin can also be oxidized by cerium(IV), which can go on to reduce the reactive intermediate BrO_2 to bromous acid if BrO_2 is present, according to the FKN model. This is one probability among other probable reaction paths, but important because the formation of bromous acid is a crucial step in the autocatalytic process due to the molecule's strong tendency to disproportionate when amassed (reactions 4, 5 and 5' in **Table 10**, discussed more later).

The reduction potential of (ferriin + $e^- \rightarrow$ ferriin) in this type of a chemical environment, determined by the voltage in 1.1 M H_2SO_4 , is 24.4(4) kcal/mol, calculated below:⁶⁰

$$24.4 \text{ kcal} = 1 \text{ mole } e^- \times F \times 1.06 \text{ Volts} ; F \sim 96,487 \frac{\text{Coulombs}}{\text{mole } e^-}$$

Using the same method as for ferriin, the reduction potential of $\text{Ce}^{4+} + e^- \rightarrow \text{Ce}^{3+}$ in 1 M H_2SO_4 comes out to 33.8(1) kcal/mol.⁶¹ Formation energy calculations using two DFT theories greatly overestimate this number; UB3LYP/6-31G** estimates the electronic formation energy difference between ferriin and ferriin to be 262.60 kcal/mol, while U ω B97X-D/6-311G** estimates a higher value: (+)272.09 kcal/mol. Neither computed quantity is near the empirical one. Using the SMD solvent model on the D-DFT method decreases the electronic energy difference to about (+)114.4 kcal/mol, though singlet ferriin does not completely converge at this level of theory. We note that in the calibration, all of the DFT methods overestimate the ionization energy of iron despite predicting accurate properties of bromine. Since the free energy correction term is relatively small, we can already see that its magnitude, even accounting for ± 6 kcal/mol (at the very most) between the queried point on the singlet ferriin PES and the true minimum, is not significant enough to approach 24.4 kcal/mol. While we might

first write this off as a failure of DFT, doing so before looking into the matter further would be shortsighted. Plugging the total electronic energy change (which is within 2 kcal/mol of the Gibbs energy change when calculated at UB3LYP/6-31G**, i.e. close enough to use as a rough estimation) into the redox reaction:



Then plugging the result of that, 22.81 kcal/mol, into the Eyring equation, found in **Equation Set 6** with appropriate substitutions, yields a value for the first-order rate constant of about $1.2 \times 10^{-4} \text{ s}^{-1}$, which is only around four times faster than empirically calculated rate constants in reference 62 ($3.1 \pm 0.2 \times 10^{-5} \text{ s}^{-1}$). Oddly enough, *their* experimental rate constants, calculated at 25 °C, are all about fifteen times faster than another group's rate constant that was experimentally determined at 40 °C, cited in their paper. Perhaps the lighting made a difference. Given the fact that the total electronic energy was used instead of the Gibbs energy herein, $1.2 \times 10^{-4} \text{ s}^{-1}$ is actually not such a bad result, especially considering how inaccurately UωB97X-D/6-311G** predicts the third ionization energy of iron. Given that the ionization energy is overestimated, it makes sense that the rate of reduction is overestimated as well. Important to note also is that the true rate constant is at least of the second-order, thus first-order approximations will always be subject to the concentrations of other species during the specific experiment(s) in which the data were obtained. Luckily for us, in the case of a BZ reaction, the initial condition regime that results in visible oscillations is fairly small. From these results, the author learned that reduction potentials are only directly useful in real electrochemical applications (not to be confused with the use of the term in the title of this thesis). We also note that the oxidation of BMA does not (usually) result in the formation of an enolic radical cation or BMA⁺; it results in the formation of the neutral bromomalonyl radical and generates a proton, determined by the agreement of the calculated reaction rate constant with empirical data.

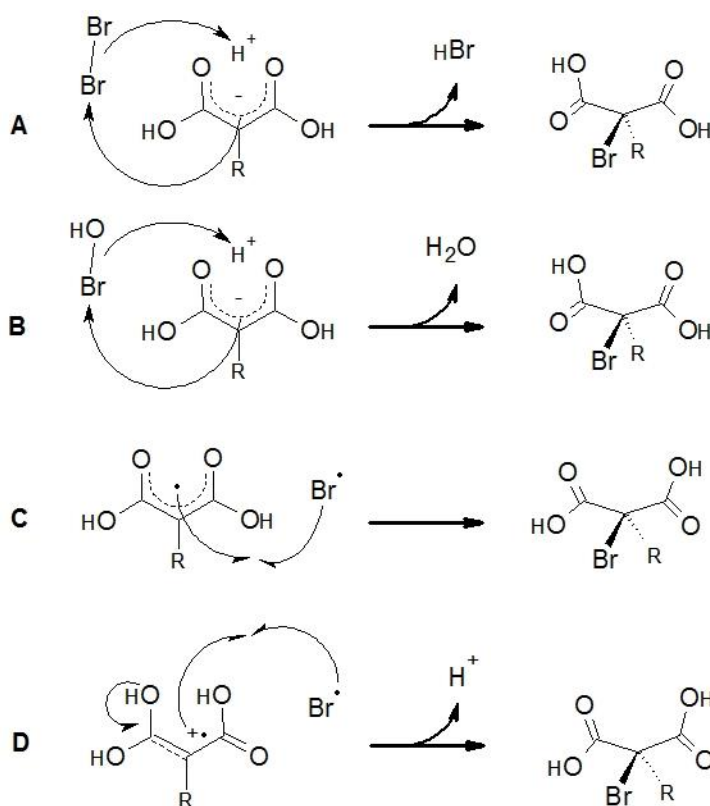
3.2 Proposed Mechanisms

3.2.1 The Induction Period and Rise of Oscillations

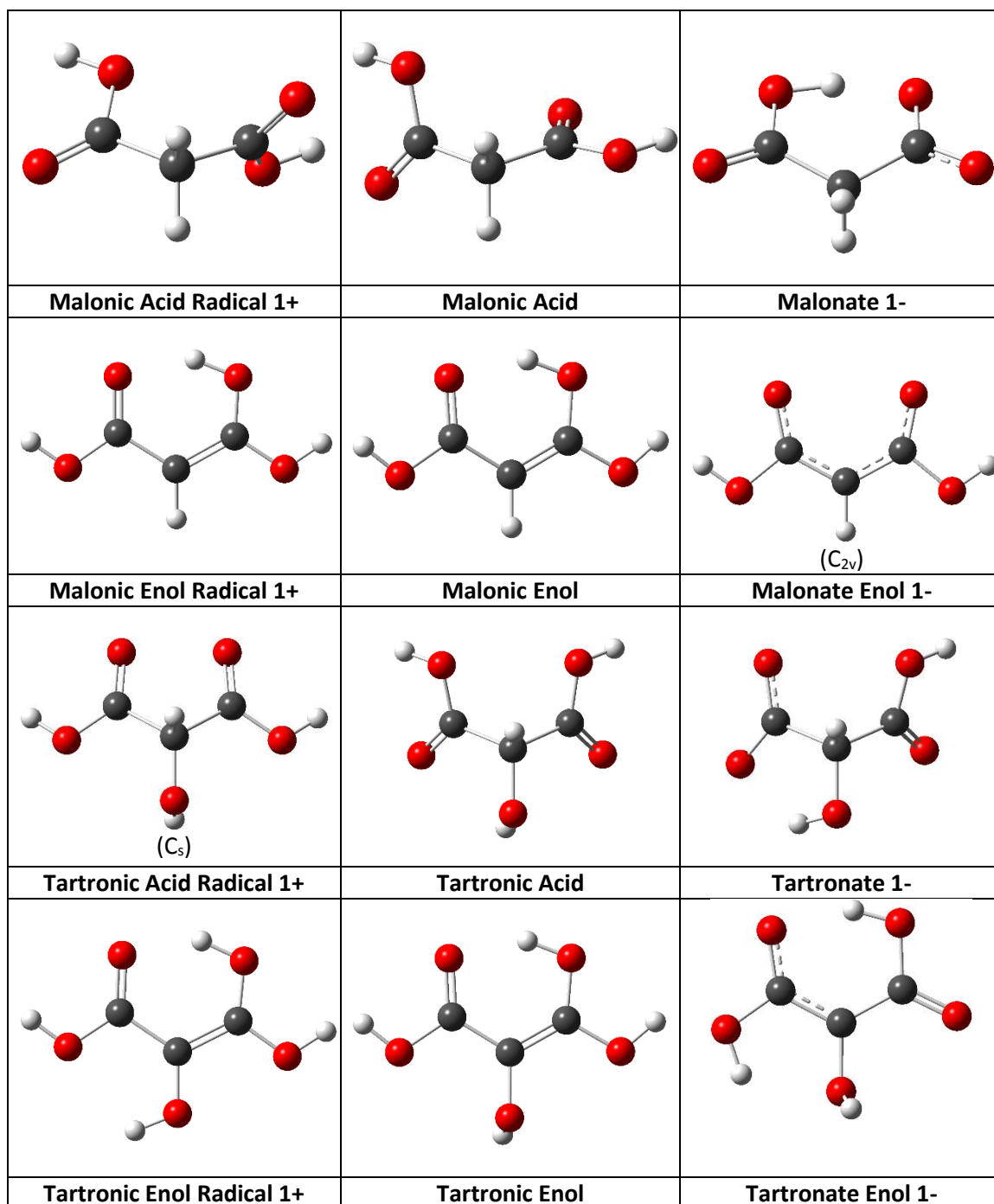
We begin with a possible sequence of reactions that lead to the formation of BMA during the induction period, starting from acidic bromate. Four different reactions are proposed in **Scheme 1**, the most likely of which to occur are probably reactions **A** and **B** during the induction period. Indeed, the MBM model of a cerium-catalyzed BZ reaction includes processes **A** and **B** as its sole generators of BMA, labeled reactions 30 and 31 therein. The rates that they give are quite fast: $2.0 \times 10^6 \text{ M}^{-1}\text{s}^{-1}$ for process **A** and $6.7 \times 10^5 \text{ M}^{-1}\text{s}^{-1}$ for process **B**. Following initiation of the reaction, when radical species run rampant, mechanisms **C** and **D** may certainly compete. Process **A**, since the rate is so high, acts as an effective bromine recycling reaction, reverting elemental bromine in the vessel to bromide so that it can feed back into the autocatalytic bromooxoacid cycle. If the bromooxoacids were not such strong oxidizing agents, all else the same, perhaps the reaction would be allowed to oscillate perpetually, however since more and more organic acids are irreversibly oxidized, the time between oscillatory periods continues to grow until the system is sufficiently close a point when all carbon has been converted to CO_2 or incorporated into inert radical recombination product(s) and/or all bromine has been converted to its elemental form. At this point, the reaction is complete. Most of the important intermediate chemical species, excluding the neutral radicals, are shown unbrominated in **Figure 2** and brominated in **Figure 3**.

The activation barrier for the formation of BMA via process **A** is calculated to be 56.41 kcal/mol in the gas phase. Realistically, though, 30 kcal/mol is around the highest barrier that can be appreciably surpassed under standard conditions. For reference, the air-combustion barrier of propane (C_3H_8) has been measured from 87.2 to 116 kcal/mol.⁶³ Oddly enough, the

rate presented in the MBM mechanism predicts the activation energy in the aqueous phase to be around 8.9 kcal/mol, which is reasonable based on other empirical observations, but not even close to the gas-phase calculation herein. As we note in reference to some of the other computational data, this is not especially uncommon. Unfortunately, the aqueous phase transition state calculation does not appear to converge, so for now we must just trust the authors of the MBM sequence.



Scheme 1. Four probable mechanisms for the formation of bromomalonic and dibromomalonic acids: **(A)** Malonic enol attacks elemental bromine, generates bromide and proton (-7.54 kcal/mol gas-phase, -5.11 kcal/mol aqueous), **(B)** Malonic enol reacts with BrOH (-31.40 kcal/mol gas-phase, -36.87 kcal/mol aqueous), **(C)** Malonyl radical combines with atomic bromine (-35.46 kcal/mol gas-phase, -35.71 kcal/mol aqueous), and **(D)** Malonic enol radical combines with atomic bromine and loses proton (+3.41 kcal/mol gas-phase, -42.12 kcal/mol aqueous). In the formation of BMA, R = H, and in the formation of DBMA, R = Br. Single-barbed arrows represent motion of one electron in **C** and **D** while thin double-barbed arrows represent motion of an electron pair in **A** and **B**.



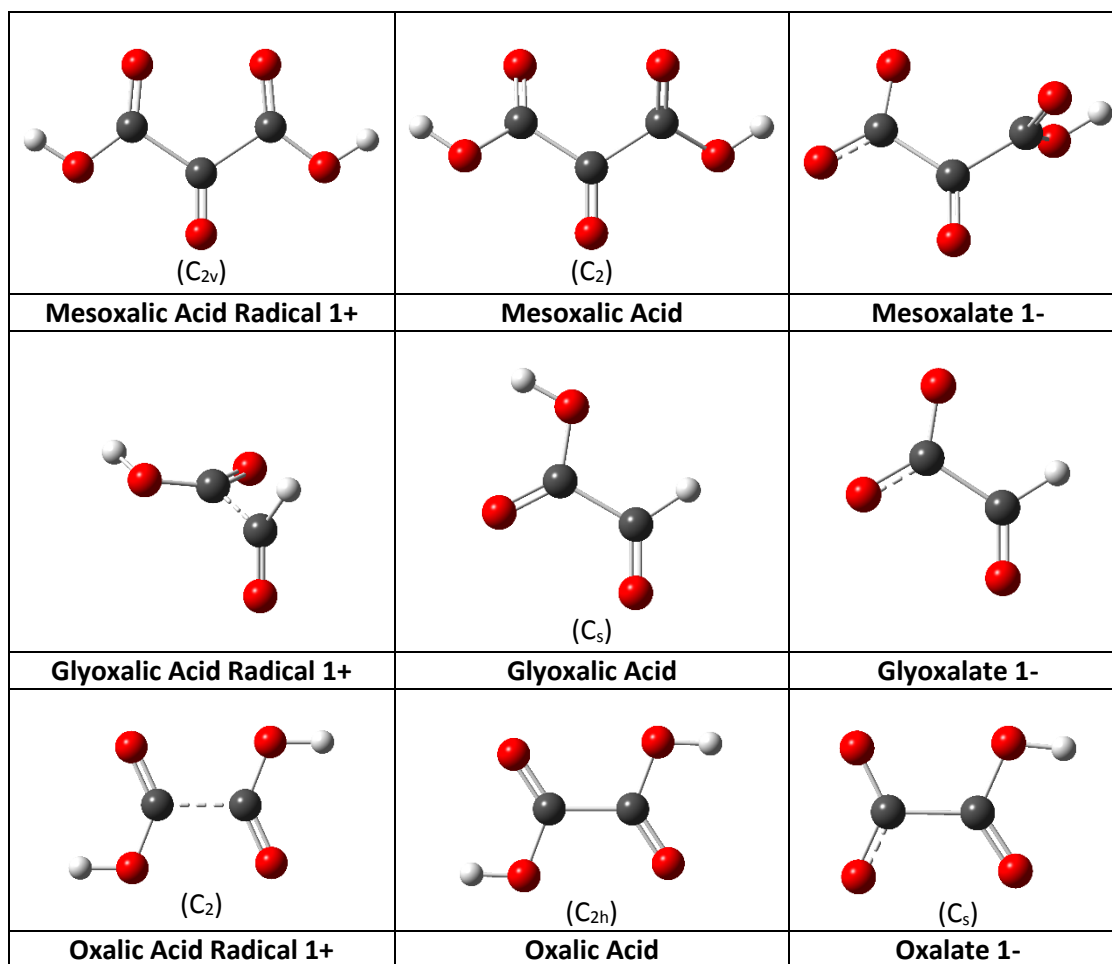
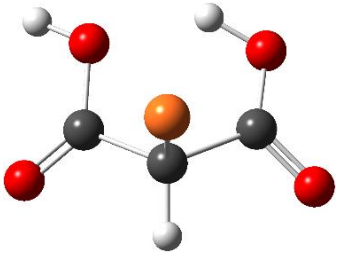
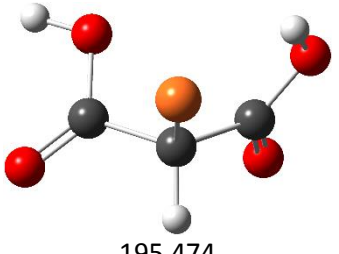
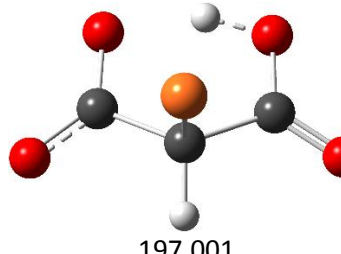
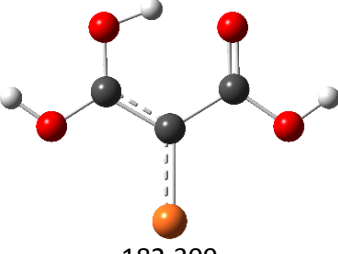
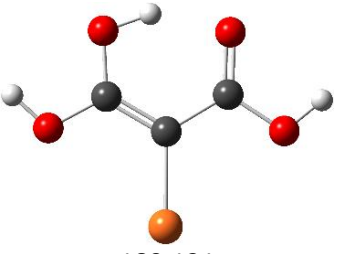
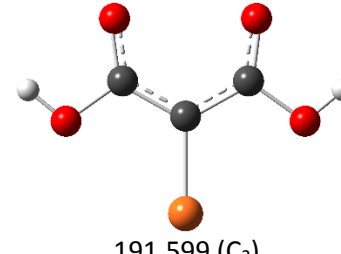
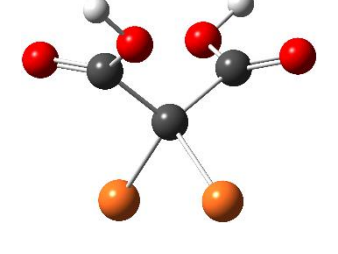
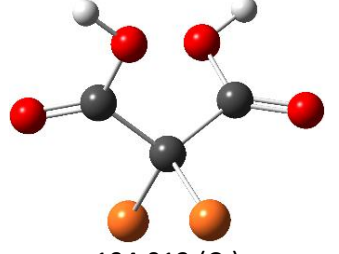
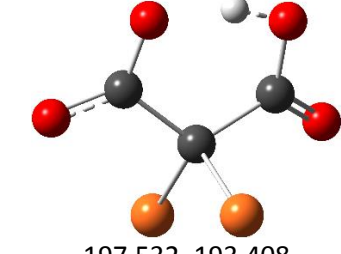
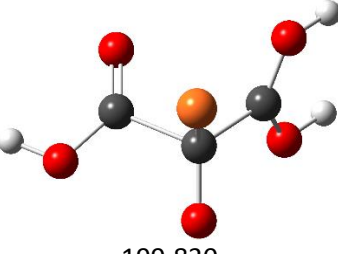
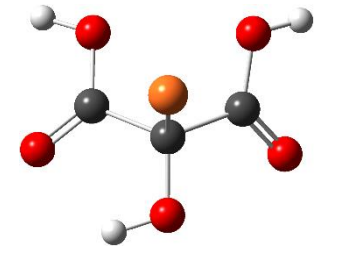
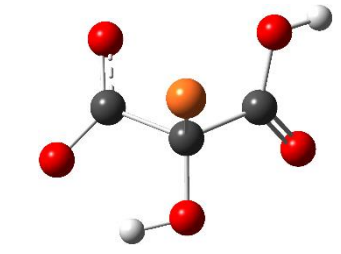


Figure 2. Aqueous-phase optimized structures at $U\omega B97X-D/6-311G^{**}$ of the major bromine-free organic acids present in a malonic acid-catalyzed BZ reaction, shown in their keto and enol forms if applicable. If multiple geometric isomers exist, the most thermodynamically stable structure determined in the aqueous-phase is pictured. One may follow a path corresponding to the oxidative degradation of malonic acid from the top to the bottom of the table. Only the singly deprotonated species are shown in addition to the fully-protonated neutral species and one-electron oxidized radical cations. If the molecule exhibits any symmetry, the point group is noted directly beneath the three-dimensional structure. Bond orders are inferred from lengths.

 191.883	 195.474	 197.001
Bromomalonic Acid Radical 1+	Bromomalonic Acid	Bromomalonate 1-
 182.309	 189.131	 191.599 (C ₂)
Bromomalonic Enol Radical 1+	Bromomalonic Enol	Bromomalonate Enol 1-
 192.678, 192.670	 194.013 (C ₂)	 197.532, 193.408
Dibromomalonic Acid Radical 1+	Dibromomalonic Acid	Dibromomalonate 1-
 199.830	 202.066	 202.742
Bromotartronic Acid Radical 1+	Bromotartronic Acid	Bromotartronate 1-

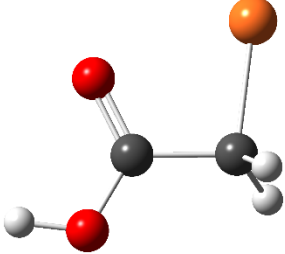
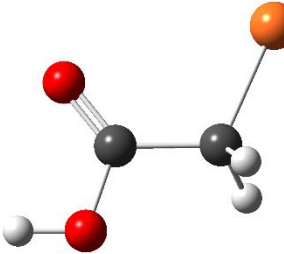
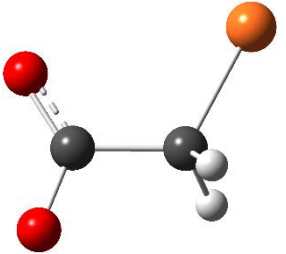
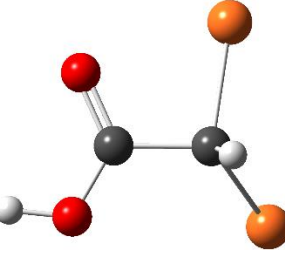
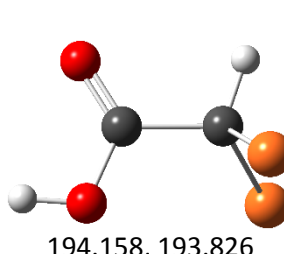
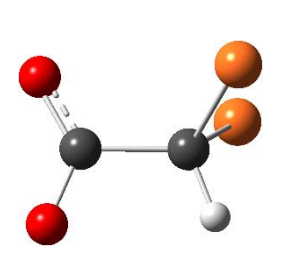
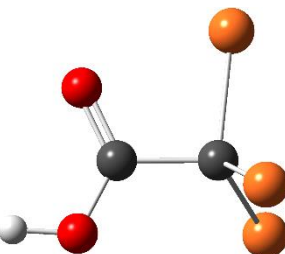
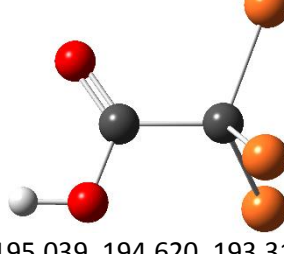
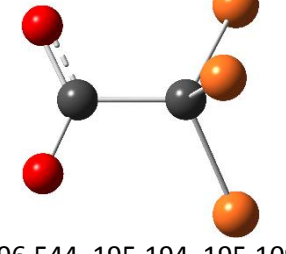
 <p>197.166</p>	 <p>193.321</p>	 <p>195.698</p>
Bromoacetic Acid Radical 1+	Bromoacetic Acid	Bromoacetate 1-
 <p>198.353, 189.839</p>	 <p>194.158, 193.826</p>	 <p>195.217, 195.033</p>
Dibromoacetic Acid Radical 1+	Dibromoacetic Acid	Dibromoacetate 1-
 <p>200.556, 190.692(x2) (C_s)</p>	 <p>195.039, 194.620, 193.317</p>	 <p>196.544, 195.194, 195.109</p>
Tribromoacetic Acid Radical 1+	Tribromoacetic Acid	Tribromoacetate 1-

Figure 3. Aqueous-phase optimized structures at U ω B97X-D/6-311G** of brominated malonic acid derivatives and some degradation products of a malonic acid-catalyzed BZ reaction. The C—Br bond length(s) in picometers are given below each optimized structure along with the point group if the molecule is symmetric. Bond orders are inferred from lengths. Every accessible minimum on each potential energy surface was not sampled explicitly, but the structures shown are the most stable of those that were sampled, which in most cases does include all feasible geometric conformers.

3.2.2 Propagation via One-Electron Oxidations

According to data gathered from this study, metal oscillations in ferriin-catalyzed BZ reactions could also be governed by acid-consuming one-electron oxidations of reduced organic acids by bromate/bromic acid, bromous acid and bromine monoxide, followed by the reduction of the resulting organic radicals by ferriin. After ferriin is oxidized to ferriin, it can be regenerated by bromide or another reduced organic acid, ultimately evolving elemental bromine and organic radical recombination products. Though MA is capable of being both oxidized and regenerated favorably, there are many more favorable redox pairs, assuming that the oxidation precedes the reduction, as follows: Tartronic acid – Tartronic enol radical cation > Bromomalonic acid – Bromomalonyl radical > Tartronic acid – Tartronyl radical > Dibromoacetic acid – Dibromoacetyl radical > Bromomalonic acid – Bromomalonic enol radical cation > Bromoacetic acid – Bromoacetyl radical > Malonic acid – Malonyl radical. Once oxidized, the favorability of reduction reverses. This elucidates a purpose for the induction period since the oxidation of MA is not only less thermodynamically favorable than oxidation of downstream organic acids, but also likely slower due to the physical mechanism. All but the most obscure non-metal redox reactions that could conceivably proceed in a BZ reaction vessel are included in **Table 5**, for gas- and aqueous-phases, respectively, which take the form of half-reaction matrices. From the table, we learn that bromous acid is the best oxidant, followed by bromine monoxide and finally bromate, although bromate requires two acidic equivalents in order for the reactions to proceed as written; the first protonation forms bromic acid and the second water. Notice that all of the oxidation events proceed more readily in the gas phase. Also notice that neither elemental nor radical bromine are included in the matrix because they are not strong enough oxidants to oxidize any of the organic acids queried, at least without accounting

for the chemical environment. As noted previously, the effects of acidity and chemical potential would definitely influence the activity of relevant chemical species.

Oxidizing Agent → Oxidation ½ Rxn ↓	HBrO ₃	BrO ₂	HBrO ₂	BrO	BrOH
Gas Phase					
MA + H ₂ O → MAyl + H ₃ O ⁺ + e ⁻	0.40	14.92	-15.35	-3.34	18.96
MA → MA ⁺ (enol) + e ⁻	-37.17	-22.65	-52.92	-40.91	-18.61
MA → MA ⁺ + e ⁻	-10.05	4.47	-25.80	-13.79	8.51
BMA + H ₂ O → BMAyl + H ₃ O ⁺ + e ⁻	-10.02	4.50	-25.77	-13.76	8.51
BMA → BMA ⁺ (enol) + e ⁻	-48.88	-34.36	-64.63	-52.62	-30.32
BMA → BMA ⁺ + e ⁻	-9.60	4.92	-25.34	-13.33	8.96
Br ₂ MA + H ₂ O → Br ₂ MAyl + H ₃ O ⁺ + e ⁻	12.94	27.47	-2.80	9.21	31.51
Br ₂ MA → Br ₂ MA ⁺ + e ⁻	-15.17	-0.65	-30.92	-18.91	3.39
TA + H ₂ O → TAYl + H ₃ O ⁺ + e ⁻	-6.83	7.70	-22.57	-10.56	11.74
TA → TA ⁺ (enol) + e ⁻	-54.93	-40.41	-70.68	-58.67	-36.37
TA → TA ⁺ + e ⁻	-15.30	-0.78	-31.05	-19.04	3.26
BTA → BTA ⁺ + e ⁻	-17.59	-3.07	-33.34	-21.33	0.97
MOA → MOA ⁺ + e ⁻	-20.32	-5.79	-36.06	-24.05	-1.75
GOA → GOA ⁺ + e ⁻	-12.31	2.21	-28.06	-16.05	6.25
OA → OA ⁺ + e ⁻	-6.82	7.70	-22.56	-10.55	11.75
FA + H ₂ O → Cbxyl + H ₃ O ⁺ + e ⁻	4.78	19.30	-10.97	1.04	23.34
FA → FA ⁺ + e ⁻	10.02	24.54	-5.72	6.29	28.58
H ₂ CO ₃ + H ₂ O → HCO ₃ + H ₃ O ⁺ + e ⁻	12.87	27.39	-2.87	9.14	31.44
H ₂ CO ₃ → H ₂ CO ₃ ⁺ + e ⁻	8.44	22.96	-7.30	4.71	27.00
BrAA + H ₂ O → BrAYl + H ₃ O ⁺ + e ⁻	-2.82	11.70	-18.57	-6.56	15.74
BrAA → BrAA ⁺ + e ⁻	-9.26	5.26	-25.00	-12.99	9.30
Br ₂ AA + H ₂ O → Br ₂ AYl + H ₃ O ⁺ + e ⁻	-6.29	8.23	-22.03	-10.02	12.27
Br ₂ AA → Br ₂ AA ⁺ + e ⁻	-11.00	3.52	-26.74	-14.73	7.57
Br ₃ AA → Br ₃ AA ⁺ + e ⁻	-13.37	1.15	-29.12	-17.11	5.19

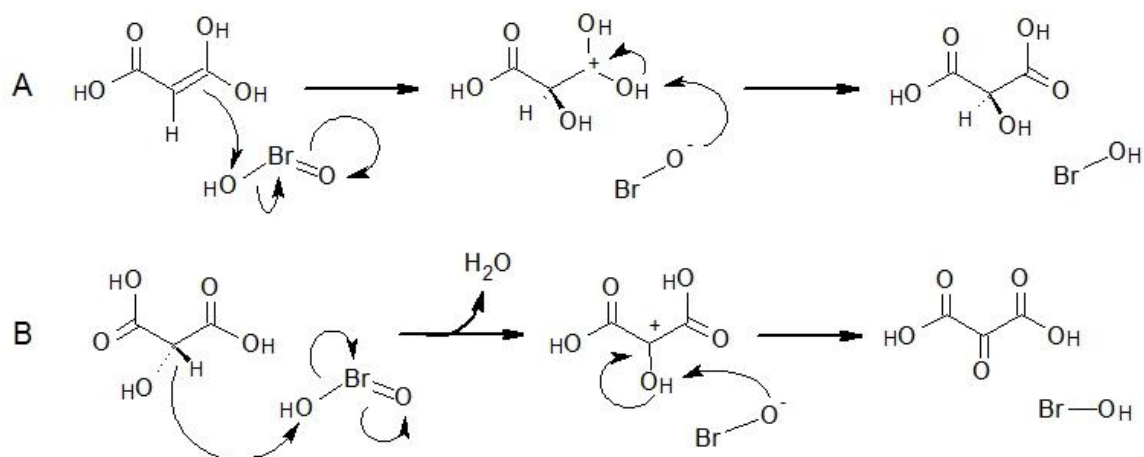
Table 4a. Gas-phase thermodynamic reaction matrix for all or most plausible acid-consuming one-electron oxidations by bromooxoacids. The Gibbs energy for each redox reaction is given, found by summing the Gibbs energies of the row half-reaction as shown and the column half-reaction, as follows: (1) HBrO₃ + H₃O⁺ + e⁻ → BrO₂ + 2 H₂O, (2) BrO₂ + H₃O⁺ + e⁻ → HBrO₂ + H₂O, (3) HBrO₂ + H₃O⁺ + e⁻ → BrO + 2 H₂O, (4) BrO + H₃O⁺ + e⁻ → BrOH + H₂O, and (5) BrOH + H₃O⁺ + e⁻ → Br⁻ + 2 H₂O. Bolded values indicate thermodynamically favorable single-electron transfers. Abbreviations are defined in the **List of Recurrent Abbreviations** on page v. Not all of these reactions may actually occur appreciably, however thermodynamics says that most of them can, especially those with bolded ΔG values. Tartronic and bromomalonic acids appear to be the most readily oxidized organic substrates in the gas phase, followed by malonic acid.

Oxidizing Agent → Oxidation ½ Rxn ↓	HBrO ₃	BrO ₂	HBrO ₂	BrO	BrOH
Aqueous Phase					
MA + H ₂ O → MAyl + H ₃ O ⁺ + e ⁻	-4.24	11.86	-16.38	-4.87	14.79
MA → MA ⁺ (enol) + e ⁻	-1.58	14.52	-13.72	-2.20	17.45
MA → MA ⁺ + e ⁻	24.92	41.02	12.77	24.29	43.95
BMA + H ₂ O → BMAyl + H ₃ O ⁺ + e ⁻	-15.70	0.41	-27.84	-16.32	3.34
BMA → BMA ⁺ (enol) + e ⁻	-9.29	6.82	-21.43	-9.91	9.74
BMA → BMA ⁺ + e ⁻	28.29	44.39	16.15	27.66	47.32
Br ₂ MA + H ₂ O → Br ₂ MAyl + H ₃ O ⁺ + e ⁻	11.75	27.85	-0.39	11.12	30.78
Br ₂ MA → Br ₂ MA ⁺ + e ⁻	34.35	50.45	22.20	33.72	53.38
TA + H ₂ O → TAyl + H ₃ O ⁺ + e ⁻	-11.74	4.36	-23.88	-12.36	7.29
TA → TA ⁺ (enol) + e ⁻	-16.02	0.08	-28.17	-16.65	3.01
TA → TA ⁺ + e ⁻	18.71	34.81	6.57	18.09	37.74
BTA → BTA ⁺ + e ⁻	18.84	34.95	6.70	18.22	37.88
MOA → MOA ⁺ + e ⁻	15.86	31.96	3.72	15.23	34.89
GOA → GOA ⁺ + e ⁻	13.62	29.72	1.48	12.99	32.65
OA → OA ⁺ + e ⁻	24.36	40.46	12.21	23.73	43.39
FA + H ₂ O → Cbxyl + H ₃ O ⁺ + e ⁻	2.12	18.23	-10.02	1.50	21.16
FA → FA ⁺ + e ⁻	26.05	42.15	13.90	25.42	45.08
H ₂ CO ₃ + H ₂ O → HCO ₃ + H ₃ O ⁺ + e ⁻	11.31	27.42	-0.83	10.69	30.35
H ₂ CO ₃ → H ₂ CO ₃ ⁺ + e ⁻	29.62	45.72	17.47	28.99	48.65
BrAA + H ₂ O → BrAyl + H ₃ O ⁺ + e ⁻	-6.00	10.10	-18.15	-6.63	13.03
BrAA → BrAA ⁺ + e ⁻	27.54	43.65	15.40	26.92	46.58
Br ₂ AA + H ₂ O → Br ₂ Ayl + H ₃ O ⁺ + e ⁻	-10.94	5.16	-23.09	-11.57	8.09
Br ₂ AA → Br ₂ AA ⁺ + e ⁻	30.67	46.77	18.52	30.04	49.70
Br ₃ AA → Br ₃ AA ⁺ + e ⁻	33.80	49.91	21.66	33.18	52.83

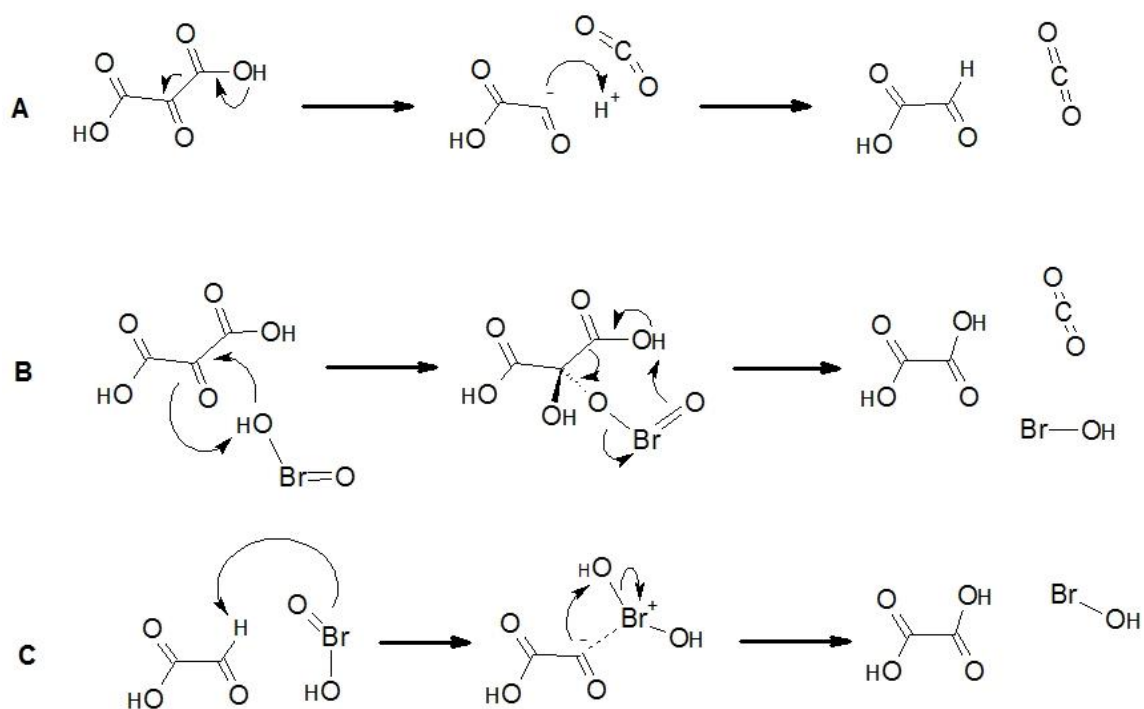
Table 5b. Simulated aqueous-phase thermodynamic reaction matrix for all or most plausible acid-consuming one-electron oxidations by bromooxoacids. The Gibbs energy for each redox reaction is given, found by summing the Gibbs energies of the row half-reaction as shown and the column half-reaction, as follows: (1) $\text{HBrO}_3 + \text{H}_3\text{O}^+ + \text{e}^- \rightarrow \text{BrO}_2 + 2 \text{H}_2\text{O}$, (2) $\text{BrO}_2 + \text{H}_3\text{O}^+ + \text{e}^- \rightarrow \text{HBrO}_2 + \text{H}_2\text{O}$, (3) $\text{HBrO}_2 + \text{H}_3\text{O}^+ + \text{e}^- \rightarrow \text{BrO} + 2 \text{H}_2\text{O}$, (4) $\text{BrO} + \text{H}_3\text{O}^+ + \text{e}^- \rightarrow \text{BrOH} + \text{H}_2\text{O}$, and (5) $\text{BrOH} + \text{H}_3\text{O}^+ + \text{e}^- \rightarrow \text{Br}^- + 2 \text{H}_2\text{O}$. Bolded values indicate thermodynamically favorable single-electron transfers. Abbreviations are defined in the **List of Recurrent Abbreviations** on page v. Not all of these reactions may occur appreciably, however thermodynamics says they are likely to occur if bolded. Tartronic and bromomalonic acids appear to be the most readily oxidized organic substrates in the aqueous phase, followed by dibromoacetic acid.

3.2.3 Termination via Two-Electron Oxidations

One-electron oxidations of the organic acids are reversible, especially when bromide has not yet been depleted, however as more time passes, the organic acids eventually become irreversibly oxidized. All three of the common bromooxoacids, including BrOH, can transfer an oxygen atom to MA, forming tartronic acid (TA) and the next reduced bromo compound in the sequence (oxidation states $+5 \rightarrow +3$, $+3 \rightarrow +1$, and $+1 \rightarrow -1$), shown in **Scheme 2A**. As noted previously, TA appears to be better at sustaining oscillations than MA, however once oxidized by two electrons rather than just one, TA is converted to mesoxalic acid (MOA) (**Scheme 2B**), which is no longer favorably oxidized by one electron in the aqueous phase. MOA can either be oxidized again to oxalic acid (**Scheme 3B**) or spontaneously decarboxylate to glyoxalic acid (**Scheme 3A**), both pathways liberating CO_2 as a secondary product. The oxidation by HBrO_2 is more than six times preferred in terms of thermodynamics, however since bromous acid may be scarce at any given moment, the spontaneous decarboxylation mechanism is also feasible. If the decarboxylation pathway is chosen, glyoxalic acid can then be oxidized one last time by a bromooxoacid (**Scheme 3C**), yielding the convergent final product of the two-electron oxidation sequence, oxalic acid. Thermodynamics of all two-electron oxidation reactions are shown in **Table 6**. Notice that bromous acid is by far the best oxygen donor despite being bonded to one less oxygen than bromic acid, with these reactions being about two-fold more favorable than the next most favorable reactions in MA and TA oxidations. No matter the initial oxidation state of bromine, it is reduced by two electrons following these types of oxidation event(s). The reaction illustrated in **Scheme 3B** is proposed as an oxygen-transfer reaction in the MBM scheme.



Scheme 2. (A) Oxidation of malonic acid enol to tartronic acid (-82.06 kcal/mol), and (B) Tartronic acid to mesoxalic acid (-72.49 kcal/mol). Bromous acid is the oxidizing agent shown, however thermodynamics indicate that any of the bromooxoacids may substitute. Note the apparent hydride transfer in **B** that results in the formation of water and hypobromate before the very fast deprotonation of the intermediate. SMD energies are reported.



Scheme 3. Two mechanisms for the degradation of mesoxalic acid into oxalic acid and CO₂. **A** shows the spontaneous decarboxylation of MOA (-19.68 kcal/mol) and feeds into **C**. **B** is about six times favored over **A** (-119.99 kcal/mol). The net Gibbs energy change, like the net chemical equation, is the same for both processes (**A**+**C**=**B**). SMD energies are reported.

Reaction	ΔE (kcal/mol)	ΔH (kcal/mol)	ΔG (kcal/mol)
Gas Phase			
MA(enol) + HBrO ₃ → TA + HBrO ₂	-41.26	-40.33	-40.25
MA(enol) + HBrO ₂ → TA + BrOH	-81.75	-80.44	-82.06
MA(enol) + BrOH → TA + HBr	-39.44	-40.39	-40.83
TA + HBrO ₃ → MOA + HBrO ₂ + H ₂ O	-27.35	-30.02	-38.49
TA + HBrO ₂ → MOA + BrOH + H ₂ O	-61.65	-64.05	-72.49
TA + BrOH → MOA + HBr + H ₂ O	-19.34	-24.00	-31.26
MOA + HBrO ₃ → OA + HBrO ₂ + CO ₂	-79.36	-78.88	-89.97
MOA + HBrO ₂ → OA + BrOH + CO ₂	-113.66	-112.92	-123.98
MOA + BrOH → OA + HBr + CO ₂	-71.35	-72.86	-82.74
MOA → GOA + CO ₂	-10.49	-11.79	-23.60
GOA + HBrO ₃ → OA + HBrO ₂	-68.87	-67.09	-66.37
GOA + HBrO ₂ → OA + BrOH	-103.17	-101.12	-100.37
GOA + BrOH → OA + HBr	-60.86	-61.07	-59.14
OA → FA + CO ₂	-12.27	-13.97	-23.94
FA + HBrO ₃ → CA + HBrO ₂	-63.65	-61.85	-61.01
FA + HBrO ₂ → CA + BrOH	-97.66	-95.89	-95.01
FA + BrOH → CA + HBr	-55.35	-55.83	-53.78
Aqueous Phase			
MA(enol) + HBrO ₃ → TA + HBrO ₂	-45.38	-44.31	-44.73
MA(enol) + HBrO ₂ → TA + BrOH	-93.32	-92.68	-95.11
MA(enol) + BrOH → TA + HBr	-48.58	-50.13	-51.31
TA + HBrO ₃ → MOA + HBrO ₂ + H ₂ O	-33.80	-35.78	-44.81
TA + HBrO ₂ → MOA + BrOH + H ₂ O	-62.59	-64.53	-73.68
TA + BrOH → MOA + HBr + H ₂ O	-17.85	-21.98	-29.88
MOA + HBrO ₃ → OA + HBrO ₂	-81.85	-81.91	-91.12
MOA + HBrO ₂ → OA + BrOH	-110.63	-110.66	-119.99
MOA + BrOH → OA + HBr	-65.89	-68.11	-76.19
MOA → GOA + CO ₂	-7.90	-9.48	-19.68
GOA + HBrO ₃ → OA + HBrO ₂	-73.95	-72.43	-71.44
GOA + HBrO ₂ → OA + BrOH	-102.73	-101.19	-100.31
GOA + BrOH → OA + HBr	-57.99	-58.63	-56.51
OA → FA + CO ₂	-7.33	-8.86	-19.33
FA + HBrO ₃ → CA + HBrO ₂	-68.54	-67.18	-66.25
FA + HBrO ₂ → CA + BrOH	-97.32	-95.94	-95.13
FA + BrOH → CA + HBr	-52.58	-53.38	-51.32

Table 6. Gas phase (above) and aqueous phase (below) energies of two-electron oxidation reactions by bromooxoacids. Appropriate substitutions of ionized bromate make the reactions more favorable, but if the pH is low enough it also exists as bromic acid. As one moves down the table, the organic acids become more oxidized. Abbreviations are defined in the text.

3.2.4 Products of a BZ Reaction

Traditionally, the products of a BZ reaction were thought to include: Bromide, CO₂, formic acid, reduced metal, and additional protons.⁵ We now know that the actual mixture is far more complex.^{6,7,65,68} In order to better their understanding, groups of researchers have taken it upon themselves to analyze the products of real-world BZ and BZ-like reactions using analytical chemistry. One reliable analytical method is high-performance liquid chromatography (HPLC), notably used by the groups that developed the MBM model (and also others) to characterize the products of BZ reactions in acidic media. Some interesting results of experiments detailed in reference 7, narrowing their studies only to reactions between cerium(IV), ferriin and either BMA or MA, suggest that significant amounts of BMA, when oxidized in an acidic solution of ferriin, condense to a brominated tricarboxylic acid. The reactions proceed very quickly, with aliquots taken after only ten seconds exhibiting peaks that don't significantly differ from reaction aliquots taken after 240 minutes. The dominant detected species after 240 minutes was always BMA, indicating the stability of the halogenated organic, but products like dibromoacetic acid (Br₂AA), bromide, and bromoethanetricarboxylic acid (BEE3CA, **Figure 4** below-left) were all detected in appreciable quantities. Their results are consistent with those obtained in this study, suggesting also that oxalic acid (OA) is the worst reducing agent since sensitive experiments did not detect CO₂ evolution from a mixture of OA and ferriin. Literature indicates that the acidic cerium(IV)-catalyzed oxidation of BMA also yields BEE3CA, but substituting MA instead reportedly yields bromine-free organic acids that are not obtained in the ferriin-catalyzed oxidation including radical recombination products ethanetricarboxylic acid (EA4CA) and malonyl malonate (MAMA).⁶⁸ An adapted mechanism for the formation of dibromoethanetricarboxylic acid (DBEA3CA, **Figure 4** above-left) is shown in **Scheme 4**.

According to the researchers in 68, the product spontaneously decomposes to BEE3CA by losing HBr, and this is verified by thermodynamics; free energy change in the gas phase is only -2.95 kcal/mol, but increases to -23.90 kcal/mol upon aqueous solvation. Given that the researchers calculated a 52% yield of BEE3CA, they also proposed DBEA3CA could debrominate to ethenetricarboxylic acid (EE3CA). Thermodynamics indicate that BEE3CA can spontaneously decarboxylate three times to bromoethene (**Figure 4** below-right), liberating (-)66.21 kcal/mol in the gas phase and (-)55.28 kcal/mol in aqueous solution, however this pathway is not likely to be traversed given only the energy supplied by room temperature fluctuations.

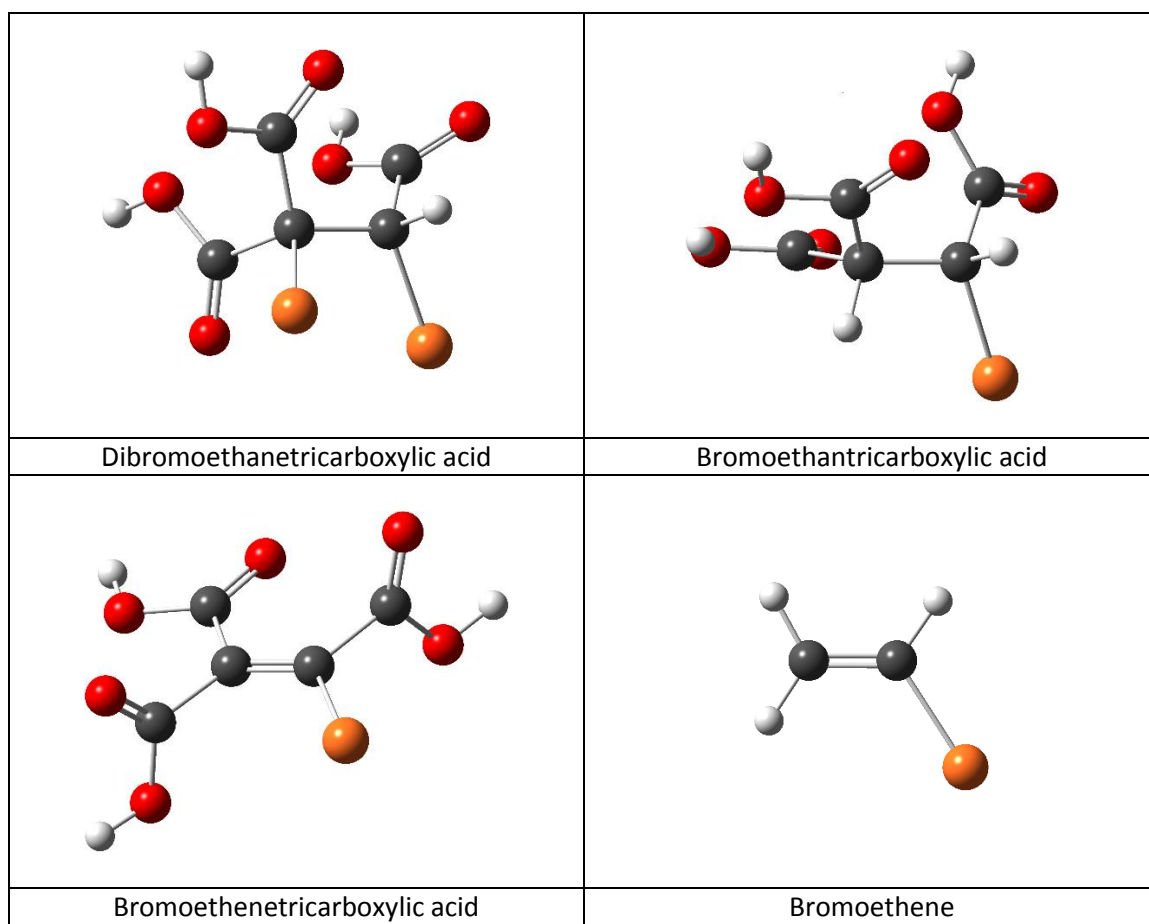
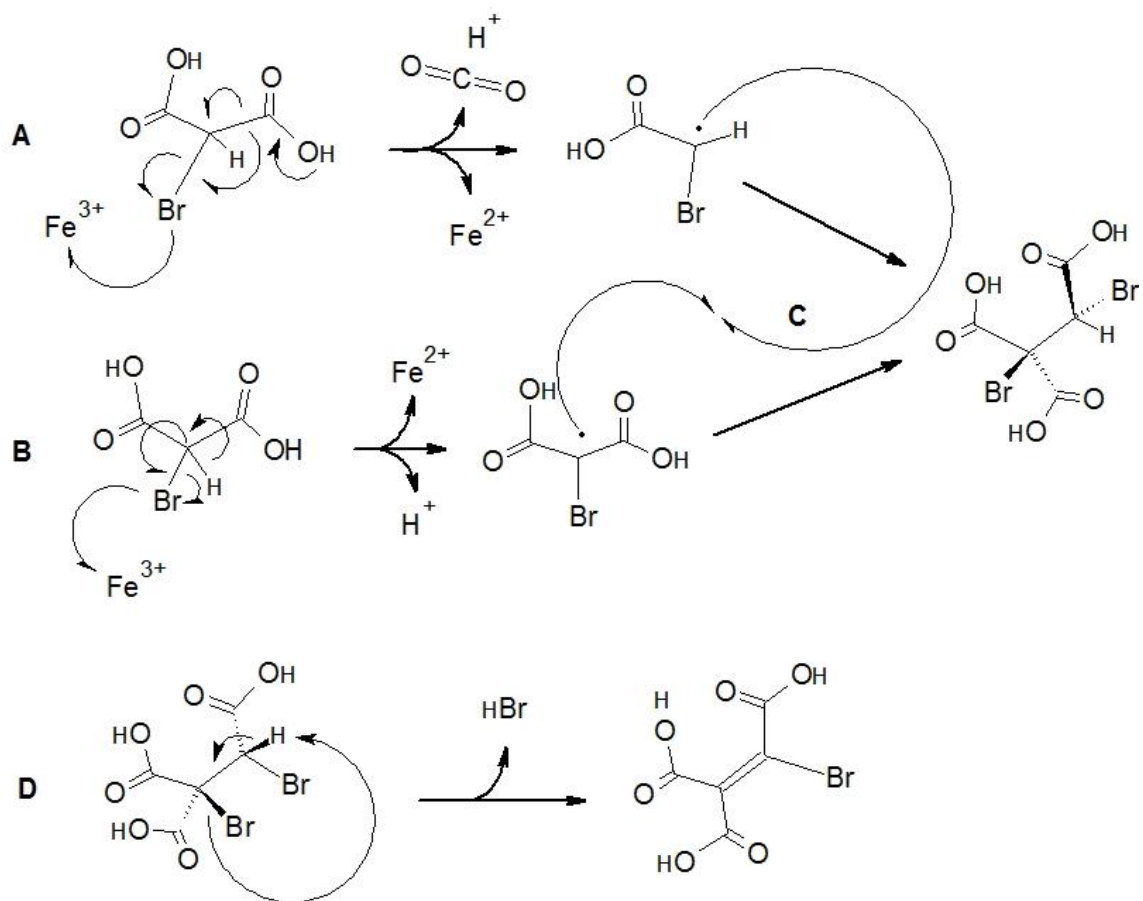


Figure 4. Radical recombination products and subsequent decompositions. Above-left is the recombination product of bromomalonyl and bromoacetyl radicals. Above-right is the recombination product of malonyl and bromoacetyl radicals. Below-left is a decomposition product of the species above it, dibromoethanetricarboxylic acid. Below-right is the hypothetical final decomposition product of all other species shown, bromoethene. Though bromoethene probably does not form appreciably in a BZ reaction, it would certainly form upon combustion of the precursors.



Scheme 4. Electron-pushing mechanisms for (A) Formation of dehydrobromoacetic acid radical (Gas: -43.68 kcal/mol, Aqueous: +19.42 kcal/mol), (B) Formation of bromomalonyl radical (Gas: -37.76 kcal/mol, Aqueous: +22.81 kcal/mol), (C) Radical termination by combination of products from A and B to form dibromoethanetricarboxylic acid (DBEATCA) (Gas: -42.62 kcal/mol, Aqueous: -19.90 kcal/mol), and (D) Decomposition of dibromoethanetricarboxylic acid to bromoethenetricarboxylic acid and HBr (Gas: -2.95 kcal/mol, Aqueous: +1.33 kcal/mol). Single-barbed arrows represent one electron while thin double-barbed arrows represent an electron pair. Ferro/iiin is denoted by Fe. Electronic SMD energies are reported for reactions involving ferriin (A and B) and Gibbs SMD energies are reported otherwise (C and D). Partially adapted from the reactions in reference 7. Since D is slightly exergonic, perhaps there is a better mechanism for its formation.

The researchers suggest that ferriin does not readily oxidize MA since they do not detect appreciable amounts of MA degradation products (i.e. CO₂ and other organic acids). Other experiments determine that the oxidation of MA by ferriin is slow, but detectable in the presence of oxygen.⁶⁴ The experimenters in reference 7 attributed their slight decrease in the

HPLC peak height assigned to MA following the four-hour observation period to a complex that forms between ferriin and MA. Results from this study both support and conflict their conclusions at different theoretical computational levels, however considering results from UωB97X-D/6-311G** theory to be more accurate, the formation of a $\text{Fe}(\text{o-phen})_2(\text{MA})^{3+}$ adduct with two oxygen atoms in direct contact to iron (favored over one oxygen and one bromine contact) would be unfavorable by slightly less than 50 kcal/mol in the gas phase. An optimized structure corresponding to this product is shown in **Figure 5**. Results computed with UB3LYP/6-31G** predict a significantly more favorable interaction (-169.07 kcal/mol), but the adduct was not examined in the aqueous phase because other evidence, notably the absence of o-phenanthroline in chromatograms, refutes its formation. Unlike the complex studied herein, some researchers suggest that the proposed adduct results from the oxidation of a phenanthroline ligand by the Fe(III) center, which reportedly occurs in basic solution.⁷ The authors rationalize that the cation-exchange resin used in their measurements only lets products that are not positively charged through to the detector, thus the slight decrease in MA peak height that they observed could be due to some other sort of unidentified, positively charged complex that somehow forms in the mixture. The only problem with that hypothesis is that the oxidation of phenanthroline may not appreciably occur in acidic solution – the researchers measured an 18% decrease in MA peak height in four hours, which almost seems like too much, but more probing would help decide what is actually happening. On the other hand, judging by the presence of MOA and OA in their chromatograms, one may speculate that O_2 from the surroundings enters the vessel and oxidizes MA or a downstream product by two electrons, which would be one possible method of forming a positively charged product. As will be discussed later, a one-electron oxidation of MA that is not followed by deprotonation could be stabilized by the tautomerization of the radical cation product to its enol form either before

or following the oxidation event. The neutral radical is more thermodynamically favored, but since the pH is very low, the formation of significant amounts of the enol radical cation are also feasible. Given that the product is a smaller cation than it is in complex, it could certainly be caught on an anionic column alone. If any of the larger adducts discussed did form, the color of the solution would probably change, at least slightly, and since a subtle color change has not been reported in any of the cited literature, it is assumed herein to not occur appreciably. Either way, in order to know for sure, we would need a way to accurately measure the remaining ferro/iin in solution following completion of the reaction. This could potentially be done spectrophotometrically (and likely has been, but maybe not in this particular context).

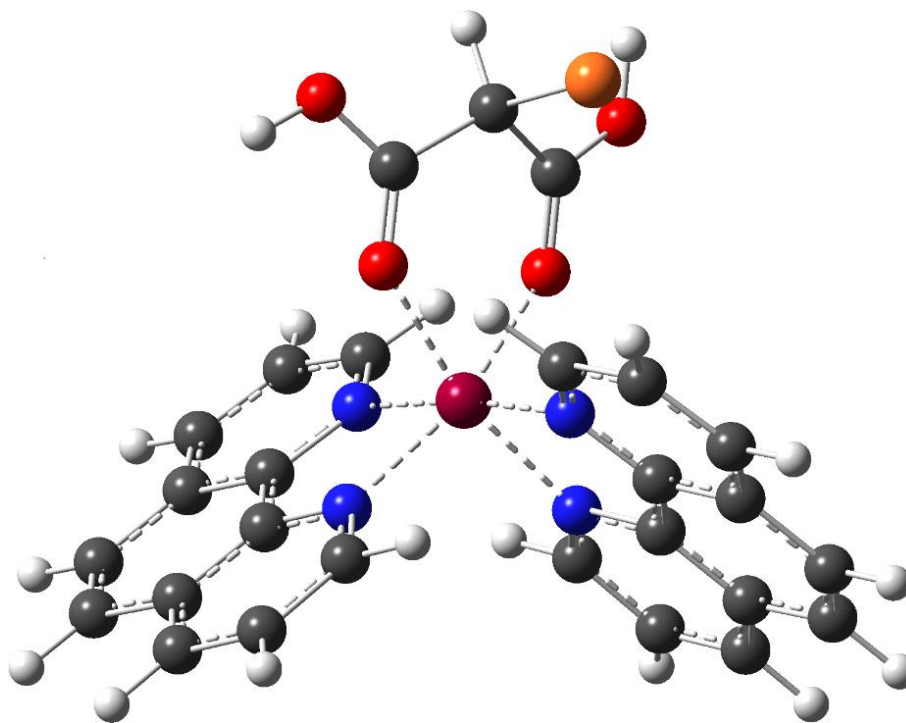


Figure 5. One hypothetical adduct that could form between ferriin and bromomalonic acid, geometrically optimized at $U\omega B97X-D/6-311G^{**}$. The structure shown above has a charge of +3 and spin $\frac{1}{2}$. The phenanthroline replacement event, starting from ferriin and BMA, was calculated at $U\omega B97X-D/6-311G^{**}$ to be unfavorable in the gas phase by 52.49 kcal/mol. On the contrary, it is favorable by -169.07 kcal/mol when queried at $UB3LYP/6-31G^{**}$. Starting from ferroin would probably make it more favorable at both levels.

3.2.5 Elusive Intermediate: Bromotartronic Acid

Though not assigned elution peaks in HPLC analyses of the cerium-catalyzed oxidation of malonic acid in literature,^{7,65} thermodynamics and rational mechanics both suggest the presence of another brominated organic intermediate called bromotartronic acid (BTA). This molecule can be formed spontaneously by a two-step attack at the central carbon of MOA by bromide and subsequent protonation of the resultant anion (-15.4 kcal/mol). Since MOA is a direct oxidation product of MA, the BTA concentration likely begins to rise during high-bromide periods, perhaps when oscillations have begun to slow. The MBM and GTF sequences both include BTA, formed from the hydrolysis of bromomalonyl bromite (BMAyl—OBrO), with oxygen bonded to the central carbon of the bromomalonyl moiety, then spontaneously decomposed to acidic bromide and MOA (+2.9 kcal/mol). The MBM paper neglects to include water in the hydrolysis reaction, however they correctly include the rate for the ‘reverse decomposition’ reaction (-0.3 kcal/mol). In agreement with thermodynamics herein, the rate of BTA formation is greater than the rate of its decomposition, which indicates that MOA is actually more likely to consume bromide and acid, thereby producing BTA, than BTA is to lose bromide. Partially oxidized radical recombination products are shown in the upper portion of **Figure 6**. Reference 65 mentions an elution peak near the characteristic TA peak in their discussion that is not heat-stable, which supports this reasoning if it corresponds to BTA since the molecule can also spontaneously decarboxylate to bromohydroxyacetic acid (BHAA), an as-of-yet unidentified decomposition product, upon heat treatment (-21.3 kcal/mol gas-phase, -20.8 kcal/mol aqueous), shown in the lower-right portion of **Figure 6**. However BTA actually decomposes (perhaps both paths are traversed), there is still rationale for the heat-sensitive elution peak. Interestingly, when BTA is oxidized, it appears to prefer either kicking out an atomic bromine

radical and transferring the charge to the central oxygen (**Figure 6**, below left), decarboxylating to bromoglyoxyl radical cation, or rearranging to a radical diol. The most former path leads to a favorable formation of MOA following deprotonation of the debromo- intermediate in the aqueous phase, the free energy change of which is about -27.9 kcal/mol. Conversely, in the gas phase, the free energy change is no longer favorable (+14.2 kcal/mol), indicating that the ‘reverse decomposition’ would be the path more likely traversed in this case.

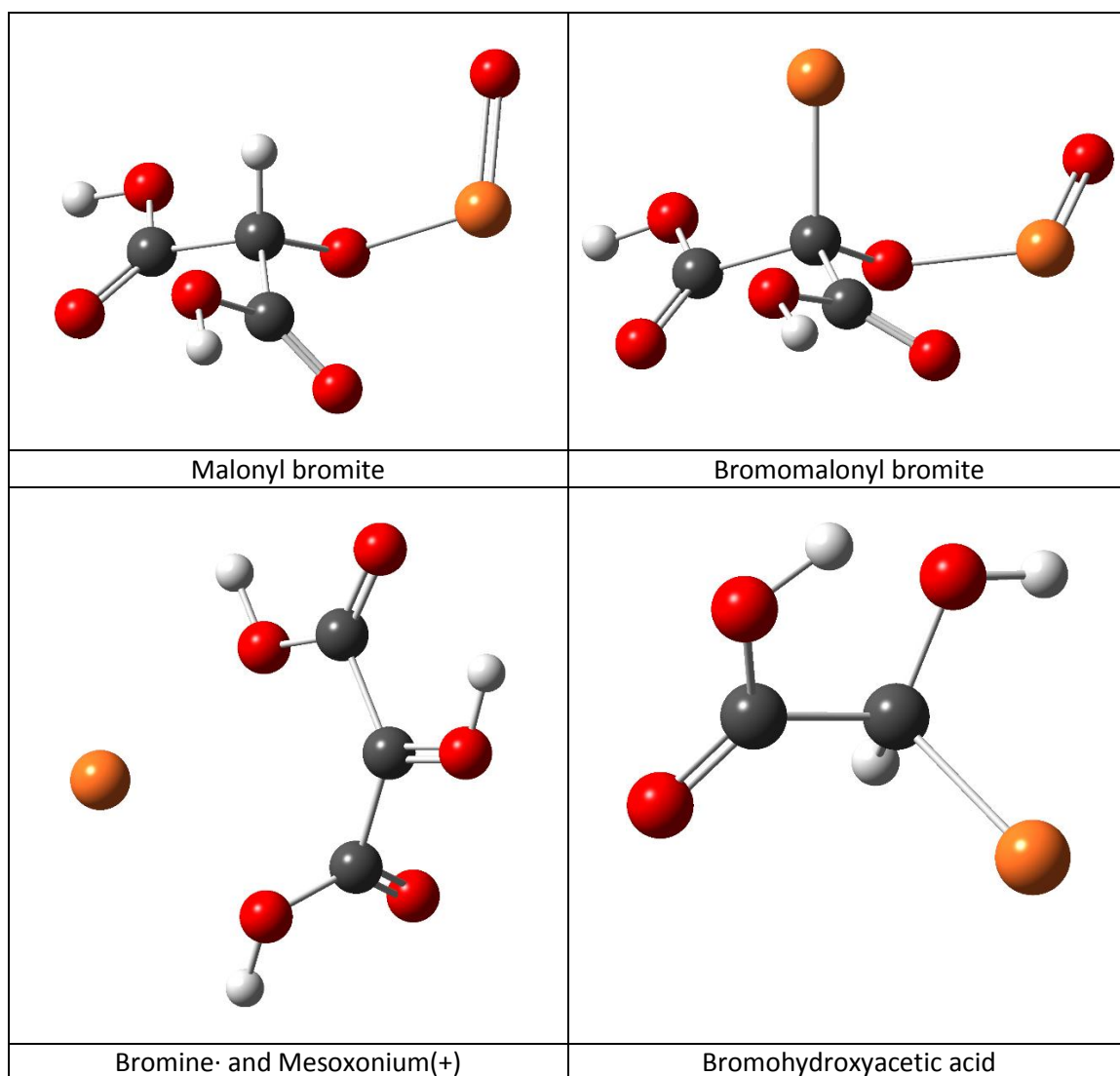


Figure 6. Additional theorized intermediates and byproducts of a BZ reaction. The upper two boxes show favorable radical recombinations of malonyl ($\Delta G_{soln} \approx -39.1$ kcal/mol) and bromomalonyl ($\Delta G_{soln} \approx -34.8$ kcal/mol) radicals with BrO_2 , which are proposed to hydrolyze into tartronic or bromotartronic acid, respectively, while generating HBrO_2 . One-electron oxidation of BTA facilitates its decomposition, an intermediate of which is shown in the lower-left.

3.3 Metal Catalysis

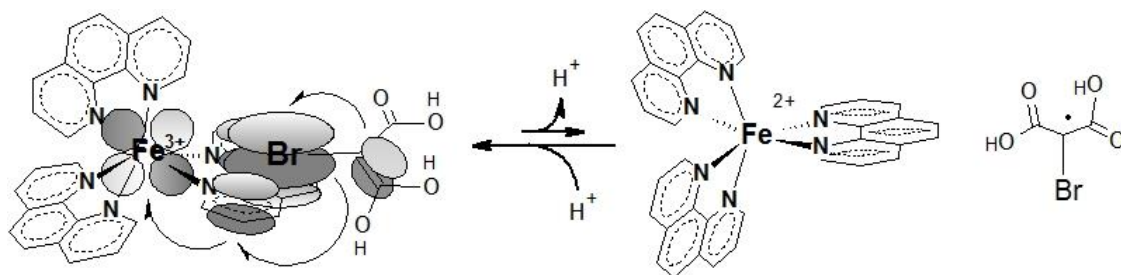
3.3.1 Evidence for and Against the Outer-Sphere Electron Transfer

In a ferriin-catalyzed BZ reaction, electron transfer to and from the metal catalyst primarily occurs via an outer-sphere mechanism, whereby two chemical species in close enough proximity exchange an electron(s) without forming a bond. If this were untrue and electron transfer were to instead proceed primarily by an inner-sphere mechanism, a metal-organic adduct with stability similar to the tris-phenanthroline complex would have to form, which is feasible in acidic solution, but unlikely. Given that time spent in the +2 oxidation state per cycle decreases as the reaction approaches equilibrium, the probability of a phenanthroline ligand dissociating and another complex forming also decreases over time since phenanthroline is much less likely to dissociate when the Coulomb attraction is strong, i.e. when iron has a formal charge of +3. Though the dissociation energy is significantly large, the aqueous-phase electronic energy difference between ferriin and $\text{Fe}[(\text{phen})_2(\text{H}_2\text{O})_2]^{2+}$ is only about 17 ± 2 kcal/mol, which means that there is definitely a very small amount of uncomplexed 1,10-phenanthroline present in ferriin solution at all times. Given this, a small fraction of iron centers could potentially be open to complexation by an organic acid, too. While this would otherwise suggest an inner-sphere electron transfer, a study examining the oxidation kinetics of several ketones by ferriin in a (loosely) similar chemical environment to that of a BZ reaction determined that the rate-limiting step in the oxidation of multiple ketones by ferriin is the tautomerization to an enol, suggesting that even if inner-sphere transfers do occur, they are less likely to occur than outer-sphere transfers.⁶⁶ Initial evidence pointing towards this conclusion were the raw oxidation rate kinetics, which appeared to be zero-order in ferriin and first-order in acid and ketone. Given that the concentrations of ferriin used were on the order of 10^{-4} - 10^{-5} molar, which is more than ten

million times the initial concentration of ferriin in a typical BZ reaction, the zero-order in ferriin could certainly be due to the *effective* zero-order saturation effect that occurs when the reaction rate is several magnitudes less than the concentration of the *effective* zero-order reactant. This approximation is often exploited in models, however it is not formally correct. Both sulfuric and perchloric acids were queried, in both lower and higher concentrations than typically found used a BZ reaction. Interestingly, the oxidation rate of the ketones *decreased* or stayed the same in response to the addition of more ferriin in almost (but not) every high ferriin, low acid trial. We can make at least four hypotheses given what we were told about the experiment, noting the high concentration of ferriin: 1) Uncomplexed phenanthroline facilitates protective π - π interactions with the enols and other complexed ligands, 2) Phenanthroline concentration on the order of 10^4 - 10^6 M (and about three times the initial concentration of ferriin) prevented the availability of free chelation spots at any given time, 3) Ferro/iin prefers to interact with itself in the experimental concentration regime, or 4) Low concentrations of acid significantly slowed tautomerization, causing ferriin to oxidize more ferriin and phenanthroline relative to ketone. If option 2 dominates, then the electron transfer actually does proceed by an inner-sphere mechanism. Though we cannot rule this out, ferriin holds onto its ligands very tightly (>20 kcal/mol in aqueous phase based on calculated 17(.58) kcal/mol for ferriin), thus it is unlikely to be the case. Though we may not be able to deduce with certainty which, if any, of the above reasons cause the oxidation rate to decrease in low acid with increasing ferriin, it does not really matter for our purposes. The paper reports that the oxidation rate is accurately modeled when the tautomerization rate constant is included in the overall rate equation, thus our faith in the authors' conclusions grows strong. In references 64 and 68, we are told that the oxidation of malonic acid by ferriin is slower than the oxidation of BMA. Given this and that data collected in **Table 7** (skipping ahead to the next section), we have all but proven that the

tautomerization is required for substantial turnover. One might suggest, however, that electronegative, sp^3 -hybridized atoms like oxygen and bromine can also chelate directly to open iron centers and proceed to do redox chemistry, which is probably accurate. In this case, the lone pair orbitals on bromine would allow BMA to bypass the thermodynamically unfavorable tautomerization step and react as soon as an open chelation site were available. While this is a sound theory, the problem is that most of the time, there is not an open chelation site available. That is okay, though, because the tautomerization of a ketone creates a π -system that can mix with any of the three large π -systems present in ferro/iin and initiate an instant through-space electron transfer when in close enough proximity. Therefore, once the enol tautomer of a carboxylic acid or ketone is present in solution, it can react with essentially any ferro/iin moiety that it happens to pass by. The data strongly suggests, based on the rate-limiting tautomerization step as opposed to a rate-limiting dissociation step, that the outer-sphere mechanism is primarily how electron transfer occurs between ferro/iin and an organic species in a BZ-like environment. In the absence of electromagnetic radiation, an outer-sphere electron transfer from BMA to ferriin (and vice versa) via π - π interaction is idealized in **Scheme 5**. The scheme models the electron transfer to or from bromine, which is conjugated to the π -system in either BMA enol or bromomalonyl radical (discussed in the next section). It does not explicitly model the transfer of electrons to or from an unbrominated organic acid, but this is fairly straightforward to imagine. Besides, the oxidation of MA by ferriin is reportedly insignificant, which is why the induction period is required before one can observe visible oscillations in ferroin-catalyzed reactions that do not initially contain BMA.^{64,68}

As is known to be the case with a cerium metal catalyst, ferriin can likely reduce bromine oxides as well as organic acids. This could be done more readily since the specific geometric alignment would not be as important. The GTF mechanism includes chemical equations for electron transfers between cerium and (H)BrO₂ with fairly large rates in both directions.⁶ The forward rate for the oxidation of cerium by BrO₂ is $6.2 \times 10^4 \text{ M}^{-2}\text{s}^{-1}$ and the forward rate for the reduction of cerium by HBrO₂ (i.e., the reverse process) is $7.0 \times 10^3 \text{ M}^{-1}\text{s}^{-1}$. Notice from the units of the rate constant that the oxidation of cerium is modeled by a second-order reaction, thus it is sensitive to the concentration of BrO₂. Also worth noting is that, since protons are gained and lost as necessary but do not factor into the rate constants as reported, the pH is assumed to be constant in these approximations (which is commonly considered to be an okay assumption). In the more recent MBM mechanism, these rate constants are slightly modified; $6.0 \times 10^4 \text{ M}^{-2}\text{s}^{-1}$ and $1.3 \times 10^4 \text{ M}^{-1}\text{s}^{-1}$ for the forward and reverse reactions, respectively.⁷ The rate constants provided are consistent with trends that we observe in this study, however the numbers are less consistent (which is okay because we were concerned with ferriin rather than cerium and we can only calculate first-order rate constants with the methods described herein anyway). Since the reduction potential of ferriin is less than the reduction potential of cerium(IV), we would expect the oxidation of ferriin to be faster than the oxidation of Ce(III) and the reduction of ferriin to be slower than the reduction of Ce(IV). The forward rate constant for the oxidation of cerium given in the MBM mechanism corresponds to an energy difference of about 11 kcal/mol when plugged into the Eyring equation, shown in **Equation Set 6**, however this is not necessarily the most accurate way to calculate it due to the higher-order nature of the reaction. Either way, it should give us a good rough estimation.



Scheme 5. Probable mechanism of outer-sphere electron transfer from bromomalonyl radical to ferriin, facilitated by the conjugated π -system (22.81 kcal/mol). The electron transfer is favorable in the reverse direction. Electron transfer from ferriin to dibromomalonic acid is even more favorable in theory (-75.86 kcal/mol). Transfer to ferriin has been shown to occur despite the large energy gap,⁶² but is likely more dependent on the unfavorable tautomerization of BMA to bromomalonic enol. Raw electronic SMD energies are reported.

Studies of a novel Minimal-Bromate Oscillator (MBO) containing bromate, ferriin and benzoquinone found that illumination increased oscillation frequencies up until a certain point, after which the light was destructive rather than constructive.¹² Several other studies note the destructive nature of illumination on chemical oscillations past a certain intensity as well.^{11, 67} One rather interesting finding reported by the authors of reference 12 is that the oxidation of bromide by ferriin is increased by illumination with 500(\pm 40) nm light. This includes the absorption peak of the ferriin/ferroin complex and, even more interestingly, the calculated first excitation wavelengths of two higher-order bromine oxides examined in this study, Br₂O₃ and Br₂O₄, which just happen to fall at the low and high ends of the reported wavelength continuum, respectively. Singlet and triplet excited states were calculated by the CIS(T) method, as noted before, but that is all we will hear of them for now. Due to the increased accessibility of excited π -states under visible irradiation, the researchers' findings are in support of outer-sphere electron transfer mechanisms governing the ferriin-catalyzed redox processes, notably including oxidations of bromomalonic acid (BMA) and dibromomalonic acid (DBMA) that are mediated by π -interactions. Though at first it may seem counter-intuitive, excitation of phenanthroline π -

electrons by visible light may open up short-lived 'holes' in the lower valence band of the ferriin complex, allowing for a more favorable electron transfer from the reducing species provided it is in close enough proximity to the ligand. The holes could also be filled by electrons from bromide, a decent reducing agent which, contrary to the organic species, does not require any special geometric alignment to quickly transfer an electron to the complex.

On the other hand, too much irradiation could cause the phenanthroline ligand to be oxidized by elemental oxygen, the presence of which has been acknowledged for decades, but has only more recently (circa 2000) been explicitly proposed to evolve from the vessel, itself, in the MBM mechanism. Oxidation of phenanthroline by elemental O_2 could proceed via excitation of oxygen from triplet to singlet and subsequent attack, or excitation of o-phenanthroline followed by a radical recombination with triplet- O_2 .

3.3.2 Tautomerizations

We speculate based on what we have learned thus far that if the one-electron transfer from MA to ferriin can proceed, the physical mechanism requires an unfavorable tautomerization of MA to its enol form immediately followed by the alignment of its very small conjugated π -system one of a phenanthroline on ferriin. This can occur more readily in strongly acidic solution due to the abundance of protons. Regardless of the specific mechanism, thermodynamics reveal that relevant oxidized organic acids that can tautomerize to an enol, namely MA^+ , BMA^+ and TA^+ , all prefer to do so, allowing the radical electron to resonate primarily among two carbon atoms at any given instant, and bromine, if present. At this point, malonic and bromomalonic cations tend to deprotonate to their neutral radical forms, which allows the radical electron to localize to an unhybridized $2p$ orbital on the central carbon, thus

regressing to the electronic state of graphite. This suggests that it can accept and eject electrons best when ligated through oxygen, as this would put a metal ligand in the conduction plane.

Table 7 lists the tautomerization energies of MA-derivatives mentioned above in both their oxidized and reduced states, then shows the stability gain following deprotonation. **Figure 7** shows spin-density isosurfaces of both MA⁺ and BMA⁺ radical enols as well as neutral malonyl and bromomalonyl radicals. Interestingly, we notice that BMA exhibits the most favorable tautomerization in the aqueous phase, which is consistent with all of the data presented thus far that suggest the necessity of the induction period before a ferriin-catalyzed BZ reaction begins to oscillate. This is not an issue in cerium-catalyzed variants of the reaction because the organic acid can ligate cerium directly, thus the single-electron reduction does not require the same shuttling through or rearrangement of a large π -system that must occur when ferriin is reduced.

Tautomerization	ΔE (kcal/mol)	ΔH (kcal/mol)	ΔG (kcal/mol)
Gas Phase			
Malonic Acid	6.19	6.08	7.81
Bromomalonic Acid	2.71	2.69	4.49
Tartronic Acid	11.37	11.15	13.10
Malonic Acid ⁺ Radical Cation	-29.00	-28.45	-27.12
Bromomalonic Acid ⁺ Radical Cation	-41.09	-40.30	-39.29
Tartronic Acid ⁺ Radical Cation	-40.97	-40.27	-39.63
Aqueous Phase			
Malonic Acid	19.15	19.62	21.51
Bromomalonic Acid	3.52	3.16	4.49
Tartronic Acid	13.36	12.84	15.43
Malonic Acid ⁺ Radical Cation	-28.04	-27.50	-26.50
Bromomalonic Acid ⁺ Radical Cation	-40.33	-38.83	-37.58
Tartronic Acid ⁺ Radical Cation	-36.25	-35.51	-34.73
Aqueous Phase			
Deprotonation by H₂O			
MA ⁺ enol \rightarrow Malonyl Radical	-1.46	-0.82	-2.67
BMA ⁺ enol \rightarrow Bromomalonyl Radical	-6.09	-5.27	-6.41
TA ⁺ enol \rightarrow Tartronyl Radical	4.42	4.94	4.28

Table 7. Ketone to enol tautomerization and deprotonation energies of all organic acids present in a standard BZ reaction that can tautomerize in the gas phase (above) and aqueous phase (below). Deprotonation energies include the appropriate ΔE for $H_2O \rightarrow H_3O^+$.

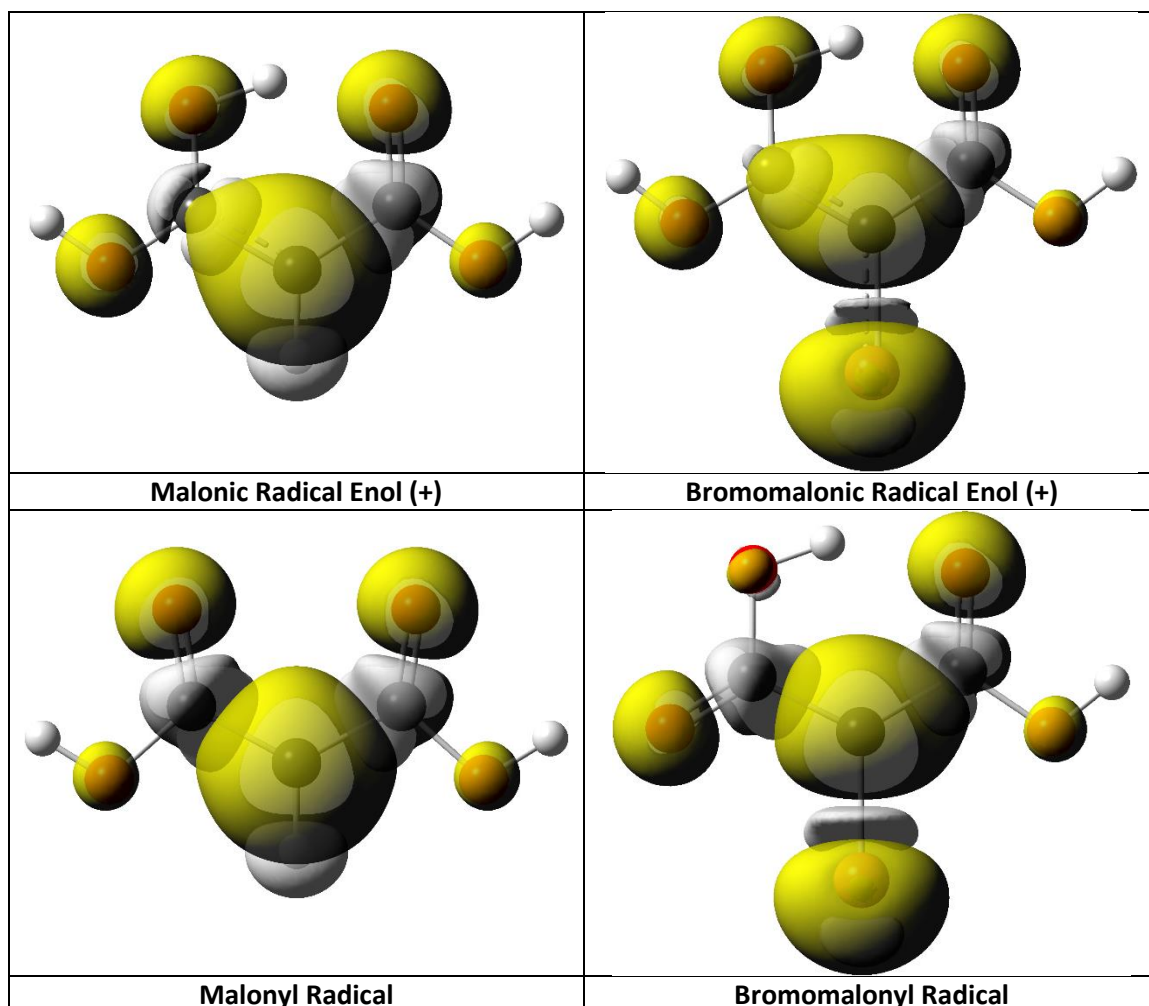


Figure 7. Spin density isosurfaces of malonic radical enol and bromomalonic radical enol (top) compared to malonyl radical and bromomalonyl radical (bottom), all optimized at UωB97X-D/6-311G** with simulated (SMD) solvation. Yellow and white surfaces represent unpaired α and β spin, respectively. The surfaces enclose regions where the unpaired electron (with given spin) density is greater than or equal to $0.001 \text{ e}^-/\text{\AA}^3$. Observe the central carbon's $2p$ orbital unhybridizing with its neighbor upon deprotonation, as evidenced by the change in shape from ovular to round. The hourglass-like shape of the orbitals are not visible from this particular viewpoint.

Taking spontaneous tautomerizations and deprotonations upon oxidation into account if applicable, the calculated order of raw Gibbs reducing power for the set of one-, two- and three-carbon malonic acid derivatives in the aqueous phase is: TA (to tartronic enol radical cation) > BMA (to bromomalonyl radical) > Dibromoacetic acid (to dibromoacetyl radical) > Bromoacetic acid (to bromoacetyl radical) > MA (to malonyl radical) > Formic acid (to carboxyl radical) > Carbonic acid (to HCO_3^-) > DBMA (to dibromomalonyl radical). Of course, the order changes in the gas phase, where water is not so plentiful as to accept any proton released – in this case, formation of enols are preferred. Thermodynamics indicate that bromide can favorably reduce all queried organic acids when they are oxidized, itself then becoming a neutral bromine radical that may combine with another that it meets to form elemental bromine. Since cerium gets reduced by means of an inner-sphere electron transfer, contrary to the outer-sphere mechanism of ferriin, a mediator atom like bromine does not appear to be required for spontaneous oxidation by cerium, hence we see why the more recently published mechanisms for cerium-catalyzed BZ reactions have been giving TA plenty due attention and why the cerium-catalyzed oxidation of MA proceeds appreciably while the ferriin-catalyzed oxidation does not.⁶⁸ The relative redox energies of all probable organic acids are collected in **Table 5**, which will be referred to again when we include bromooxoacids in the discussion. Notice that the ability of an oxidized organic acid to tautomerize to an enol decreases the redox energy and consequently favors the species as a reducing agent. This is especially true in acidic solution, where the activation barrier to tautomerization is much lower.

3.4 Modeling the Metal Catalysis

3.4.1 First Attempts

This project originally began as a study of the iron hexammonia complex ($\text{Fe}(\text{NH}_3)_6^{2+/3+}$), proposed as an attempt to model interactions between iron and its nitrogen-containing ligands. Following many months of work, the study was finally discontinued due primarily to the failure of the model system to reproduce defining characteristics of a ferro/iin system, namely the ground state spin multiplicity and redox energy. As the spectrochemical series predicts, o-phenanthroline splits the relative energies of doubly- (e_g , “high-spin”) and triply- (t_{2g} , “low-spin”) degenerate orbitals centered on iron, thereby facilitating the preference of a low-spin ground state in both ferriin and ferriin, where the field-splitting energy (Δ) imposed by the ligands is greater than the pairing energy of the t_{2g} electrons, and a high-spin ground state in the hexammonia complex, where the opposite is true and Hund filling is favored. This phenomenon is likely due to the difference in flexibility of the hybridized orbitals on nitrogen, the structural rigidity of the tri-bidentate tris-phenanthroline complex, or perhaps parts of both rationales. The model system did elucidate the shallow nature of a potential well with essentially unhindered ligand rotations, as energy differences among minima and even some of the lower-energy saddles are less than $1 k_B T$ per mole (or RT) at room temperature (~ 0.59 kcal/mol). **Table 8** contains geometric and energetic data for ferric model complexes in their high-spin ground state computed at the MP2(full)/cc-pVDZ theoretical level. This particular data set is selected as an example because of its fairly robust characterization of the potential energy surface; the rest of the data are not included. One interesting observation is that the average Fe—N virtual bond length is directly proportional to the order of the saddle calculated at this level for transition structures in their high-spin ground state ($S=5/2$). The Fe—N virtual bond length in D_{3d}

conformation as a sixth-order saddle is 2.4 pm greater than in S_6 conformation and 2.5 pm greater than the shortest average bond length. The dihedral angles between opposing ammonia hydrogen atoms are less than 15° in *all* obtained minima of accessible ferrous and ferric states and are usually less than 5° , indicating that near-eclipsed geometry is preferred.

Complex	Entropy (cal/mol/K)	Avg. Fe—N (pm)	RMS δ_1 ($^\circ$)	RMS δ_2 ($^\circ$)	RMS δ_3 ($^\circ$)	$\Delta E_{\text{tot}} / C_1$ (kcal/mol)
${}^6\text{Fe}(\text{NH}_3)_6^{3+} C_1$	129.04	217.11	1.98	1.92	1.95	0.00000
${}^6\text{Fe}(\text{NH}_3)_6^{3+} C_1\text{-2OSP}$	122.42	217.25	179.98	179.98	179.98	0.42381
${}^6\text{Fe}(\text{NH}_3)_6^{3+} C_2$	127.66	217.11	1.94	1.94	1.94	0.00001
${}^6\text{Fe}(\text{NH}_3)_6^{3+} C_3$	126.88	217.10	1.91	1.91	1.91	0.00003
${}^6\text{Fe}(\text{NH}_3)_6^{3+} C_3\text{-3OSP}$	116.33	217.30	159.59	159.61	159.61	0.74395
${}^6\text{Fe}(\text{NH}_3)_6^{3+} C_{2v}\text{-1OSP}$	122.96	217.12	0.10	0.00	0.10	0.04640
${}^6\text{Fe}(\text{NH}_3)_6^{3+} D_3$	125.43	217.11	1.99	1.99	1.99	0.00001
${}^6\text{Fe}(\text{NH}_3)_6^{3+} D_3\text{-4OSP}$	113.15	217.30	179.99	179.99	179.99	0.93791
${}^6\text{Fe}(\text{NH}_3)_6^{3+} S_6\text{-2OSP}$	121.74	217.25	180.00	180.00	180.00	0.40792
${}^6\text{Fe}(\text{NH}_3)_6^{3+} D_{3d}\text{-6OSP}$	104.88	219.62	180.00	180.00	180.00	13.20632

Table 8. Data at the MP2(full)/cc-pVDZ theoretical level for $\text{Fe}(\text{NH}_3)_6^{3+}$ in different geometric conformations. All (Fe—N) distances are given in picometers, RMS δ refers to the root-mean square of the three dihedral angles between each pair of opposite ammonia hydrogen atoms in degrees, and nOSP classifies a structure as an n-order saddle point. Note that entropy is in units of calories/mole/Kelvin; not kilocalories.

3.4.2 Ligand Field Analysis

The model system predicts a more thermodynamically stable electron transfer from BMA by almost a factor of two in the gas phase when compared to ferriin data at the same theoretical level. Though the transfer would be more favorable, the mechanism by which it could occur would be different, relying instead on the dissociation of an ammonia ligand followed by an inner-sphere electron transfer with either bromine or oxygen in direct contact with the iron center. The dissociation of ammonia is many times more feasible than the dissociation of a bidentate o-phenanthroline ligand, and in the case of the model, this would

have to occur in order to allow compatible orbitals to overlap. In contrast, the ligands bound to iron in ferriin are large conjugated π -systems that can both freely interact with the $4p$ -orbitals centered on bromine and shuttle the liberated electron to an available t_{2g} orbital centered on iron. Calculated thermodynamics for the electron transfer reactions as well as spin-crossovers, pure redox energies, and ligation energies were calculated in the gas phase and are provided in **Table 9**. Examining the data, we notice that phenanthroline is by far the most attracted to the free cation of all species examined, likely due to its bidentate binding, and ligation to ferric iron is more favorable due its greater positive charge, as expected. In accordance with the spectrochemical series, the preference for a high-spin center decreases from water to ammonia and switches upon sp^2 -hybridization of the lone-pair orbital in o-phenanthroline. Interestingly, data collected at UB3LYP/6-31G** suggests that ferroin would slightly prefer to exist in its high-spin state, however this is one of the reasons why a different theoretical level was chosen, as it conflicts with both empirical observations and findings of a more rigorous computational study.⁶⁹ That being said, the fairly low spin-crossover energy of ferroin invites us to postulate other interesting mechanisms for transferring electrons, perhaps relying first on the switch from a low- to high-spin electronic state for a sub-femtosecond slice of time immediately preceding the electron transfer. Speculation aside, something that we can say with relative certainty is that the low-spin ground state is more favorable in ferriin than it is in ferroin, which has one additional electron. This is likely attributed to the increased structural rigidity of ferriin caused by its greater positive charge that attracts the ligands more tightly. We notice that this also occurs in the $\text{Fe}(\text{NH}_3)_6^{n+}$ system, but not the $\text{Fe}(\text{H}_2\text{O})_6^{n+}$ system, and can be rationalized by considering the shapes of the ligand orbitals and their constructive overlap with the d orbitals. Evidence for the structural rigidity hypothesis, i.e., that it is inversely proportional to the number of unpaired electrons, will be presented in the next section. **Figure 8** illustrates

examples of constructive and non-constructive orbital overlap in ammonia- and water-ligated ferric iron. The ferric case is not shown because, though similar in essence, it is more complex.

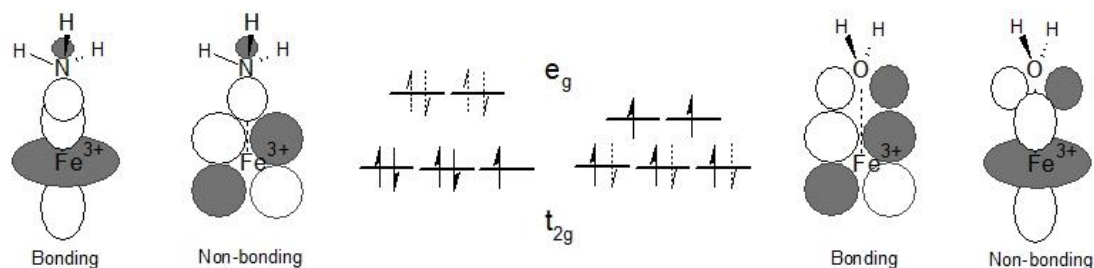


Figure 8. Molecular orbital bonding scheme between iron(III) and its ligands, shown as ammonia on the left and water on the right. The remaining five ligands and four d orbitals are omitted for clarity. The orbital shading indicates electron phase. Two orbitals feel a constructive, bonding interaction when like phases overlap and a destructive, anti-bonding interaction when opposite phases overlap. Dotted arrows indicate dative bonding ligand electrons while dark arrows indicate $3d$ metal electrons. Notice that ammonia interacts more favorably with both of the e_g orbitals, though only d_{z^2} is shown. Consequently, the hexammonia complex is more likely to be found in a low-spin state than the hexaquo complex.

Since nitrogen atoms in both ammonia and phenanthroline have one lone pair of electrons that face towards the metal center, they constructively interact with e_g -type orbitals on iron. Ligand overlap with iron's t_{2g} orbitals is partially destructive, so metal electrons are preferentially pushed into these orbitals to permit the constructive, sub first-order dative bonding interaction among lone pairs on nitrogen and the e_g orbitals around iron. Conversely, the two lone pairs on water overlap more constructively with metal t_{2g} orbitals. Since the metal has too many electrons to push exclusively into its e_g orbitals, iron retains its high-spin ground state and forms constructive ligand-metal MOs without distorting the preferred geometric arrangement of its ligands. The aquo complex could exist in a low-spin electronic state without introducing too much steric strain, however this would require hybridization of the empty e_g orbitals with a different pair of ligand electrons, thereby drawing electron density from and weakening the O—H σ -bonds, which causes the complex to become less stable by about 30 kcal/mol in the gas phase. Ammonia is the middle-ground between phenanthroline and water

since valent metal orbitals can overlap constructively with more than one of the valence orbitals on nitrogen. The more localized nature of the single lone pair on nitrogen allows ligand electrons to fill metal e_g orbitals, if necessary, while drawing less electron density away from their own substituents. This is one likely explanation for the increasing formation enthalpy from H_2O - to ammonia- to phenanthroline-ligated iron complexes as well, shown in **Table 9**.

Phenomenon	ΔE (kcal/mol)	ΔH (kcal/mol)	ΔG (kcal/mol)
${}^6\text{Ferriin} + \text{BMA} \rightarrow {}^5\text{Ferriin} + \text{BMA}^+ \text{ enol}$	-79.97	-80.95	-82.19
${}^2\text{Ferriin} + \text{BMA} \rightarrow {}^1\text{Ferriin} + \text{BMA}^+ \text{ enol}$	-77.02	-79*	-79*
Low-Spin Redox Energy	272.09	273*	273*
High-Spin Redox Energy	275.04	275.70	278.26
Ferrous Spin-Crossing ($S=2 \leftarrow S=0$)	4.92	2*	-1*
Ferric Spin-Crossing ($S=5/2 \leftarrow S=1/2$)	7.87	7.21	4.20
${}^5\text{Fe}^{2+} + 3 \text{ o-phenanthroline} \rightarrow {}^1\text{Ferriin}$	-449.16	-444*	-400*
${}^5\text{Fe}^{2+} + 3 \text{ o-phenanthroline} \rightarrow {}^5\text{Ferriin}$	-444.24	-438.23	-403.59
${}^6\text{Fe}^{3+} + 3 \text{ o-phenanthroline} \rightarrow {}^2\text{Ferriin}$	-892.49	-885.16	-844.84
${}^6\text{Fe}^{3+} + 3 \text{ o-phenanthroline} \rightarrow {}^6\text{Ferriin}$	-884.63	-877.96	-840.64
${}^6\text{Fe}(\text{NH}_3)_6^{3+} + \text{BMA} \rightarrow {}^5\text{Fe}(\text{NH}_3)_6^{2+} + \text{BMA}^+ \text{ enol}$	-156.71	-157.70	-159.17
${}^2\text{Fe}(\text{NH}_3)_6^{3+} + \text{BMA} \rightarrow {}^1\text{Fe}(\text{NH}_3)_6^{2+} + \text{BMA}^+ \text{ enol}$	-145.07	-146.34	-150.64
Low-Spin Redox Energy	381.90	381.20	383.67
High-Spin Redox Energy	382.35	379.30	381.71
Ferrous Spin-Crossing ($S=0 \leftarrow S=2$)	11.87	14.02	15.32
Ferric Spin-Crossing ($S=1/2 \leftarrow S=5/2$)	0.22	2.66	6.79
${}^5\text{Fe}^{2+} + 6 \text{ NH}_3 \rightarrow {}^1\text{Fe}(\text{NH}_3)_6^{2+}$	-377.04	-362.67	-307.90
${}^5\text{Fe}^{2+} + 6 \text{ NH}_3 \rightarrow {}^5\text{Fe}(\text{NH}_3)_6^{2+}$	-388.91	-376.69	-323.22
${}^6\text{Fe}^{3+} + 6 \text{ NH}_3 \rightarrow {}^2\text{Fe}(\text{NH}_3)_6^{3+}$	-752.33	-736.99	-676.50
${}^6\text{Fe}^{3+} + 6 \text{ NH}_3 \rightarrow {}^6\text{Fe}(\text{NH}_3)_6^{3+}$	-752.55	-739.66	-683.29
${}^6\text{Fe}(\text{H}_2\text{O})_6^{3+} + \text{BMA} \rightarrow {}^5\text{Fe}(\text{H}_2\text{O})_6^{2+} + \text{BMA}^+ \text{ enol}$	-187.28	-184.55	-185.64
${}^2\text{Fe}(\text{H}_2\text{O})_6^{3+} + \text{BMA} \rightarrow {}^1\text{Fe}(\text{H}_2\text{O})_6^{2+} + \text{BMA}^+ \text{ enol}$	-186.84	-186.45	-187.60
Low-Spin Redox Energy	381.90	381.20	383.67
High-Spin Redox Energy	382.35	379.30	381.71
Ferrous Spin-Crossing ($S=0 \leftarrow S=2$)	30.94	28.83	30.17
Ferric Spin-Crossing ($S=1/2 \leftarrow S=5/2$)	30.49	30.73	32.13
${}^5\text{Fe}^{2+} + 6 \text{ H}_2\text{O} \rightarrow {}^1\text{Fe}(\text{H}_2\text{O})_6^{2+}$	-325.60	-314.22	-256.78
${}^5\text{Fe}^{2+} + 6 \text{ H}_2\text{O} \rightarrow {}^5\text{Fe}(\text{H}_2\text{O})_6^{2+}$	-356.54	-343.06	-286.95
${}^6\text{Fe}^{3+} + 6 \text{ H}_2\text{O} \rightarrow {}^2\text{Fe}(\text{H}_2\text{O})_6^{3+}$	-659.12	-648.45	-588.43
${}^6\text{Fe}^{3+} + 6 \text{ H}_2\text{O} \rightarrow {}^6\text{Fe}(\text{H}_2\text{O})_6^{3+}$	-689.62	-679.18	-620.56

Table 9. Gas phase thermodynamics of electron transfer from BMA, intersystem crossing, pure redox processes, and ligation for Ferro/iin, $\text{Fe}(\text{NH}_3)_6^{2+/3+}$, and $\text{Fe}(\text{H}_2\text{O})_6^{2+/3+}$ computed at UωB97X-D/6-311G**. Values marked with an asterisk (*) are estimated with additional data obtained at the UB3LYP/6-31G** theoretical level. Note that the magnitude of the ligation energies are much greater than they would be in the aqueous phase and DFT sometimes has trouble predicting energies of reactions in which the spin-state changes.⁷⁸ It is also known to artificially favor high-spin states in some instances.⁶⁹

3.4.3 Ligand Fields in Another Practical Model

Given this collection of data and the spectrochemical series itself, much evidence points to structural rigidity being the major contributor to the field-splitting energy; i.e., a more rigid complex splits the energy of the high- and low-spin d orbitals to a greater degree. Evidence in support of this hypothesis includes the experimentally observed tendency of ferric cytochrome P450 enzymes, usually with axial cysteine sulfur ligands and low-spin ground states, to distort upon the binding of substrate to the surrounding protein, pulling the iron center below the equatorial plane and facilitating a spin-crossover to the high-spin state just before accepting an electron from a nearby cofactor. Once in the ferrous state, elemental oxygen can associate in the open axial position, restoring the rigid octahedral geometry and reverting the porphyrin back to its low-spin state. In contrast, heme proteins like myoglobin that coordinate the central iron with a single axial histidine instead of sulfur (non-covalent axial bond, still the same porphyrin; b_5) reportedly exhibit high-spin ground states before binding an oxygen molecule and reverting temporarily to the low-spin form before its release, indicated by the rigid octahedral geometry of the O_2 -bound complex. More information on heme-containing oxygenase proteins, including visual representations of the mechanisms outlined above, can be found in an excellent review cited as reference 70. Further support for the rigidity hypothesis in intermediate cases is found in at least two studies; one examining a natural bacterial protein called ferricytochrome c and another examining a synthetic porphyrin complex. Though the particular 1974 study of ferricytochrome c was not completely conclusive, researchers were able to resolve a spin crossover from the low-spin state, when an axial methionine sulfur coordinates to the iron center, to an intermediate magnetic state, reported as an admixture of $S=3/2$ and $S=5/2$ states (an interesting finding on its own), when the iron-sulfur bond breaks and a histidine residue

associates on the other side of the ring.⁷¹ There appeared to be only five coordinating ligands (not including water) at once. In 1982, a different magnetic susceptibility study of horse heart ferricytochrome c reported a low-pH, temperature-dependent high-spin state that they also hypothesized occurred due to cleavage of the methionine sulfur—heme iron bond, however they make no mention of histidine and instead suggest that a different weak-field ligand (like water) is associated to the heme center when in the high-spin state.⁷² Perhaps this particular cytochrome did not contain a nearby histidine at all, but support for the high flexibility, high spin hypothesis is apparent either way, especially considering the increased probability of the protein denaturing at low pH. Solution-phase NMR and X-ray studies of a 107-amino acid *Desulfovibrio vulgaris* cytochrome c that contains four Heme C moieties reports that all of the hemes are ligated with two histidine residues and in a low-spin state. They are not equivalent, however, and somehow all involved in coordinating the transfer of two electrons at once to the respiratory chain.⁷³ Though the spin states were not discussed any further than their classification in the aforementioned study, given what we have learned about ferroin in this one, it makes sense that six sp^2 -nitrogen ligands would hold iron in a low-spin state. To examine the intermediate-spin case, some crafty researchers were able to coax a synthetic, nonplanar ferric porphyrin complex from low-spin to a definitive $S=3/2$ state at room temperature by replacing axial imidazole ligands with either 4-cyanopyridine or tetrahydrofuran.⁷⁴ We note, once again, that in all of the examples provided, iron-porphyrin complexes unpair electrons as they become less structurally rigid, which appears to be facilitated in many cases by breaking a strong interaction and forming a weaker one.

3.5 Bromine Oxide/Oxoacid Equilibria

3.5.1 What is Known

Given that bromine oxide chemistry is the main driving force of autocatalytic behavior in BZ reactions and also intricately related to ozone destruction all the way up to the stratosphere, it makes sense to examine some of the more obscure, inorganic mechanisms at play as well since these are just as important in elucidating the oscillating nature of the bromine oxide chemistry. Of the 48 reactions in the most recent MBM mechanism, 9 of them exclusively describe the chemistry of bromine oxides and oxoacids, not including the oxidation of cerium by BrO_2 . Raw thermodynamics of the bromooxoacid reactions corresponding to the MBM sequence are computed and shown in **Table 10**, replacing cerium with ferriin. While it should not be difficult to add cerium into the calculations, unfortunately it cannot be directly incorporated into this model because atomic orbitals are not defined at the chosen theoretical level. The parameterized MBM system of equations reproduces the behavior of a cerium-catalyzed BZ reaction fairly well, though the researchers note that the reverse rate of reaction **8** depends strongly on the solution's ionic strength, which was not examined in depth herein, but does make a lot of sense since ionic strength is directly related to the ease of electron transfer.

Reaction	ΔE (kcal/mol)	ΔH (kcal/mol)	ΔG (kcal/mol)
Gas Phase			
1. $\text{HBrO} + \text{HBr} \rightarrow \text{Br}_2 + \text{H}_2\text{O}$	-27.03	-24.75	-23.86
2. $\text{HBrO}_2 + \text{HBr} \rightarrow 2 \text{HBrO}$	-42.31	-40.06	-41.23
3. $\text{HBrO}_3 + \text{HBr} \rightarrow \text{HBrO}_2 + \text{HBrO}$	-12.18	-10.18	-11.64
4. $\text{HBrO}_2 + \text{H}_3\text{O}^+ \rightarrow \text{H}_2\text{BrO}_2^+ + \text{H}_2\text{O}$	-40.90	-41.51	-40.64
5. $\text{HBrO}_2 + \text{H}_2\text{BrO}_2^+ + \text{H}_2\text{O} \rightarrow \text{HBrO}_3 + \text{HBrO} + \text{H}_3\text{O}^+$	6.60	7.47	6.64
5.' $2 \text{HBrO}_2 \rightarrow \text{HBrO}_3 + \text{HBrO}$	-30.13	-29.87	-29.59
6. $\text{HBrO}_2 + \text{HBrO}_3 \rightarrow \text{Br}_2\text{O}_4 + \text{H}_2\text{O}$	-8.74	-8.98	-7.73
7. $\text{Br}_2\text{O}_4 \rightarrow 2 \text{BrO}_2$	1.36	-0.03	-11.20
8.' $\text{BrO}_2 + \text{Fe}^{2+} + \text{H}_3\text{O}^+ \rightarrow \text{HBrO}_2 + \text{Fe}^{3+} + \text{H}_2\text{O}$	42.48	--	--
9. $2 \text{HBrO}_3 \rightarrow 2 \text{HBrO}_2 + \text{O}_2$	-23.21	-24.13	-34.64
10.' $\text{BrO}_2 \rightarrow \text{Br} + \text{O}_2$	-34.22	-33.85	-41.25

Aqueous Phase			
1. $\text{HBrO} + \text{HBr} \rightarrow \text{Br}_2 + \text{H}_2\text{O}$	-33.85	-31.56	-30.69
2. $\text{HBrO}_2 + \text{HBr} \rightarrow 2 \text{HBrO}$	-44.74	-42.55	-43.80
3. $\text{HBrO}_3 + \text{HBr} \rightarrow \text{HBrO}_2 + \text{HBrO}$	-15.96	-13.80	-14.93
4. $\text{HBrO}_2 + \text{H}_3\text{O}^+ \rightarrow \text{H}_2\text{BrO}_2^+ + \text{H}_2\text{O}$	3.72	2.71	3.49
5. $\text{HBrO}_2 + \text{H}_2\text{BrO}_2^+ + \text{H}_2\text{O} \rightarrow \text{HBrO}_3 + \text{HBrO} + \text{H}_3\text{O}^+$	-32.51	-31.46	-32.36
5.' $2 \text{HBrO}_2 \rightarrow \text{HBrO}_3 + \text{HBrO}$	-28.78	-28.75	-28.87
6. $\text{HBrO}_2 + \text{HBrO}_3 \rightarrow \text{Br}_2\text{O}_4 + \text{H}_2\text{O}$	-4.18	-4.57	-2.98
7. $\text{Br}_2\text{O}_4 \rightarrow 2 \text{BrO}_2$	-0.44	-1.76	-13.12
8.' $\text{BrO}_2 + \text{Fe}^{2+} + \text{H}_3\text{O}^+ \rightarrow \text{HBrO}_2 + \text{Fe}^{3+} + \text{H}_2\text{O}$	-21.88	--	--
9. $2 \text{HBrO}_3 \rightarrow 2 \text{HBrO}_2 + \text{O}_2$	-17.88	-18.54	-28.39
10.' $\text{BrO}_2 \rightarrow \text{Br} + \text{O}_2$	-31.23	-30.84	-38.24

Table 10. Thermodynamics of a slightly modified MBM reaction scheme without activation energies in both gas and aqueous phases. Reactions modified from the original scheme are denoted with a 'prime' symbol and ferro/iin is abbreviated simply as Fe.

3.5.2 What is Less Known

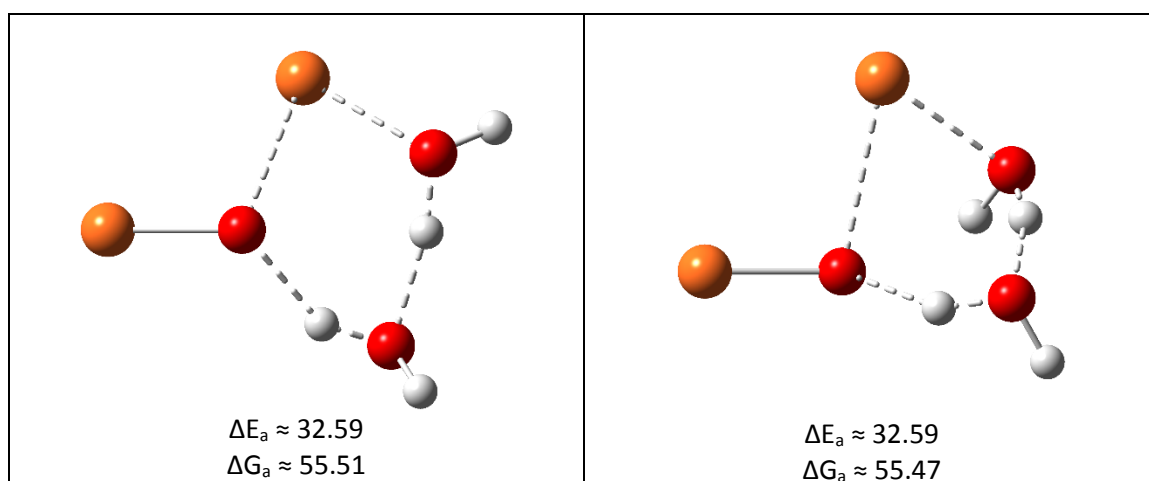
Reactions 9-12 in the GTF scheme introduce higher-order bromine oxides into the mainstream BZ sequence for the first time (to my knowledge) as the asymmetric condensation of HOBrO and HOBrO₂ to Br₂O₄, followed by three modes of decomposition. Br₂O₄ has been observed directly with infrared spectroscopy at temperatures less than or equal to 233 K,⁷⁵ but that is okay in this case since it is only present in the model as a reactive intermediate. The same study reports that BrOO is more thermodynamically stable than OBrO, which is verified in this study, by about 37.96 kcal/mol in the gas phase and 35.33 kcal/mol in the aqueous phase. This provides rationale as to how some of the peroxy higher-order bromine oxides tend to form. Calculated thermodynamics from this study and solid-state data collected in the cited reference also indicate that Br₂O₄ is more thermodynamically stable in its peroxy conformation (BrOOBrO₂), however we assume (BrOOBrO₂), however we assume that the kinetic, pro-symproportionation (to two OBrO) conformer, OBrOBrO₂, is likely the chemical species of interest in the more recent BZ reaction schemes. According to data obtained at the UωB97X-D/6-311G** theoretical level, BrOOBrO₂ appears to be the most

appears to be the most favorable radical recombination product of BrO and OBrO₂ radicals, OBrOBrO₂ the most OBrOBrO₂ the most favorable condensation product of BrOH and HOBrO₂ (as reaction 6 in Table 10 suggests), and 10 suggests), and BrOBrO₂ the most favorable condensation product of two HOBrO molecules. If BrOOBrO₂ forms, the probability of it decomposing appears to be very low at first glance. Interestingly, though, CIS(T) predicts that the most stable isomer of Br₂O₄, peroxy-BrOOBrO₂, also decomposes most readily when irradiated with 816(.85) nm infrared light in the gas phase or 784(.83) nm light in the aqueous phase, which is consistent with its low observed lifetime in experimental studies. The first excited state of the Br₂O₄ isomer of interest, OBrOBrO₂, is a triplet, calculated to be triplet, calculated to be excited by 540(.48) nm visible radiation. Both Br₂O₄ isomers have excitation energies less than excitation energies less than queried Br₂O₃ and Br₂O₅ isomers. In addition, the peroxy form has the lowest excitation the lowest excitation energy of all queried higher bromine oxides (1.52 eV), as might be expected based on the expected based on the molecular connectivity, and presumably decomposes upon irradiation in the aqueous phase to the aqueous phase to OBrO and BrOO, the latter of which has an extremely low calculated excitation energy (0.5023 eV) that corresponds to its elemental decomposition. In general, longer oxygen chains are longer oxygen chains are thermodynamically preferred and easier to excite, but Br₂O₄ appears to be inherently less to be inherently less stable, as inferred from its lower excitation energies (by more than 0.2 eV). When the geometry of OBrOBrO₂ is optimized to fit the wavefunction of its first triplet excited state (2.29 eV), the state (2.29 eV), the molecule decomposes to atomic oxygen and BrOBrO₂. Given these observations, one may observations, one may speculate that despite the fairly deep nature of these thermodynamic sinks, perhaps they are sinks, perhaps they are not so easily observed because they decompose rapidly upon irradiation. Knowing that they Knowing that they form favorably and definitely decompose, one also speculates that perhaps the higher-order the higher-order bromine oxides play deeper roles in regulating the stoichiometry of the oscillating species. Their oscillating species. Their decomposition is likely involved in the changes observed when a BZ solution is irradiated with solution is irradiated with high-intensity light, which often leads to termination or slowing of oscillations.⁶⁷ Irradiation oscillations.⁶⁷ Irradiation experiments have different effects on different variants of the reaction because ferriin and because ferriin and Ru(bipy)₃³⁺ both contain conjugated π-systems that also absorb visible and ultraviolet light. ultraviolet light. Definite effects of irradiation on cerium-catalyzed batch reactions hint that bromine oxides in the

bromine oxides in the vessel are also absorbing light and their chemical activities are changed as a result. In fact, Zhabotinsky's own team reportedly found that as the $[OBrO_2^-]/[MA]$ ratio increases in a reactor irradiated with ultraviolet light, the oscillation domain also increases. Reading between the lines a bit, one may speculate that adding more bromate allows more higher-order bromine oxides to form, which would normally be a detriment to the rate and domain of oscillations, however in this case may prolong the reaction by providing a reservoir of readily available readily available bromate and bromous acid upon irradiative decomposition. We know that all electrons can absorb electrons can absorb electromagnetic radiation, so it is also important to consider organic species like MA in the species like MA in the vessel, however the non-aromatic organic species do not likely contribute significantly, if at all, significantly, if at all, to processes observed upon irradiation. As enticing as the realm of mysterious higher-order mysterious higher-order bromine oxide chemistry is, we return now to perhaps the most significant of the oft-significant of the oft-overlooked species in a BZ reaction, BrOBr. The strange, dark brown solid has been isolated at has been isolated at low temperatures, but is reported to decompose at -23°C .⁷⁶ Due to its apparent labile nature, it is apparent labile nature, it is treated as a short-lived intermediate in the reaction sequence, quickly rearranging to quickly rearranging to something else upon its formation. One plausible method for this is the rearrangement to two rearrangement to two hypobromous acid molecules upon hydrolysis, however the activation barrier for this process is barrier for this process is calculated to be quite high in seclusion. Interestingly, the electronic activation barrier activation barrier decreases from 44 to around 19 kcal/mol as spectator water molecules are included in the gas-included in the gas-phase calculation, leading us to appreciate how important the specific geometry of the transition geometry of the transition state is in any given chemical reaction. At least one successful model has been has been independently formulated that includes the hydrolysis of BrOBr.⁷⁷ The model accurately predicts the accurately predicts the temporal distribution of bromide potential waves and almost predicts the shapes. Rate the shapes. Rate constants used in the model match thermodynamic trends herein, but not kinetics. Despite being kinetics. Despite being determined at 30 and 40 °C instead of 25 °C, correcting for this still leaves us far from the us far from the reported rate constant for the hydrolysis of BrOBr, which is $3.22 \times 10^3 \text{ M s}^{-1}$ (the units may be a units may be a mistake, as M/s is a unit of reaction rate), however the first-order rate constant that we would that we would calculate given the lowest computationally obtained barrier is $1.93 \times 10^{-25} \text{ s}^{-1}$. Substituting the

Substituting the electronic barrier for the Gibbs barrier yields $7.61 \times 10^{-2} \text{ s}^{-1}$, which is still about 40,000 times too small. Assuming that the units reported are not a mistake, the researchers may have treated the concentration of BrOBr as constant, on the order of 10^{-9} , and multiplied that by an empirically determined first-order rate constant (which still would have given them a rate, not a rate constant). The value could have also been chosen to artificially fit data, but it was not clarified. Interestingly, the rate constant of BrOBr formation from the bromide-mediated decomposition of Br_2O_4 , shown in **Figure 16**, does come within an order of magnitude of the formation rate constant reported in 77, which may or may not be a coincidence. We also must consider the possibility of the harmonic approximation severely overestimating the bond enthalpy. Either way, this forces us to acknowledge some of these models for what they really are: Sets of equations designed specifically to reproduce certain observable behavior(s). Manipulating the rate constants that govern calculated concentration fluctuations can produce numbers that fit obtained data even if the specific equations used have little physical ground, like fitting a polynomial to a random dataset. As of now, all we can say is that BrOBr deserves further study in (and out of) the context of a BZ reaction. Optimized transition states for its hydrolysis are shown in **Figure 9**

Figure 9. Results of thermodynamics calculations in this study suggest, in addition to the formation process described previously, that BrOBr is likely consumed as it reacts with bromic acid to form BrOBrO_2 and BrOH. A transition state describing this is shown in **Figure 12**. The 14-16 kcal/mol barrier from either direction means that BrOBr is likely involved in both the formation and decomposition of BrOBrO_2 , presumably in response to the dominant chemical species. When bromate dominates, it converts BrOBr to BrOH and is in the process converted to a much less labile sink that may function as a reservoir. When BrO_3^- is scarce and BrOH is present, the reaction proceeds in reverse, converting the thermodynamic sink back to OBrOH and BrOBr.



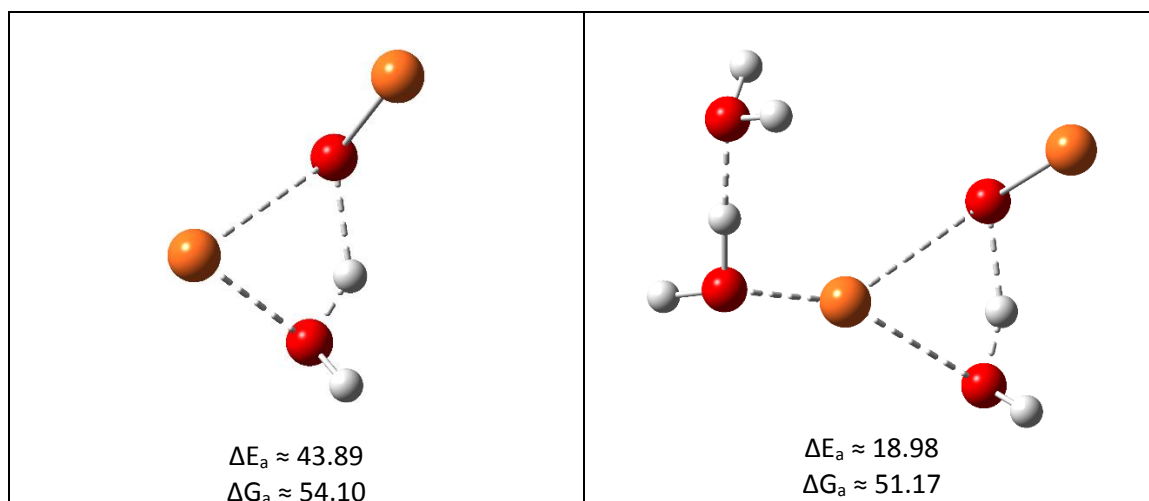
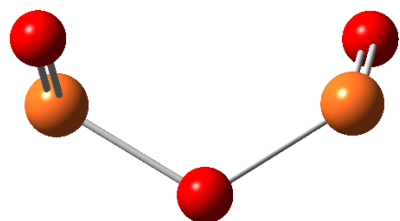
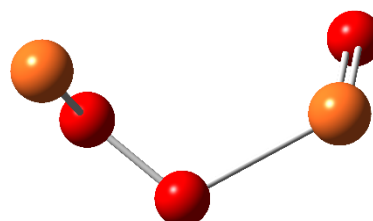


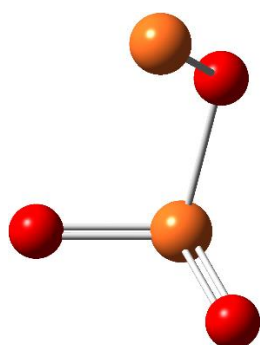
Figure 9. Select optimized, simulated aqueous-phase transition states corresponding to the hydrolysis of BrOBr at the U ω B97X-D/6-311G** theoretical level. Notice that adding more water molecules to the proton transfer chain actually appears to increase the activation energy, contrary to what may occur in other proton-transfer reactions. In the bottom-right structure, two spectator water molecules are added to the structure, one of which appears to form a halogen bond to the bromine that is pulled off of BrOBr, clearly stabilizing the transition state. Intrinsic reaction coordinate (IRC) calculations verify the validity of obtained transition states.



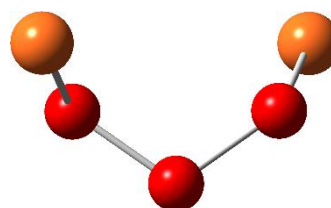
OBrOBrO
(0, 0)



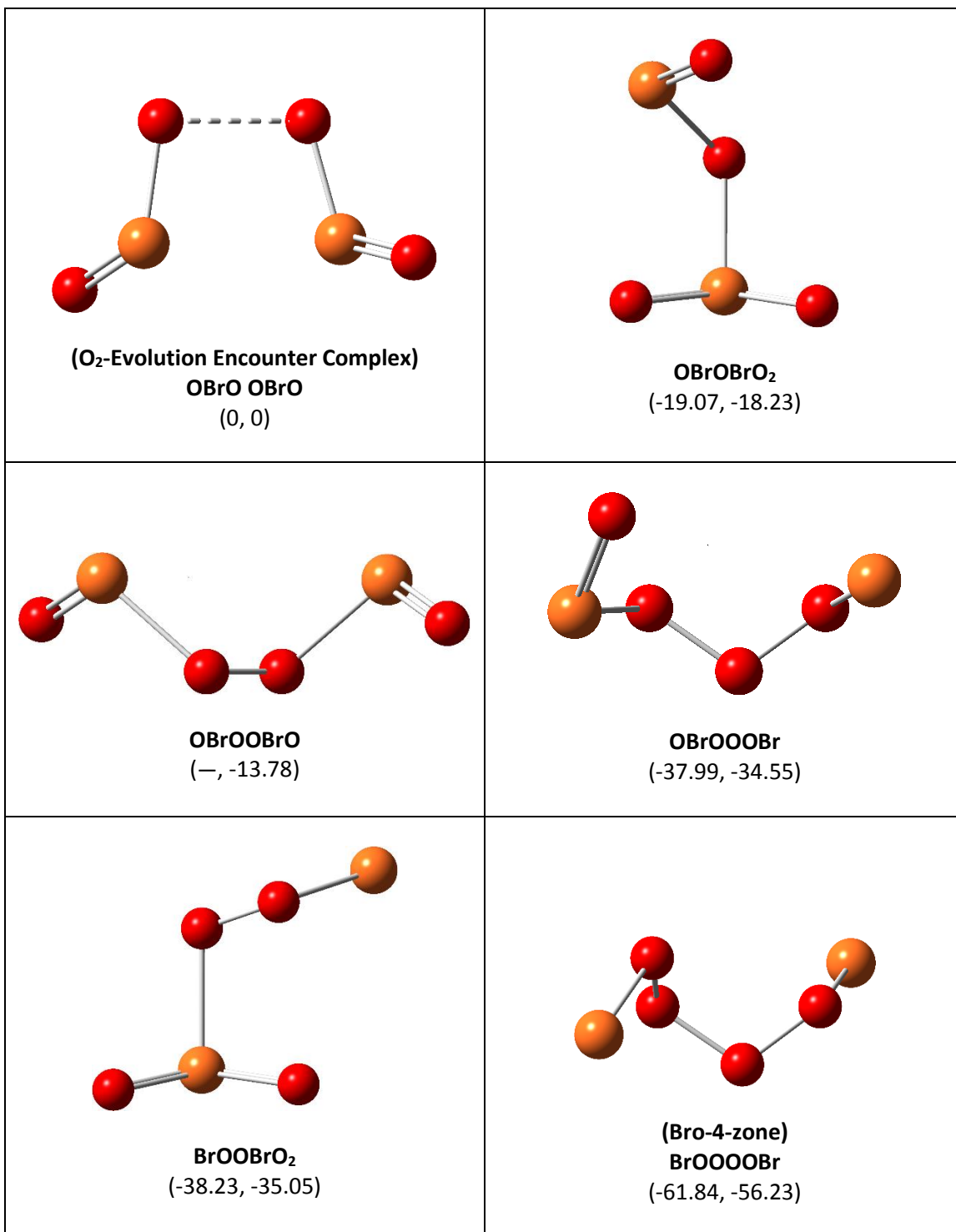
BrOOBrO
(-, -17.49)



BrOBrO₂
(-22.64, -20.73)



(Brozone)
BrOOOBr
(-42.60, -38.33)



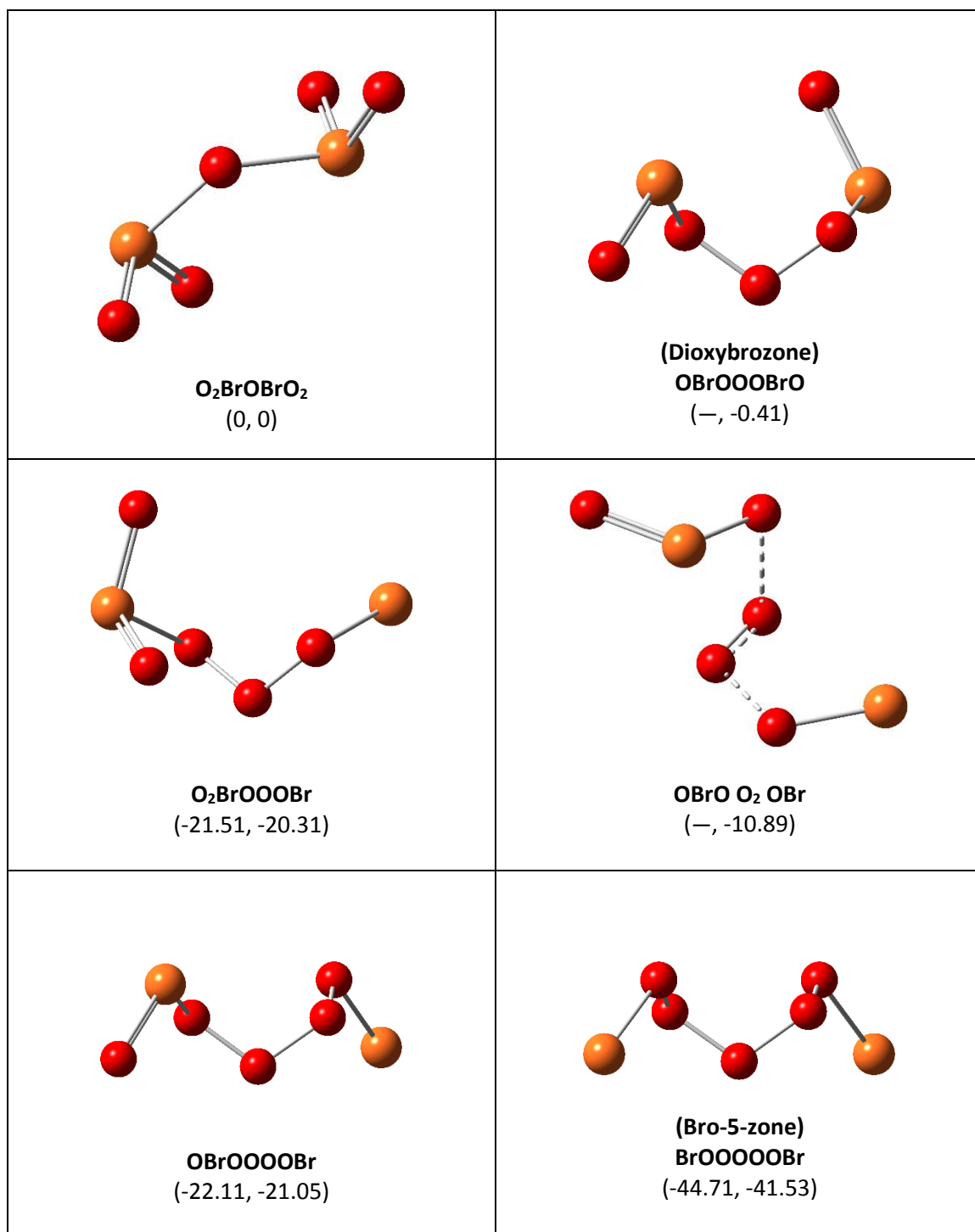


Figure 10. Assortment of singlet ($S=0$) bromine oxides, labeled with their thermodynamic Gibbs energy relative to one of the least stable bromine oxides with the same stoichiometry. Relative energies are in kcal/mol in the form: (gas phase, SMD). Some species were not optimized in the gas phase and are denoted with ‘—’. Only the most stable identified conformer in any given connectivity well is shown. Bond orders are calculated based on formal charge and length. Molecules are pictured in aqueous geometries, optimized at the $U\omega B97X-D/6-311G^{**}$ theoretical level.

3.5.3 What We Can Speculate – Brozone and Bonding

The compound with the chemical structure BrOOBr , and the global thermodynamic sink on the potential energy surface defined by the stoichiometry Br_2O_3 , will be henceforth referred to as brozone. Thermodynamics indicate that brozone is more stable than BrOBrO_2 by around $(-)$ 19.96 kcal/mol in the gas phase and $(-)$ 17.59 kcal/mol in the aqueous phase, meaning that the global minimum can be escaped, especially as it is bombarded with ultraviolet light, but the probability is low. Rather unexpectedly, the $[-\text{O}-\text{O}-]_n$ (n being a multiple of $\frac{1}{2}$) bonding motif ends up being very prominent among the global minima on all examined potential energy surfaces. Since we know that in its elemental form, sulfur appears in clusters of eight, it would not be so outrageous to consider the possibility of oxygen forming clusters, too, specifically in chemical environments where atomic oxygen evolution/liberation is not as uncommon as one might initially expect. Additional bonded oxygen atoms appear to make the complexes more stable, though it is likely (but not yet surveyed) that the stability drops off in chains longer than those discussed herein. According to the electrostatic potential (ESP) plot of the global minimum with Br_2O_5 stoichiometry pictured in **Figure 11**, the oxygen atom(s) nearest to the center in a linear chain have the most sp^3 -character and also (oddly) appear to be more electrophilic than those closer to the outer edges of the molecule, meaning that they could be sensitive to attack by halides and/or other nucleophiles.

Though oxygen often tends to steal valence density from bromine when the two atoms are bonded, in certain situations bromine may instead receive valence density from a formally unbonded electronegative element such as oxygen in what is known as a halogen bond. This is a special case of molecular orbital-driven dative bonding, as opposed to being Coulomb-mediated. The availability of an empty anti-bonding σ^* orbital on bromine, particularly opposite a single

bonded substituent, allows an unbonded, electron-rich oxygen to dump some of its charge there, forming a fairly strong interaction that sometimes approaches the strength of a covalent bond, shared then among bonded substituents (similar to a 3-center, 2-electron bond). This type of interaction may hold some of the higher-order bromine oxides together, particularly in the solid phase. As noted previously, oxygen that is formally bonded to two bromine atoms often appears to be more electrophilic than oxygen bonded to only one bromine. Curiously, calculating the oxidation number of both bromine atoms in BrO₅Br as we would in general chemistry for most normal molecules gives +5 for each bromine, however this is certainly inaccurate according to the literal values on the ESP surface (the charges are deliberately exaggerated in **Figure 11**), meaning that we are dealing with one of those few-and-far-between exceptions to the normal rules of chemical bonding. If both bromine atoms are in their +1 oxidation state, -2 charge units would have to be partitioned among the remaining five oxygen atoms. According to the ESP, the most likely whole number oxidation distribution is likely: Br(I)—O(-II)—O(I)—O(0)—O(I)—O(-II)—Br(I), but could also be more like: Br(I)—O(-I)—O(-I)—O(II)—O(-I)—O(-I)—Br(I). There are certainly other acceptable spreads.

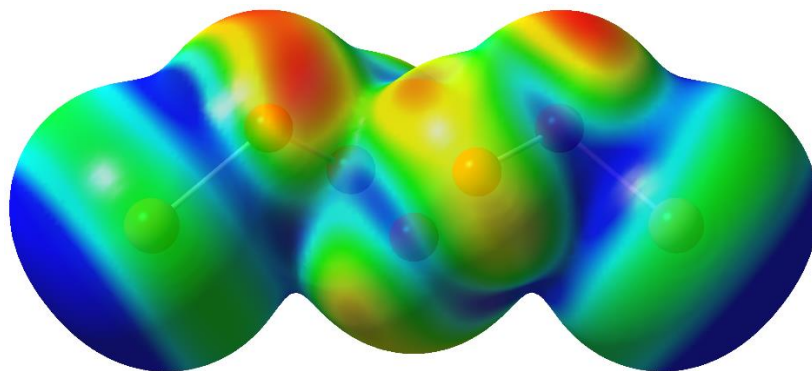


Figure 11. Electrostatic potential of the global minimum on the singlet BrO₅Br potential energy surface at U ω B97X-D/6-311G**. Colors represent a range from (-)0.025 electron charge (red, negative charge) to (+)0.025 electron charge units (blue), hence partial charges are exaggerated. The isosurface density shown is 0.004 electrons per cubic Ångstrom.

Somewhat perplexingly, the O—O—O bonding motif is only well characterized in computational studies that present similar results. Since we have determined that bromine oxides are fairly good oxygen donors and very abundant in a BZ solution, we note that they have the potential to feed the spontaneous generation of ozone, process **2** in **Table 11**, which proceeds naturally in the sky and could be the source of another reactive intermediate in solution. Since the formation of the O₃ motif is favorable in the presence of atomic oxygen, even in aqueous solution, the bromine oxides could feasibly fall into this sink if irradiated or allowed to accumulate. Since ultraviolet radiation in the troposphere and stratosphere produces ozone in addition to many radical species, we might expect brozones to form there as well.

Reaction	ΔE (kcal/mol)	ΔH (kcal/mol)	ΔG (kcal/mol)
Gas Phase			
1. $(3/2) \text{}^3\text{O}_2 \rightarrow \text{}^1\text{O}_3$	50.58	51.13	56.11
2. $\text{}^3\text{O}_2 + \text{}^3\text{O} \rightarrow \text{}^1\text{O}_3$	-10.40	-9.07	-0.52
Aqueous Phase			
1. $(3/2) \text{}^3\text{O}_2 \rightarrow \text{}^1\text{O}_3$	47.73	48.22	53.20
2. $\text{}^3\text{O}_2 + \text{}^3\text{O} \rightarrow \text{}^1\text{O}_3$	-13.16	-11.88	-3.33

Table 11. Thermodynamics of ozone formation from two triplet oxygen molecules or one triplet oxygen molecule and one triplet atomic oxygen indicate that ozone forms spontaneously if provided with atomic oxygen. The spin multiplicity of each species is indicated with superscript.

No model published thus far is perfect, and it stands to reason that successes met by modeling one higher-order bromine oxide, Br₂O₄, into the GTF and MBM schema and BrOBr into another⁷⁷ invite us to consider many more plausible reactions involving other chemical species. While models adequately reproduced behavior characteristic of a BZ reaction for at least twenty years before Br₂O₄ and other higher-order bromine oxides were introduced, the quirks that keep these models from perfectly reproducing BZ behavior can likely be addressed by including terms for more of these processes (as is generally true for all incomplete model systems). Following

the example, the new reactions proposed in the following section were tested for thermodynamic viability and, amongst hundreds of others, represent the most seemingly useful, novel additions to general models of Belousov-Zhabotinsky reactions that this particular study has to offer. There are undoubtedly still more processes that occur, and a fair share of them likely involve the many more bromine oxides left to discover. For now, though, we will just analyze what we can. First-order rate constants, which should be modified for higher-order reactions, are calculated and provided in the next section by plugging obtained activation energies into an appropriate version of the Eyring equation:

$$k = Ae^{-\Delta G^\ddagger/RT}$$

Known Parameters:

$$A \equiv \frac{k_B T}{h} \approx \frac{(1.3806 \times 10^{-23} \frac{J}{K})(298.15 K)}{6.6261 \times 10^{-34} J \cdot s} \approx 6.2122 \times 10^{12} s^{-1}$$

$$RT = k_B N_A T \approx \left(1.3806 \times 10^{-23} \frac{J}{K}\right) (6.0221 \times 10^{23} mol^{-1})(298.15 K)$$

$$RT \approx 0.5925 \frac{kcal}{mol} \approx (2.4789 \frac{kJ}{mol}) / (4.184 \frac{kJ}{kcal})$$

Equation Set 6. The simplest form of the Eyring equation (top) is used to calculate first-order rate constants for reactions whose Gibbs energy of activation can be determined. The pre-exponential factor, A , can be defined in multiple ways, depending on the specific application, but the definition shown above is perhaps the most useful when applied to true first-order reactions. Higher-order reactions are only accurately modeled when the concentrations of other reactants are effectively constant and/or if k is multiplied by one or more additional variables to correct for their presence. The value of RT is calculated and converted to kilocalories per mole in the lower two equations.

3.6 Fruits of Labor

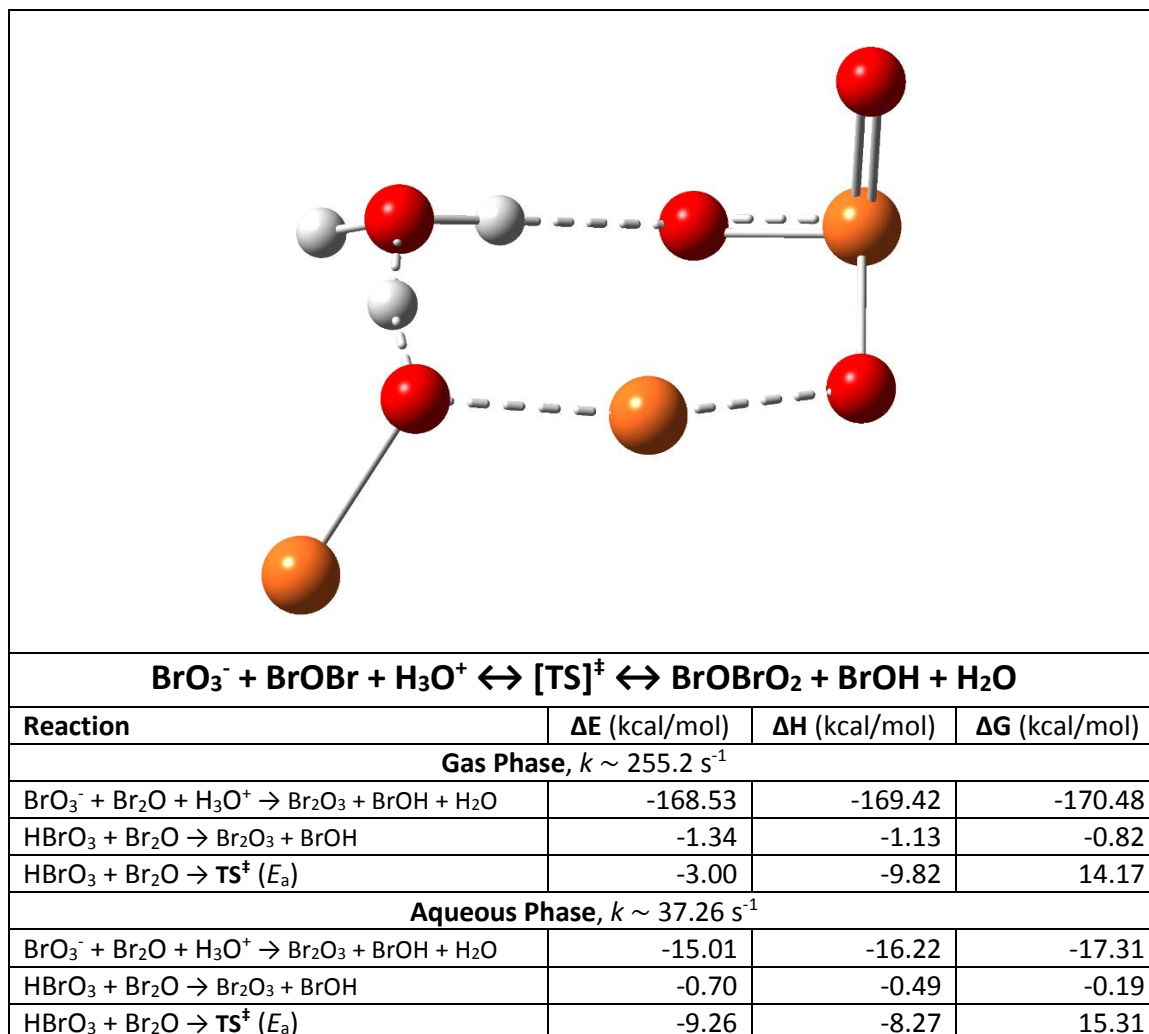


Figure 12. The oxidation of BrOBr by acidic bromate is thermodynamically favorable no matter the initial protonation state of bromate and has a modest activation barrier. In practice, this reaction can proceed in both directions, thus regenerating bromate if enough of the BrOBrO₂ sink accumulates.

As described previously, the reaction shown in **Figure 12** may function as a reversible reservoir for bromic acid, which shortly deprotonates to bromate upon its formation. Bromate's oxidizing capacity is 'deactivated' by BrOBr and regenerated when the BrOH concentration rises, which may also act as a makeshift feedback mechanism because [BrOH] should rise steadily as [BrO₃⁻] falls, according to the established chemistry.

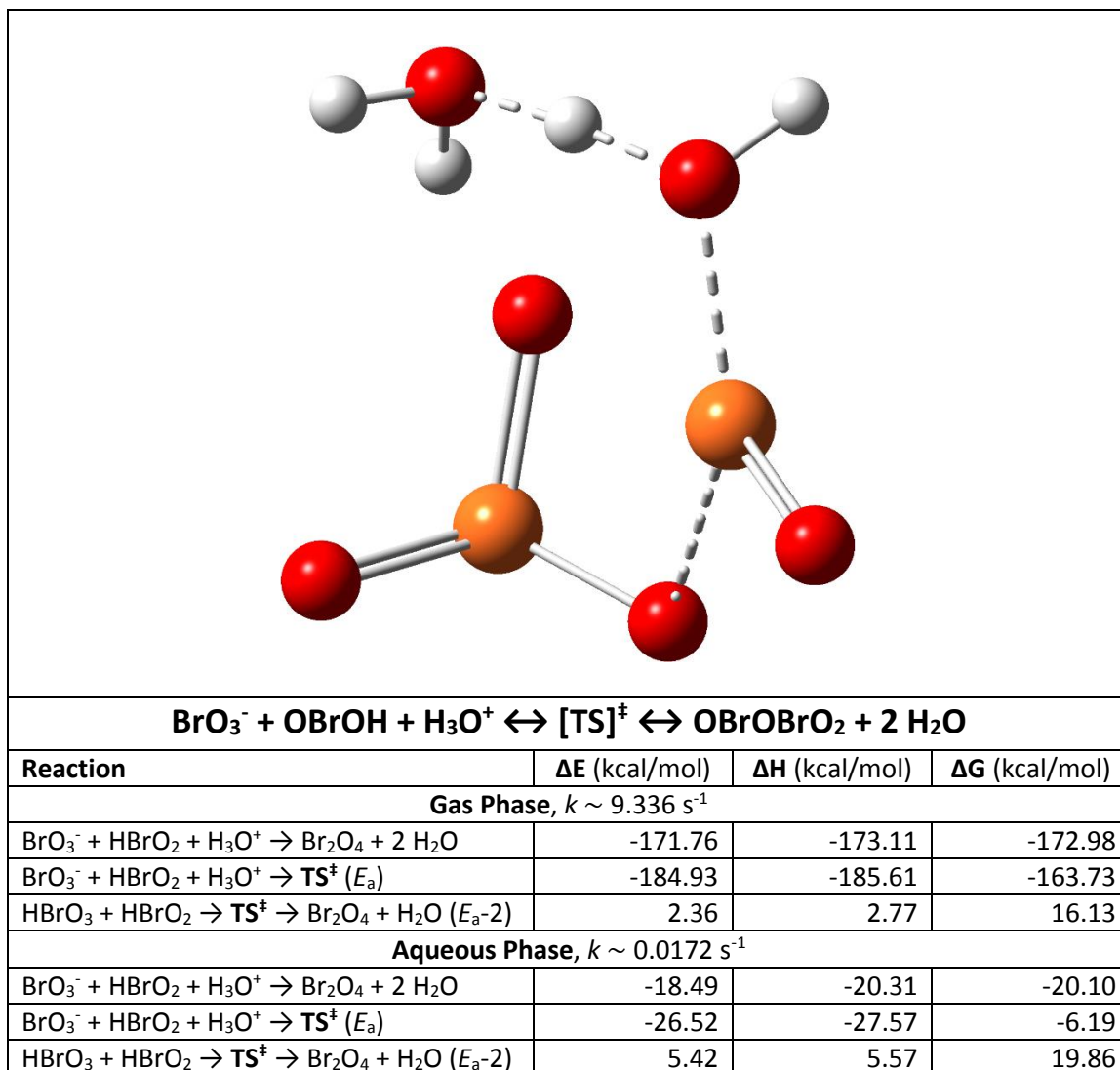


Figure 13. Acid-mediated condensation of bromate and bromous acids to OBrOBrO₂. The activation barrier, though greater for the reverse process, is reachable from both sides. This is MBM reaction 6.

The reaction in **Figure 13** is still feasible without hydronium. In this case, the primary activation barrier would be the formation of bromic acid, around 17.12 kcal/mol. Once formed, the (-)2.98 kcal/mol difference in product energy would allow the process to reverse. The negative activation energy for the pictured reaction as well as its reversibility both suggest that this process competes with others in the reaction vessel. The MBM scheme reports a second-order rate constant for the forward reaction of $48 \text{ M}^{-2}\text{s}^{-1}$ and $3.2 \times 10^3 \text{ M}^{-1}\text{s}^{-1}$ in reverse.⁷

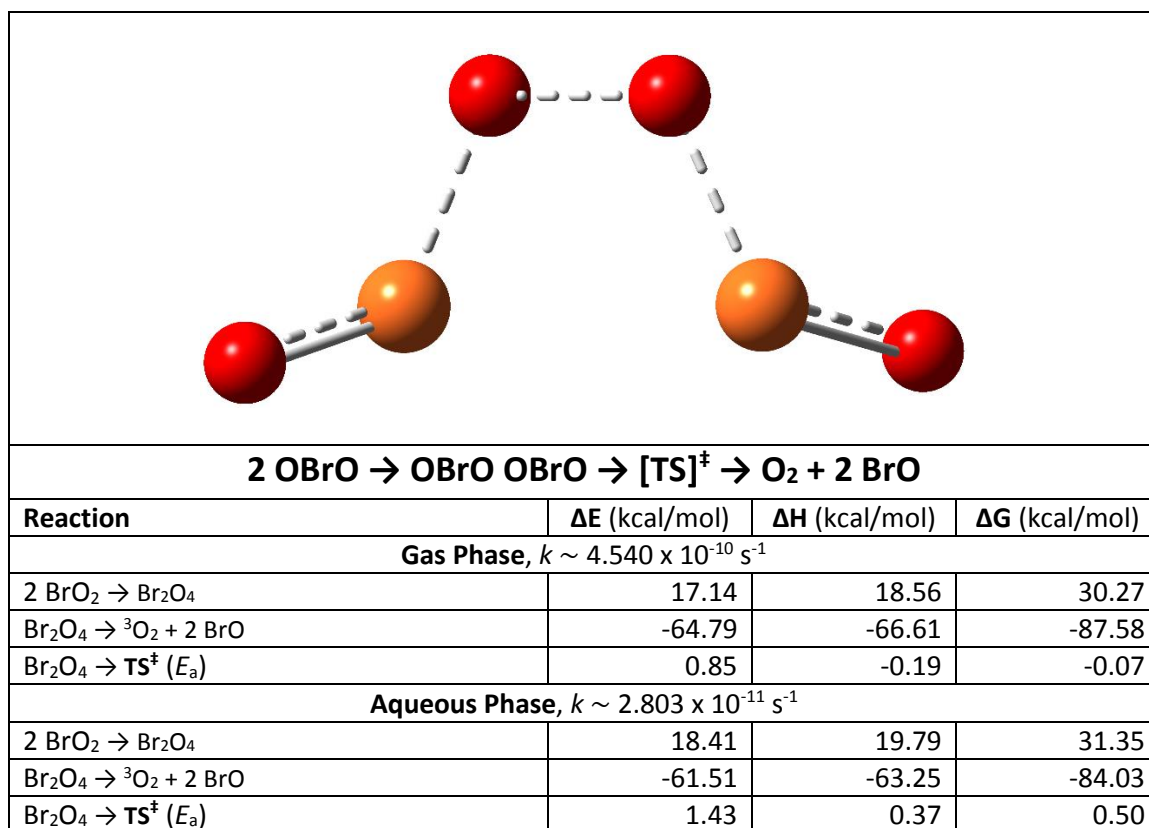


Figure 14. The decomposition rate of a bromine dioxide dimer is limited by the 30+ kcal/mol association step. Once locked into the proper conformation, oxygen is rapidly evolved, leaving two bromine monoxide radicals behind. The transition structure was optimized with a mixed electronic state because the actual electronic state rapidly changes from reactant to products.

The process shown in **Figure 14** could be important to modern BZ models because the mainstream now incorporates elemental oxygen into its description, which had only been written about in the distant past. Following the rate-limiting rearrangement of Br₂O₄ or encounter between two OBrO radicals, elemental oxygen evolves almost effortlessly and completely irreversibly. Attempts to optimize the OBrO dimer as a triplet have failed, despite the certain existence of many triplet ($S=3/2$) species, so for now this is written off as another weird property of the bromine oxides. The activation energy of the oxygen evolution process is very high, but the calculated rate constant agrees (by around a factor of 20) with the value given for reaction **9** in the MBM model, one of their oxygen evolution reactions ($6 \times 10^{-10} \text{ M}^{-3} \text{ s}^{-1}$).

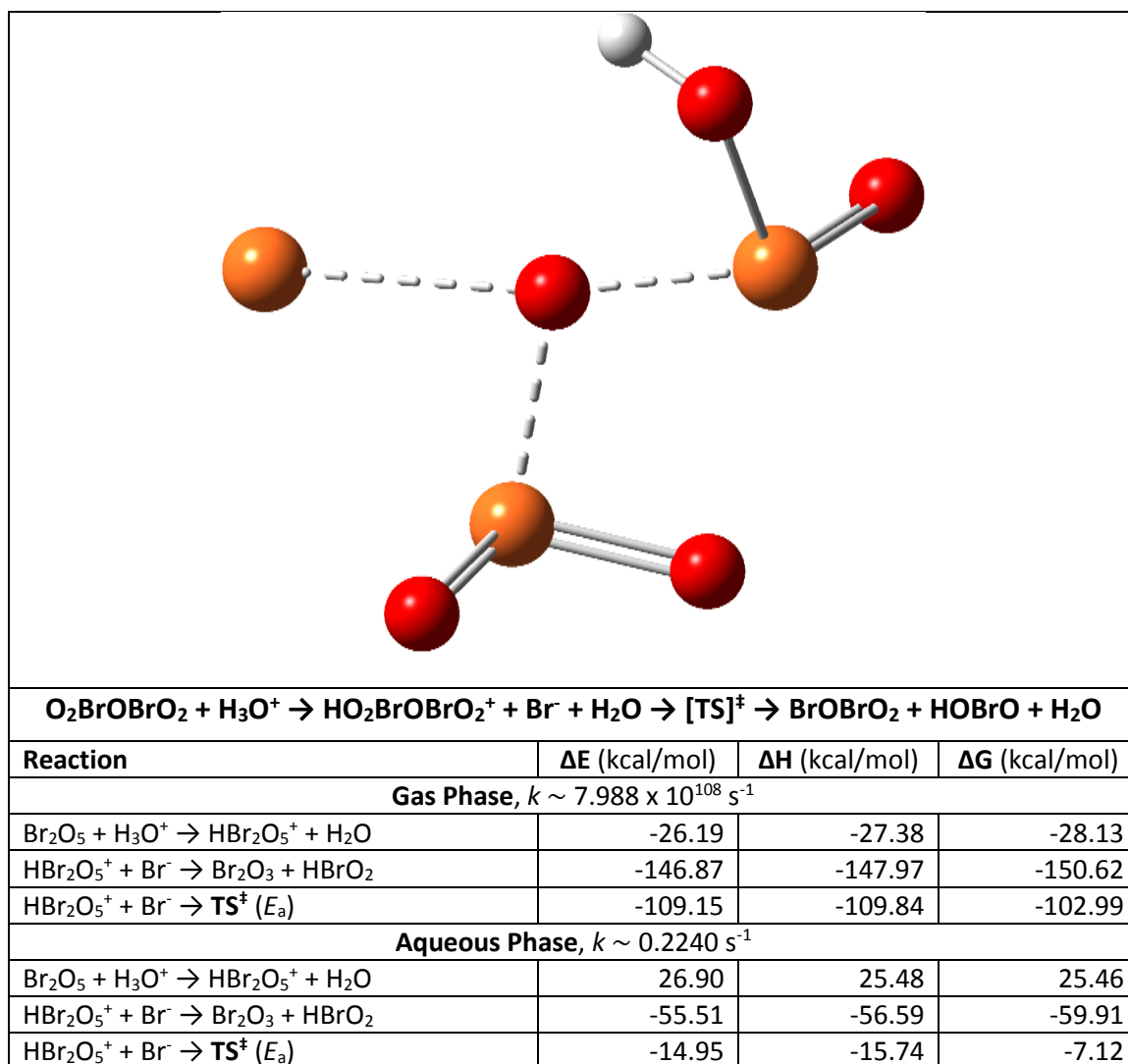


Figure 15. Decomposition of Br_2O_5 by acid and bromide. Following the protonation of Br_2O_5 at a terminal oxygen, the bromine that it is bonded to draws electron density from the central oxygen, weakening its bond and ultimately evolving $HOBrO$ as bromide secures a bond on the opposite side.

The reaction shown in **Figure 15** may act as another bromine oxide reservoir, however this time it holds onto $HOBrO$, the most reactive of the small bromine oxides. Since the reactant is one of the least stable Br_2O_5 isomers, the fact that it decomposes into a highly reactive species is not surprising, and in doing so, the much less labile $BrOBrO_2$ sink is also formed. We note that, despite the extremely large rate constant in the gas phase, the upper limit of reaction frequency is on the order of a bond vibration, around 10^{13} s^{-1} .⁷⁸ The protonation is the activation step.

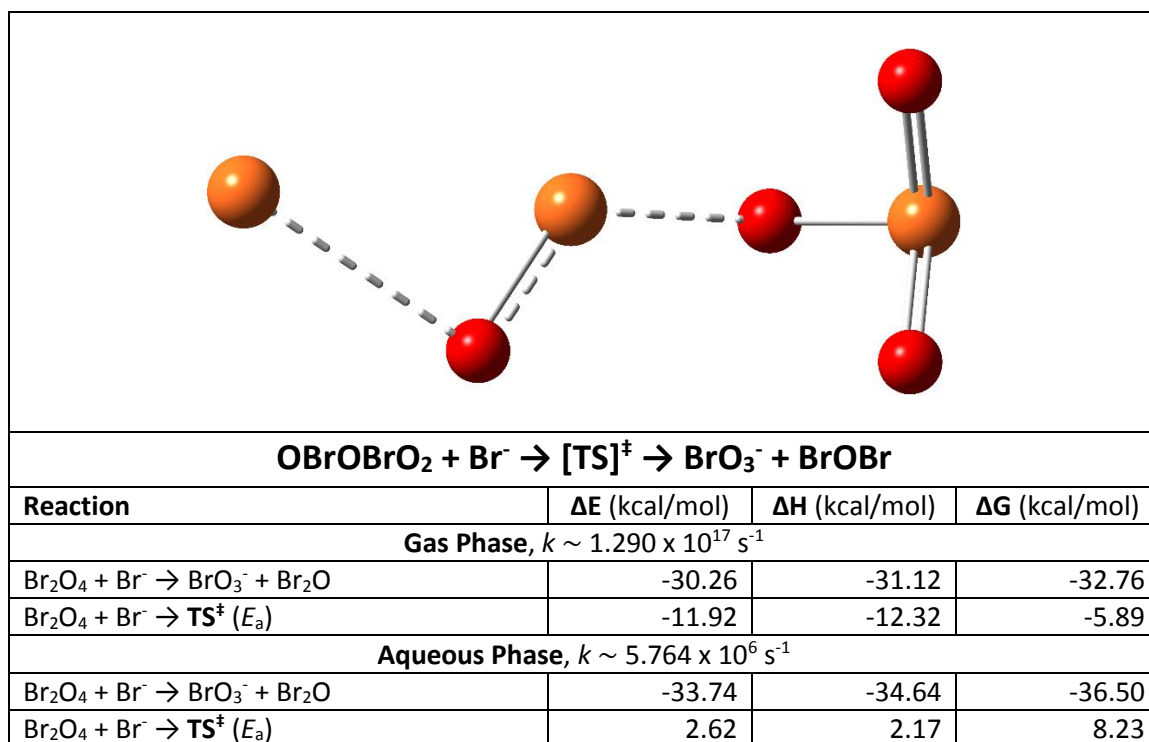


Figure 16. The bromide-mediated decomposition of OBrOBrO₂ has a low activation energy and is one of the few sources of BrOBr. Bromate is also a product, thus this reaction is amongst the most important of those presented in this section.

*A somewhat surprising feature of multiple higher-order bromine oxide reactions is that they appear to be initiated when bromide attacks an electron-deficient oxygen atom. While **Figure 13** describes the formation of OBrOBrO₂, **Figure 16***

***Figure 16**, above, describes the bromide-dependent decomposition of the same isomer, meaning that this reaction describes a novel path from bromous acid to bromate, also generating BrOBr, which could then feed into the reaction in **Figure 12**. This particular pathway is essentially irreversible. As it all comes together, we note that Br₂O₄ has the same stoichiometry as BrO₂, which, when reduced to bromous acid, was thought to be the species that caused the observed autocatalysis in the mixture for so long. While older models tend to sufficiently explain the basic behavior of a BZ reaction, perhaps someone will devise a model one day that *never* fails, and perhaps it will include this equation.*

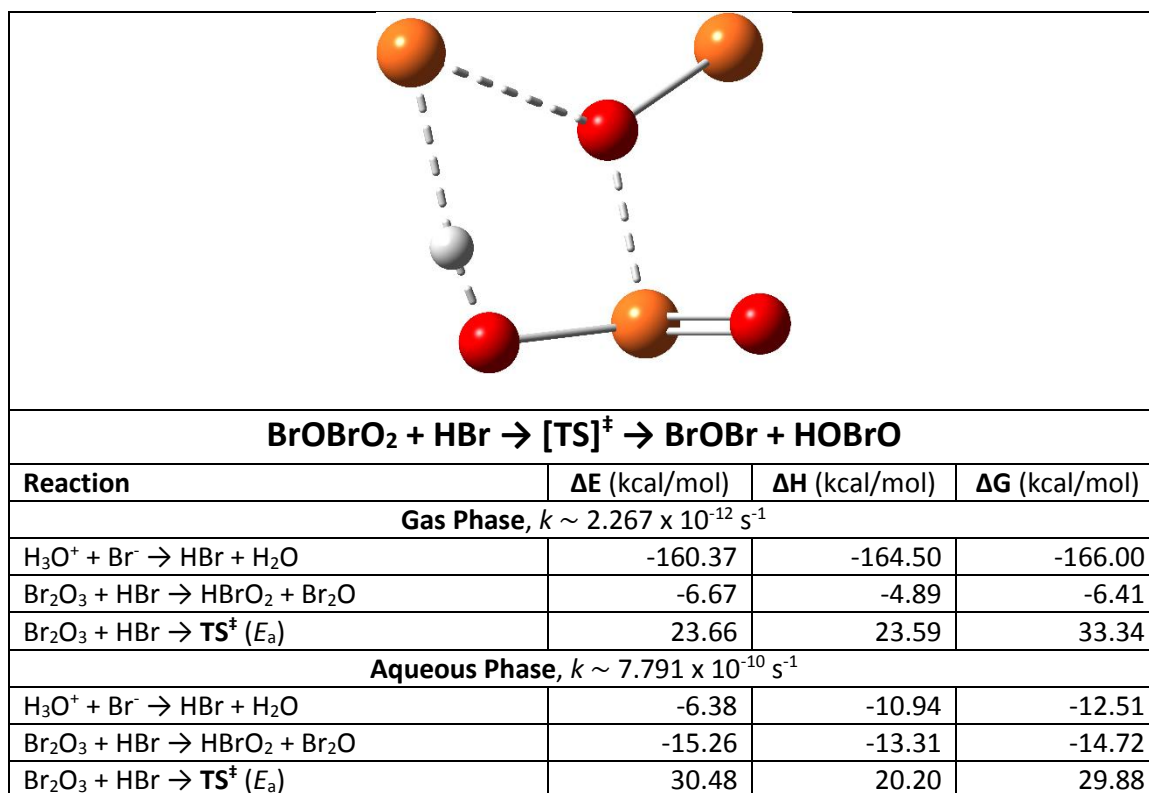


Figure 17. The acidic bromide-mediated decomposition of BrOBrO₂ has an activation energy that is skirting on the edge of feasibility, however the reaction can still proceed at 25 °C, generating BrOBr and HOBrO, which feed back into the autocatalytic cycle. The protonation of bromide is shown, but not factored into the rate constants, hence why they are so small.

Like the reaction presented in **Figure 16**, bromide appears to attack a relatively electrophilic oxygen atom in **Figure 17**, above. Unlike the previous reaction, however, this time bromide carries a proton with it, which is abstracted as the activated complex forms. We notice a pattern now in this and the two preceding figures that might pave the way to the discovery of even more novel disproportionation reactions: Higher-order bromine oxides, similar to bromate, bromous acid and hypobromous acid, appear to decompose upon attack by bromide. This is significant because we have now figured out how lower bromine oxides and oxoacids can be liberated from the higher bromine oxides, which may be thought of as effective ‘autocatalytic reservoirs’ in the context of bromate chemical oscillators.

4. Discussion

4.1 Potential Flaws, Fixes, and Side Notes

A flaw that could lead to multiple inaccurate numbers, specifically referring to the bromine oxides and oxoacids, is the neglect of diffuse functions in the chosen basis set. While the chosen basis set does reproduce properties of elemental bromine very well, bromine oxides contain many lone pairs of electrons that could potentially be modeled more accurately if allowed to venture further from the nuclei. The reason that they were not used is due to the fact that many of the molecules examined are either neutral or positively charged, and, interestingly, the calibration indicated that the Pople series triple- ζ basis with additional diffuse functions actually *decreased* the empirical agreement when passed to the chosen functional. It likely has something to do with the empirical dispersion interaction, which is also likely the reason that some of the molecules fail to converge at this level of theory. Since we note multiple cases in which diffuse functions *decrease* the accuracy of results, particularly when concerned with the transition metal, iron, we acknowledge that this should be considered in the future.

Another potential flaw is the neglect of ^{81}Br . According to slightly dated IUPAC data cited previously,³⁵ bromine is the element with the most even distribution of naturally occurring isotopes, of which there are two (^{79}Br and ^{81}Br). Gaussian calculations use the mass of ^{79}Br in calculations by default, however since ^{81}Br is essentially as abundant as ^{79}Br , all calculations herein suffer from isotope bias, slightly affecting unweighted accuracies of the numbers. Given what we know about the kinetic isotope effect, we might expect rates calculated with light bromine to be very slightly overestimated compared to the true rates, which would be more accurately found using a linear combination of both isotopomer energies of every bromine-

containing molecule weighted by their actual natural abundance. The formation of $^{81}\text{Br}_2$ is only favorable over $^{79}\text{Br}_2$ by around $1/20^{\text{th}}$ of a kcal/mol in the gas phase, as calculated at the same level of theory as everything else, so ideally the isotope bias would not have a significant effect on the obtained data, however we know that in chaotic systems, the smallest numerical difference can result in an entirely different outcome, so we must also acknowledge this.

As in any computational study, it is often difficult to sample every single possible minimum on every single potential energy surface included, thus there may be a few chemical species whose absolute free energies are slightly underestimated (in magnitude). While this could introduce small errors into the thermochemistry, it is not really that big a deal because many of the potential energy surfaces *were* sampled completely and, even if some of them were not, the differences in absolute energy that arise from these types of mistakes are often on the order of less than 3 kcal/mol, which falls somewhere near the inherent computational error bar anyway. Calculating raw energy differences for each plausible reaction and comparing them to proposed schemes in literature yields varied results – had a model reaction sequence for the ferrioxalate-catalyzed BZ reaction been proposed herein, it could have been simulated by solving the set of differential rate equations for each reaction in the sequence that depend on activation parameters determined by the relative energies of first-order saddle points on the potential energy surface. Given the shortage of available resources and time, no model was devised or solved. This study does provide raw data that orient the thermodynamic path through the components of the system considered, but it is important to take that thermodynamic data for what it is. It is also important to note that the low pH and fairly high ionic strength of BZ solutions are not accounted for in these calculations. Had they been accounted for, we likely would have found that redox reaction rates increase with ionic strength and decrease with pH (at least up to a certain point).

Certainly worth noting is that bromine oxides with different structural formulas that the ones described herein have been observed in the gas phase, namely Br_3O_6 , which was detected using a chemical ionization mass spectrometer following microwave discharge of a sample containing elemental bromine, oxygen and helium.⁷⁹ The presence of species with this stoichiometric ratio begs the study of many more potential inorganic reactions that may or may not proceed, for example the symproportionation of Br_3O_6 to three BrO_2 . Also note that we did not cover any bromine oxide species with higher spin multiplicities, of which triplets ($S = 3/2$) definitely exist and could be almost as numerous as the singlets (but are probably quite a bit less numerous).

The stationary state assumption currently used in Gaussian, that assumes all excited electronic states have excitation energies many times greater than $k_B T$ and therefore may be neglected in the partition function, is generally good, except for in rare cases like bromate, whose lowest excitation energy is about 15 kcal/mol.⁸⁰ Higher neutral halogen oxides may have lower excitation energies. While this is not so common, unfortunately for us, bromate is one of the most important chemical species in this study, thus the stationary electronic state assumption should probably be corrected for in future computational studies.

Since studies of bromine oxides could span hundreds of pages alone, I certainly do not pretend to have covered everything important. The mixture of organic and inorganic chemistry in a BZ reaction is quite perplexing, even to accomplished chemists. While my interpretations may well be inaccurate, they may also be more accurate than the interpretations formulated yesterday. Since we do not actually know for certain, keeping an open mind is very important.

4.2 Conclusions and Future Direction

Though there is still much to learn, we are slowly resolving more and more components of the grand scheme. Examining the same problem from so many different perspectives has allowed researchers to derive many – in some cases radically different – systems of equations that describe or reasonably approximate the actual chemistry of a BZ reaction. When compared to empirical results, however, all of the well-known systems currently accepted as reasonably accurate are flawed. Perhaps adding one or more of the chemical equations proposed in this thesis to the simulations would improve them, if only marginally. The challenge up until recently has been figuring out which reactions *occur*, but the future will be more so figuring out which *dominate* the chemical activity since we now have the means to query kinetics of individual steps in the reaction sequence, which are more important than thermodynamics on second-minute timescales. We cannot truly know what happens without a way to test it, so finding one that minimizes noise and maximizes reproducible results would be the obvious first step in future studies, whether this be by simulation or physical experiment. Rate constants for important chemical equations can be derived given calculated activation energies, so the process of sifting through old equations and adding new ones would only be limited by the time commitments of interested theorists. Some findings of this study may also elicit such questions as whether or not similar autocatalytic mechanisms exhibited by the bromine oxides can be applied to other systems. Do the higher oxides of other halogens behave in the same way, or is this a property unique to bromine? A broader focus would require us to examine more oscillating reactions, which could also potentially be more environmentally friendly since catalytically converting malonic acid to CO₂ (and CO) does not benefit anyone (the plants and phytoplankton already have plenty on reserve) and there is plenty of literature available to

peruse. Sorting through the fact and fallacy to discover the true mechanisms by which chemical reactions ‘oscillate’ could eventually be useful in applications such as more efficient conversion of chemical energy, or perhaps in the development of some sort of oscillating-current generator for use in new-age electronics. Halogen oxide chemistry is also definitely applicable to climate science. In fact, it has been shown that BrO and IO alone account for approximately 34% of total ozone loss in the tropical and subtropical troposphere,²⁰ thus knowing the ultra-fine details of their chemistry would allow us to more accurately model happenings in the atmosphere, which is relevant to every living thing on the surface of the planet. The more we learn, the more closely we can approach a faithful reproduction of the world as we know it *in silico* – another noble, yet daunting goal of many theorists worldwide. Perhaps some of this research will be useful to them. Then again, perhaps we can still find better uses of our time. Maybe the chemistries of life, planet Earth, and the largely unknown frontier that is the cosmos have been harboring the answers we were searching for this whole time while we allowed ourselves to be distracted by drawn-out tangents and unnecessary details. Whatever the truth may be, the real journey begins now.

All schemes were drawn in ACD/ChemSketch (Freeware).⁸¹ Thank you, good people of Earth!

-
- ¹ A.T. Winfree. "The Prehistory of the Belousov-Zhabotinsky Oscillator", *J. Chem. Edu.*, **16**(8), 661-663. (1984)
- ² A. M. Turing. "The Chemical Basis of Morphogenesis", *Philosophical Trans. Royal Soc. London Series B, Biol. Sci.*, **237**(641), 37-72. (1952)
- ³ I. Prigogine, R. Lefever. "Symmetry Breaking Instabilities in Dissipative Systems. II", *J. Chem. Phys.*, **48**(4), 1695-1700. (1968)
- ⁴ Richard J. Field, Richard M. Noyes. "Oscillations in chemical systems. IV. Limit cycle behavior in a model of a real chemical reaction", *J. Chem. Phys.*, **60**(5), 1877-1884. (1974)
- ⁵ Richard Field, Endre Körös, Richard Noyes. "Oscillations in Chemical Systems. II. Thorough Analysis of Temporal Oscillation in the Bromate-Cerium-Malonic Acid System", *J. Amer. Chem. Soc.*, **94**(25), 8649-8664. (1972)
- ⁶ László Györgyi, Tamás Turányi, Richard Field. "Mechanistic Details of the Oscillatory Belousov-Zhabotinskii Reaction", *J. Phys. Chem.*, **94**(18), 7162-7170. (1990)
- ⁷ László Hegedüs, Mária Wittmann, Zoltán Noszticzius, *et al.* "HPLC analysis of complete BZ systems. Evolution of the chemical composition in cerium and ferroin catalysed batch oscillators: experiments and model calculations", *Faraday Discuss.*, **120**, 21-38. (2001)
- ⁸ Harati Mohammad, Li Nan. "Chemical oscillations in the metal ion-catalyzed bromate—4-aminophenol reaction", *Sci. China Chem.*, **55**(9), 1916-1921. (2012)
- ⁹ Nadeem Ganaie, G. M. Peerzada. "Catalyst, Co-ion and the Media Effect on the Oscillatory Behavior of Resorcinol in the BZ Reaction", *J. Braz. Chem. Soc.*, **20**(7), 1262-1267. (2009)
- ¹⁰ Nadeem Ganaie, G. Peerzada. "Effect of Manganese Salts on an Oscillatory Chemical Reaction in Different Acidic Media", *Intern. J. Chem. Engineering Applications*, **1**(3), 256-260. (2010)
- ¹¹ Sho Kitawaki, *et al.* "Control of the Self-Motion of a Ruthenium-Catalyzed Belousov-Zhabotinsky Droplet", *J. Phys. Chem. C*, **116**, 26805-26809. (2012)
- ¹² Alberto P. Muñozuri, *et al.* "Control of the Chlorine Dioxide-Iodine-Malonic Acid Oscillating Reaction by Illumination", *J. Am. Chem. Soc.*, **121**, 8065-8069. (1999)
- ¹³ Archana Garg. "A Significant Case Study of Uncatalyzed Bromate Oscillator Through the Temperature Effect During Acidic Bromate Oxidation of Catachol", *Int. J. Sci. Enviro.*, **2**(4), 672-675. (2013)
- ¹⁴ Ishfaq Ahmah Shah, *et al.* "A Kinetic Study on Catechol-Based Belousov-Zhabotinsky Reaction", *Intern. J. Chem. Kinetics*, **45**(3), 141-151. (2013)
- ¹⁵ J. Sreekantha Babu, K. Srinivasulu. "Belousov-Zhabotinskii Oscillating Reaction in Solutions containing Gallic Acid", *J. Chem. Soc. Faraday Trans. 1*, **73**, 1843-1844. (1977)
- ¹⁶ Jun Li, Jichang Wang. "Subtle Photochemical Behavior in Ferroin—Bromate—Benzoquinone Reaction", *J. Phys. Chem. A*, **116**, 386-390. (2012)
- ¹⁷ J. Maselko, *et al.* "Oscillation Reactions in the System: Metabolites of the Krebs Cycle-Mn²⁺-KBrO₃-H₂SO₄", *Bioinorg. Chem.*, **9**, 529-536. (1978)
- ¹⁸ István Szalai, *et al.* "Dynamics and Mechanism of Bromate Oscillators with 1,4-Cyclohexanedione", *J. Phys. Chem. A*, **107**, 10074-10081. (2003)
- ¹⁹ Miklós Orbán, *et al.*, "Minimal Bromate Oscillator: Bromate—Bromide—Catalyst", *J. Am. Chem. Soc.*, **104**, 2657-2658. (1982)
- ²⁰ Siyuan Wang, *et al.* "Active and widespread halogen chemistry in the tropical and subtropical free troposphere", *PNAS*, **112**(30), 9281-9286. (2015)
- ²¹ Rainer Vogt, *et al.* "Iodine Chemistry and its Role in Halogen Activation and Ozone Loss in the Marine Boundary Layer: A Model Study", *J. Atmospheric Chem.*, **32**, 375-395. (1999)
- ²² William C. Bray. "A Periodic Reaction in Homogeneous Solution and its Relation to Catalysis", *J. Am. Chem. Soc.*, **43**(6), 1262-1267. (1921)
- ²³ Thomas S. Briggs, Warren C. Rauscher. "An Oscillating Iodine Clock", *J. Chem. Educ.*, **50**(7), 496. (1973)
- ²⁴ Miklós Orbán, *et al.* "New family of homogeneous chemical oscillators: chlorite-iodate-substrate", *Nature*, **292**(27), 816-818. (1981)
- ²⁵ Natalya Gavrilenko, *et al.* "Polymethylacrylate Colorimetric Sensor for Evaluation of Total Antioxidant Capacity", *Procedia Chemistry*, **10**, 97-102. (2014)
- ²⁶ M. Naeem Khan, *et al.* "Spectrophotometric method for quantitative determination of cefixime in bulk and pharmaceutical preparations using ferroin complex", *Journal of Applied Spectroscopy*, **82**(4), 705-711. (2015)

- ²⁷ Masoud Rohani Moghadam, *et al.* "Chemometric-assisted kinetic–spectrophotometric method for simultaneous determination of ascorbic acid, uric acid, and dopamine", *Analytical Biochemistry*, **410**, 289-295. (2011)
- ²⁸ Cong Qian Cheng, Shu Kai Yang, Jie Zhao. "Use of color-change indicators to quantify passive films on the stainless-steel valves of nuclear power plants", *Nuclear Engineering and Design*, **297**, 267-275. (2016)
- ²⁹ Dionysios Christodouleas, *et al.* "Evaluation of total reducing power of edible oils", *Talanta*, **130**, 233-240. (2014)
- ³⁰ Xueqi Xing, Yicheng Zhao, Yongdan Li. "A non-aqueous redox flow battery based on tris(1,10-phenanthroline) complexes of iron(II) and cobalt(II)", *Journal of Power Sources*, **293**, 778-783. (2015)
- ³¹ Arie Borenstein, *et al.* "Metal-organic complexes as redox candidates for carbon-based supercapacitors", *J. Mater. Chem. A*, **2**, 18132-18138. (2014)
- ³² Koji Nakano, *et al.* "Potentiometric DNA sensing platform using redox-active DNA probe pair for sandwich-type dual hybridization at indicator electrode surface", *J. Electroanal. Chem.*, **720-721**, 71-75. (2014)
- ³³ Gaussian 09, Revision D.01, M.J. Frisch, G.W. Trucks, H.B. Schlegel, G.E. Scuseria, M.A. Robb, J.R. Cheeseman, G. Scalmani, V. Barone, B. Mennucci, G.A. Petersson, H. Nakatsuji, M. Caricato, X. Li, H.P. Hratchian, A.F. Izmaylov, J. Bloino, G. Zheng, J.L. Sonnenberg, M. Hada, M. Ehara, K. Toyota, R. Fukuda, J. Hasegawa, M. Ishida, T. Nakajima, Y. Honda, O. Kitao, H. Nakai, T. Vreven, J. A. Montgomery, Jr., J.E. Peralta, F. Ogliaro, M. Bearpark, J.J. Heyd, E. Brothers, K.N. Kudin, V.N. Staroverov, T. Keith, R. Kobayashi, J. Normand, K. Raghavachari, A. Rendell, J.C. Burant, S.S. Iyengar, J. Tomasi, M. Cossi, N. Rega, J.M. Millam, M. Klene, J.E. Knox, J.B. Cross, V. Bakken, C. Adamo, J. Jaramillo, R. Gomperts, R.E. Stratmann, O. Yazyev, A.J. Austin, R. Cammi, C. Pomelli, J.W. Ochterski, R.L. Martin, K. Morokuma, V.G. Zakrzewski, G.A. Voth, P. Salvador, J.J. Dannenberg, S. Dapprich, A.D. Daniels, O. Farkas, J.B. Foresman, J.V. Ortiz, J. Cioslowski, D.J. Fox. *Gaussian, Inc.*, Wallingford, CT. (2010)
- ³⁴ GaussView, Version 5.0.9. Roy Dennington, Todd Keith, John Millam. *Semichem Inc.*, Shawnee Mission, KS. (2009)
- ³⁵ K. Rossman, P. Taylor. "Isotopic Compositions of the Elements 1997", *Pure & Appl. Chem.*, **70**(1), 217-235. (1998)
- ³⁶ Joseph W. Ochterski. "Thermochemistry in *Gaussian*", *Gaussian, Inc.* Available from: http://www.gaussian.com/g_whitepap/thermo.htm. (2000)
- ³⁷ Courtney Holmberg. *Spectroscopic and Vibrational Energy Transfer Studies in Molecular Bromine*, PhD dissertation, Airforce Institute of Technology, August 1993. (Publication No. 93-30483.)
- ³⁸ A. D. Becke. "Density-functional exchange-energy approximation with correct asymptotic-behavior", *Phys. Rev. A*, **38**, 3098-3100. (1988)
- ³⁹ B. Miehlich, A. Savin, H. Stoll, and H. Preuss. "Results obtained with the correlation-energy density functionals of Becke and Lee, Yang and Parr", *Chem. Phys. Lett.*, **157**, 200-206. (1989)
- ⁴⁰ J. P. Perdew, K. Burke, and M. Ernzerhof. "Generalized gradient approximation made simple", *Phys. Rev. Lett.*, **77**, 3865-3868. (1996)
- ⁴¹ J. P. Perdew, K. Burke, and M. Ernzerhof. "Errata: Generalized gradient approximation made simple", *Phys. Rev. Lett.*, **78**, 1396. (1997)
- ⁴² M. Head-Gordon, J. A. Pople, and M. J. Frisch. "MP2 energy evaluation by direct methods", *Chem. Phys. Lett.*, **153**, 503-506. (1988)
- ⁴³ G. E. Scuseria, C. L. Janssen, and H. F. Schaefer III. "An efficient reformulation of the closed-shell coupled cluster single and double excitation (CCSD) equations", *J. Chem. Phys.*, **89**, 7382-7387. (1988)
- ⁴⁴ J. A. Pople, M. Head-Gordon, and K. Raghavachari. "Quadratic configuration interaction - a general technique for determining electron correlation energies", *J. Chem. Phys.*, **87**, 5968-5975. (1987)
- ⁴⁵ R. Ditchfield, W. J. Hehre, and J. A. Pople. "Self-Consistent Molecular Orbital Methods. 9. Extended Gaussian-type basis for molecular-orbital studies of organic molecules", *J. Chem. Phys.*, **54**, 724. (1971)
- ⁴⁶ V. A. Rassolov, M. A. Ratner, J. A. Pople, P. C. Redfern, and L. A. Curtiss. "6-31G* Basis Set for Third-Row Atoms", *J. Comp. Chem.*, **22**, 976-984. (2001)
- ⁴⁷ K. Raghavachari and G. W. Trucks. "Highly correlated systems: Excitation energies of first row transition metals Sc-Cu", *J. Chem. Phys.*, **91**, 1062-1065. (1989)
- ⁴⁸ M. P. McGrath and L. Radom. "Extension of Gaussian-1 (G1) theory to bromine-containing molecules", *J. Chem. Phys.*, **94**, 511-516. (1991)
- ⁴⁹ Nikolai Balabanov, Kirk Peterson. "Systematically convergent basis sets for transition metals. I. All electron correlation consistent basis sets for the 3d elements Sc-Zn", *J. Chem. Phys.*, **123**, 064107. (2005)
- ⁵⁰ A.K. Wilson, D.E. Woon, K.A. Peterson, T.H. Dunning, Jr. "Gaussian basis sets for use in correlated molecular calculations. IX. The atoms gallium through krypton", *J. Chem. Phys.*, **110**, 7667-7676. (1999)
- ⁵¹ A.V. Marenich, C.J. Cramer, D.G. Truhlar. "Universal solvation model based on solute electron density and a continuum model of the solvent defined by the bulk dielectric constant and atomic surface tensions", *J. Phys. Chem. B*, **113**, 6378-6396. (2009)
- ⁵² J. B. Foresman, M. Head-Gordon, J. A. Pople, and M. J. Frisch. "Toward a Systematic Molecular Orbital Theory for Excited States", *J. Phys. Chem.*, **96**, 135-149. (1992)

- ⁵³ Frank Jensen. *Introduction to Computational Chemistry*, 2nd Edition, John Wiley & Sons Inc., Hoboken, NJ. (2007)
- ⁵⁴ Jeng-Da Chai, Martin Head-Gordon. "Long-range corrected hybrid density functionals with damped atom-atom dispersion corrections[†]", *Phys. Chem. Chemical Physics*, **10**, 6615-6620. (2008)
- ⁵⁵ Dipankar Roy, *et al.* "Comparison of some dispersion-corrected and traditional functionals with CCSD(T) and MP2 *ab initio* methods: Dispersion, induction, and basis set superposition error", *J. Chem. Phys.*, **137**(13), 134109. (2012)
- ⁵⁶ K. P. Huber, G. Herzberg. *Molecular Spectra and Molecular Structure IV. Constants of Diatomic Molecules*, Van Nostrand Reinhold Company, New York, NY. (1979)
- ⁵⁷ C. Blondel, *et al.* "High-resolution determination of the electron affinity of fluorine and bromine using crossed ion and laser beams", *Physical Rev. A*, **40**(7), 3698-3701. (1989)
- ⁵⁸ Peter Atkins, *et al.* *Shriver & Atkins Inorganic Chemistry*, Fourth Edition, W. H. Freeman and Company, New York, NY. (2006)
- ⁵⁹ G. G. Camiletti, *et al.* "Augmented Gaussian basis sets of double and triple zeta valence qualities for the atoms K and Sc-Kr: Applications in HF, MP2, and DFT calculations of molecular electronic properties", *J. Mol. Struct.: THEOCHEM*, **910**, 122-125. (2009)
- ⁶⁰ A. Hulaniki, S. Glab. "Redox Indicators. Characteristics and Applications", *Pure and Appl. Chem.*, **50**, 463-498. (1978)
- ⁶¹ A. Paulenova, *et al.* "Redox potentials and kinetics of the Ce³⁺/Ce⁴⁺ redox reaction and solubility of cerium sulfates in sulfuric acid solutions", *J. of Power Sources*, **109**(2), 431-438. (2002)
- ⁶² J. Ungvarai, *et al.* "Effective rate constant of the ferriin reduction in the Belousov-Zhabotinsky reaction", *J. Chem. Soc., Faraday Trans.*, **93**(1), 69-71. (1997)
- ⁶³ Venera Brînzea, *et al.* "Overall Activation Energy of Propane-Air Combustion in Laminar Flames", *Chimie, Anul XVIII*, **1**, 35-41. (2009)
- ⁶⁴ Yao-Chu Chou, *et al.* "Kinetic Study of the Ferriin Oxidation of Malonic Acid and Its Derivatives. Implication in the Belousov-Zhabotinsky Reaction", *J. Phys. Chem.*, **97**, 8450-8457. (1993)
- ⁶⁵ Lázló Hegedüs, *et al.* "Chemical mechanism of the radical feedback loop in the classical BZ reaction. Malonyl bromite and oxalic acid as flow-through intermediates", *Phys. Chem. Chem. Phys.*, **2**, 4023-4028. (2000)
- ⁶⁶ Flora T. T. Ng, Patrick M. Henry. "Kinetics and mechanism of the oxidation of several ketones by tris(1,10-phenanthroline)Fe(III) in aqueous acid medium", *Can. J. Chem.*, **55**, 2900-2908. (1977)
- ⁶⁷ Hans-Jürgen Krug, *et al.* "Analysis of the Modified Complete Oregonator Accounting for Oxygen Sensitivity and Photosensitivity of Belousov-Zhabotinsky Systems", *J. Phys. Chem.*, **94**, 4862-4866. (1990)
- ⁶⁸ László Hegedüs, *et al.* "Contribution to the Chemistry of the Belousov-Zhabotinsky Reaction. Products of the Ferriin-Bromomalonic Acid and Ferriin-Malonic Acid Reactions", *J. Phys. Chem. A*, **110**, 12839-12844. (2006)
- ⁶⁹ David Bowman, Elena Jakubikova. "Low-spin versus High-spin Ground State in Pseudo-Octahedral Iron Complexes", *Inorg. Chem.*, **51**, 6011-6019. (2012)
- ⁷⁰ Masanori Sono, *et al.* "Heme-Containing Oxygenases", *Chem. Rev.*, **96**, 2841-2887. (1996)
- ⁷¹ Martin Maltempo, "Magnetic state of an unusual bacterial heme protein", *J. Chem. Phys.*, **61**(7), 2540-2547. (1974)
- ⁷² Jonas Angström, *et al.* "The Magnetic Susceptibility of Ferricytochrome c", *Biochimica et Biophysica Acta*, **703**, 87-94. (1982)
- ⁷³ Ana C. Messias, *et al.* "Solution structures of tetrahaem ferricytochrome c₃ from *Desulfovibrio vulgaris* (Hildenborough) and its K45Q mutant: The molecular basis of cooperativity", *Biochimica et Biophysica Acta*, **1757**, 143-153. (2006)
- ⁷⁴ Takahisa Ikeue, *et al.* "Saddle-Shaped Six-Coordinate Iron(III) Porphyrin Complexes Showing a Novel Spin Crossover between S=1/2 and S=3/2 Spin States", *Angew. Chem.*, **113**(14), 2687-2690. (2001)
- ⁷⁵ Savilov S.V., *et al.* "Chlorine and bromine oxides: synthesis, structure, role in heterogeneous processes of stratospheric ozone decomposition", *Proc. of SPIE*, **5026**, 7-12. (2003)
- ⁷⁶ William Levason, *et al.* "Characterization of Dibromine Monoxide (Br₂O) by Bromine K-Edge EXAFS, and IR Spectroscopy", *J. Am. Chem. Soc.*, **112**, 1019-1022. (1990)
- ⁷⁷ S. M. Blagojević, *et al.* "Role of Br₂O Species in the Model of Belousov-Zhabotinsky Reaction", *Physical Chemistry* **2006**, **1**, 252-254. (2006)
- ⁷⁸ Christopher J. Cramer. *Essentials of Computational Chemistry Theories and Models*, Second ed.; Wiley: Chippingham. (2008)
- ⁷⁹ Zhuangjie Li, Joseph Francisco. "A density functional study of structure and heat of formation for Br₂O₄ and Br₂O₅", *Chem. Phys. Letters*, **354**, 109-119. (2002)
- ⁸⁰ Hui Wen, *et al.* "Photoelectron spectroscopy of higher bromine and iodine oxide anions: Electron affinities and electronic structures of BrO_{2,3} and IO₂₋₄ radicals", *J. Chem. Phys.*, **135**, 184309. (2011)
- ⁸¹ ACD/ChemSketch (Freeware) 2015, Version C10E41, Build 76694. *Advanced Chemistry Development, Inc.*, Toronto, Canada. (2015)